University of Nevada, Reno

3D-Move Simulation of TSDDs for Pavement Characterizations

A dissertation submitted in partial fulfillment of the requirements for the degree of Doctor of Philosophy in Civil & Environmental Engineering

by

Seyyedmahdi Nasimifar

Dr. Rajaratnam Siddharthan/Dissertation Advisor

December, 2015

THE GRADUATE SCHOOL

We recommend that the dissertation
prepared under our supervision by

SEYYEDMAHDI NASIMIFAR

entitled

3d-Move Simulation Of Tsdds For Pavement Characterizations

be accepted in partial fulfillment of the
requirements for the degree of

DOCTOR OF PHILOSOPHY

Rajaratnam Siddharthan, Ph.D., Advisor

Elie Y. Hajj, Ph.D., Committee Member

Ramin Motamed, Ph.D., Committee Member

Raj R. Kallu, Ph.D., Committee Member

Sherif Elfass, Ph.D., Committee Member

Raj R. Kallu, Ph.D., Graduate School Representative

David W. Zeh, Ph. D., Dean, Graduate School

December, 2015

Abstract

State highway agencies (SHAs) spend billions of dollars each year on various transportation infrastructure assets to meet legislative, agency and public expectations. Recently, some organizations in the USA and Europe have developed devices that continuously measure pavement deflection and can reduce the cost associated for network-level pavement data collection. Traffic Speed Deflectometer (TSD), Rolling Wheel Deflectometer (RWD) and Euroconsult, Curviametro (CRV) are such devices that are being used around the world and were evaluated in this study. The proper incorporation of the measurements from these devices to network level pavement management system (PMS) applications requires appropriate, device-specific, analysis methodology. To assess the appropriateness of any proposed methodology, field evaluations in conjunction with analytical models to simulate the TSDDs measurements are required important steps. The Federal Highway Administration (FHWA) commissioned the evaluation of these devices at the MnROAD facility in September 2013. 3D-Move program that has the capability of modeling moving loads and the resulting dynamic pavement responses was used as an analytical tool in this study. Using a variety of independent pavement responses that included surface deflection bowls as well as horizontal strains at the bottom of the AC layers confirmed the ability of the 3D-Move model to simulate TSDD loading under realistic pavement conditions. Using the calibrated 3D-Move software, an analytical investigation was then undertaken to explore relationships between load-induced pavement structural-related response and the corresponding surface deflection basin related indices. A key element was the simulation

of pavement deflections using the 3D-Move model with a focus on understanding the parameters that affect the TSDD measurements that included vehicle speed and loadings, and pavement layer properties (thicknesses and stiffnesses). This step enables the use of TSDDs in PMS applications. The outcome of this study facilitated use of TSDDs in network level pavement management system by categorizing pavements based only on AC thickness and then relating $DSI_{200\text{-}300}$ (D_{200} - D_{300}) and $DSI_{300\text{-}900}$ (D_{300} − D_{900}) to fatigue and rutting strain, respectively through appropriate equations. The study also provided some practical suggestions to improve the performance of TSDDs in PMS applications.

DEDICATION

This dissertation is dedicated to my wife Hanie who has encouraged and supported me on this journey. This is also dedicated to my parents, for their sacrifice and indulgence to make education a priority for me.

ACKNOWLEDGEMENTS

This study was funded through the FHWA study DTFH61-12-C-00031 and the support is gratefully acknowledged.

I would like to express my deepest gratitude to my advisor, Dr. Raj Siddharthan for his practical advices, recommendations and instructions which have enabled me to finish the research effectively. His enduring encouragements have been an inestimable source of support for me during this process. It is not sufficient to express my gratitude with only a few words.

I would especially like to thank Dr. Elie Y. Hajj. This research has certainly benefited from his insightful suggestions. I owe him my sincere gratitude for his generous and timely help.

I would like to thank the rest of my dissertation committee: Dr. Ramin Motamed, Dr. Sherif Elfass and Dr. Raj Kallu who asked me good questions and gave me perspicacious comments.

I welcome this opportunity to acknowledge a true debt of gratitude to Dr. Senthilmurugan Thyagarajan for his tremendous support and assistant in completing this study. Not only did he freely share his thoughts and work and truthful inspiration, but he was also always there to recommend what really mattered in the research.

I would also like to thank Dr. Nadarajah Sivaneswaran of the FHWA for his kind support without their help the successful outcome of the research would not have been possible.

I acknowledge Dr. Gonzalo Rada of AMEC Inc. and Dr. Soheil Nazarian of University of Texas at El Paso for their leadership in FHWA study and encouragement.

My deep appreciation goes out to my best friends, Reihaneh and Esmaeel, for their friendship and the warmth they extended to my family. I always turned to them whenever I felt stressed out and they were always there to do anything to relieve my anxiety.

I have been very privileged to get to know and to collaborate with many other great people who became friends over the last three years. I sincerely appreciate their generosity, mercy and munificence. Special mention goes to Sami, Melody, Salman, Nasim, Mehdi and Farzaneh for a great time I had in Reno. You will always be my friends.

Finally, I would greatly like to show appreciation to my lovely wife Hanie. Her tolerance of my occasional naughty attitudes is a testimony of her adamant devotion and love. Hanie, you should know that your support, clemency and encouragement were worth more than I can express on paper.

Mahdi Nasimifar

December, 2015

Notice

This research was a part of FHWA study DTFH61-12-C-00031 and some of the texts are excerpts from the FHWA report entitled “Pavement Structural Evaluation at the Network Level”.

Rada, G., Nazarian, S., Visintine, B., Siddharthan, R.V., and Thyagarajan, S. *Pavement Structural Evaluation at the Network Level.* FHWA- DTFH61-12-C-00031, FHWA, U.S. Department of Transportation, 2015.

Contents

List of Figures

List of Tables

1. Introduction

1.1. Overview of the study and objectives

State highway agencies (SHAs) spend billions of dollars each year on various transportation infrastructure assets to meet legislative, agency and public expectations. Pavements are a major component of those transportation assets and pavement rehabilitation is one of the most critical, costly and complex element. This is especially true at present, since a large percentage of pavement networks are reaching the end of their serviceable life, and pavement rehabilitation has become even more daunting given the funding constraints faced by the SHAs.

At the heart of rehabilitation decisions is the Pavement Management System (PMS), which provides network level condition indices or scores for each pavement segment in the system. A few SHAs are beginning to consider structural adequacy as part of their routine PMS activities by incorporating deflection testing based pavement condition assessment especially at the network level. Such efforts can then be used as a critical input in prioritize of the rehabilitation projects so that the best use of the state resources is achieved.

At present, there is a large array of equipment that can be used to measure the deflection basin resulting from an applied load. The most commonly used device in United States since the 1980s has been the Falling Weight Deflectometer (FWD). FWDs rely on impact loads to produce a vertical pavement deflection response similar to that

produced by actual traffic loadings that is measured by deflection sensors located at varying distances from the load.

While FWD represents the state-of-the-practice, it is not without shortcomings. Since FWDs are a stop-and-go operation, lane closures are required, which cause traffic disruptions. A part from being a serious inconvenience, it is a safety hazard to personnel involved in the operation and the traveling public. Their frequency of testing is also significantly less than a continuous operation, which affects operational costs. These shortcomings are especially important in terms of network level pavement management applications, which by their nature require information on a large pavement network representing hundreds of miles.

To overcome the FWD shortcomings, several organizations in the USA and Europe have developed devices over the past several decades that can continuously measure pavement deflections at posted traffic speeds (80 – 96 kph). The modern versions of the moving deflection testing devices that are actively used today include:

- Greenwood Engineering A/S Traffic Speed Deflectometer (TSD).
- Applied Research Associates, Inc. (ARA) Rolling Wheel Deflectometer (RWD).
- Euroconsult, Curviametro (CRV)

The last device (CRV) operates at a lower speed (up to 18 kph), which is significantly slower than traffic speed devices.

Much work has been done over the past decade towards the advancement of the state-of-the-technology of moving pavement deflection testing. However, the burning

question is: are these devices ready for immediate implementation in the structural evaluation of pavements for network level PMS applications? If so, how should the measurements from one or more of these devices be used within the context of network level PMS?

The evaluation of accuracy and the precision of these devices are beyond of the scope of this research. The main objective of this research is to find a methodology for enabling the use of the devices in network level PMS application.

1.2. Description of Traffic Speed Deflection Devices (TSDDs)

As explained earlier, three devices were evaluated in this study. The description of these devices from manufacturers' perspectives is as follow:

1.2.1. Rolling Wheel Deflectometer (RWD)

The manufacturer of this device is applied research associates located in United States. Figure 1-1 shows a RWD truck. The RWD uses six spot lasers mounted on a horizontal aluminum beam to measure the deflected pavement surface (longitudinally along the mid-point between the dual tires). Two sensors (Sensor D located at 184 mm (7.25 inches) behind and Sensor F located at 197 mm (7.75 inches) in front of the axle in Figure 1-2) are within the deflection bowl, while the other four sensors represent locations within the undeflected pavement surface. The A, B, C and E sensor readings are used to obtain the load-induced surface deflection at the location of Sensors D and F.

Figure 1-1. *RWD truck*

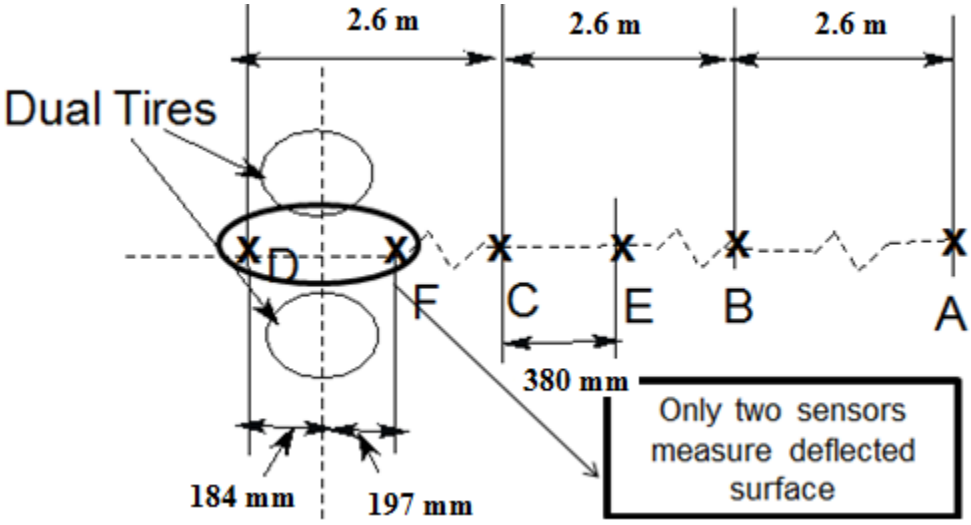

Figure 1-2. RWD sensor locations

1.2.2. Traffic Speed Deflectometer (TSD)

This device is developed by Greenwood engineering located in Denmark. Figure 1-3 shows a TSD truck. The TSD utilizes Doppler lasers to estimate the vertical surface deflection velocity of the road profile that is the velocity the pavement deflects due to the moving load. The Greenwood TSD provides deflection velocities at between three and nine points, with the model that evaluated in this study measuring six (at 100, 200, 300,

600, 900 and 1500 mm) as shown in Figure 1-4. A theoretical algorithm is used to compute the deflection basin that matches with the TSD measurements.

Figure 1-3. TSD Truck

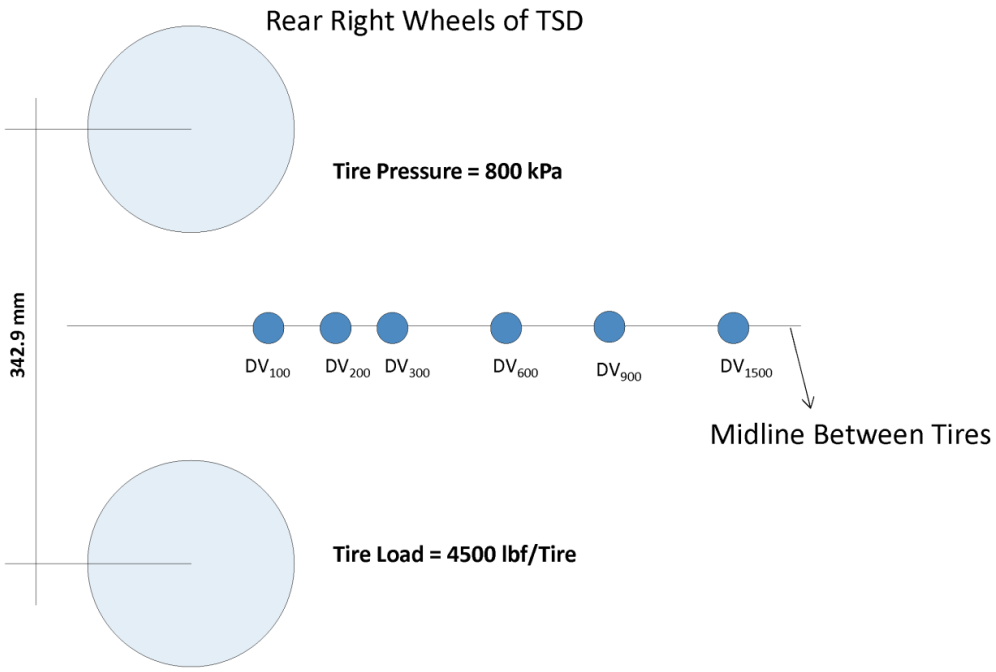

Figure 1-4. TSD rear axle configuration and location of Doppler sensors (DV= Deflection velocity)

1.2.3. Curviametro (CRV)

The curviametro has been developed by Euroconsult located in Spain. Figure 1-5 shows a Curviametro and the methodology used to measure surface deflections. The vehicle is equipped with three geophones on a chain, but only one collects the deflection bowl at a particular point at a time. The constant speed and opposing directions of travel of the Curviametro vehicle and chain allow the geophone measurements to represent deflections at a stationary location on the pavement surface.. The Curviametro geophone starts collecting data as soon as the rear axle is about 1 m (39 inches) away from the geophone's location and it stops collecting data once the rear axle has passed the geophone's location by approximately 3 m (118 inches). Therfore, it can measure the entire deflection bowl.

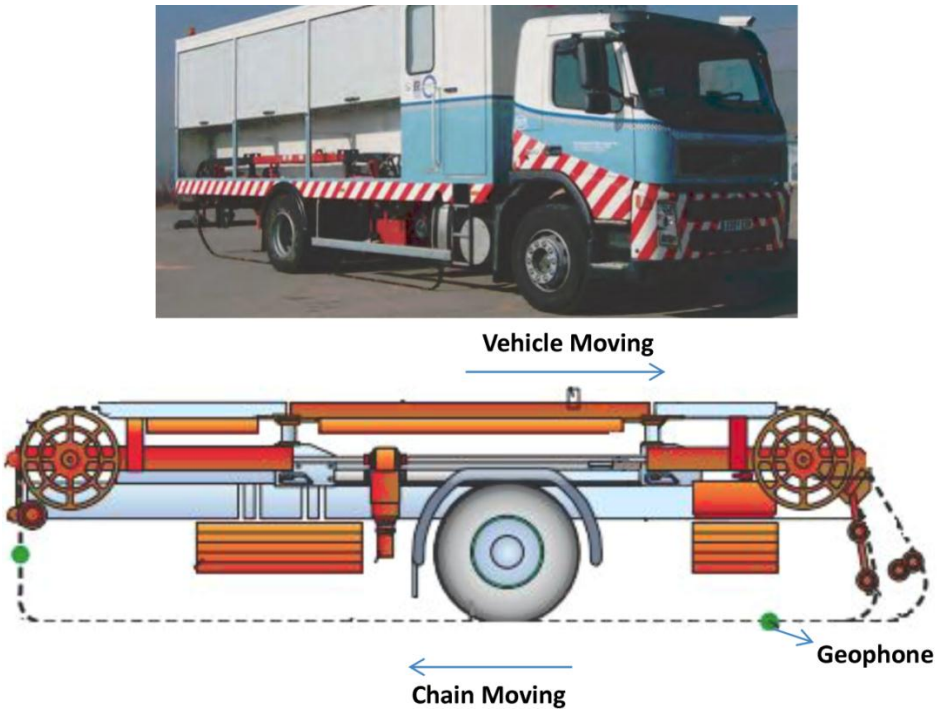

Figure 1-5. Curviametro device and schema during surface deflection measurements

1.2.4. Summary of device descriptions

Table 1-1 provides a summary of the devices presented in the previous sections that were considered viable to pursue evaluation under the study – the RWD, Greenwood TSD and Curviametro. This represents the initial information provided by the manufacturers and was the basis for the decision.

Table 1-1. Summary sheet: device comparison

Device / Parameter	RWD	TSD	CURVIAMETRO
Manufacturer	Applied Research Associates	Greenwood Engineering	Euroconsult
Measurement type	Deflection	Deflection Velocity	Deflection
Measurement location	behind and ahead the centerline of the load axle(two points)	ahead the centerline of the load axle (several points)	from 1m ahead of wheel to 3m behind of wheel in a particular point
Operation speed	30-96 (kph)	80 (kph)	18 (kph)
Sampling frequency	15 (mm)	20 (mm)	5000 (mm)
Deflection accuracy	63 (μm)	102 (μm/s)	20 (μm)
Applied load	40 (kN)	49 (kN)	67 (kN)
Complete deflection bowl	NO	NO/YES	YES

1.3. Description of the methodology used in the study

3D-Move program was used as analytical tool in this study. The analytical model (3D-Move) evaluates pavement response using a continuum-based finite-layer approach. The 3D-Move model can account for important pavement response factors such as the moving traffic-induced complex 3D contact stress distributions (normal and shear) of any shape, vehicle speed, and viscoelastic material characterization for the pavement layers. The finite-layer approach treats each pavement layer as a continuum and uses the Fourier transform technique; therefore, it can handle complex surface loadings such as multiple loads, non-uniform tire pavement contact stress distributions, and any shaped tire imprints, including those generated by wide-base tires. Since 3D-Move has the capability of modeling moving loads and the resulting dynamic pavement responses, it is ideally-suited to evaluate and compare pavement responses measured using load-response devices that move at high-speeds (e.g., TSD and RWD devices). 3D-Move program formulation will be explained later in this chapter.

FHWA study (DTFH61-12-C-00031) conducted field trials that used TSDDs where in-situ pavement response measurements were made and calibration of 3D-Move model for application with TSDD loading was carried out.

The MnROAD facility near Maplewood, Minnesota was selected as the primary site for the field trials since it provided a multitude of test sections in one location as well as a wealth of readily available information, including pavement structure, pavement condition, and environmental and TSDD load response data. In addition to the existing MnROAD sensors (strain gauges, pressure cells, etc.), four geophones and one

accelerometer were installed near the pavement surface to measure deflections at three cells called accuracy cells.

The methodology used in this study can be summarized as two following steps:

1. The 3D-Move model was calibrated as an initial undertaking before use in the development of a methodology for incorporating TSDD measurements into network-level PMS applications. Many calibration runs were performed and the results were compared with measured deflection time histories (peak and basin) from the project geophones and strain measurements taken by MnROAD strain gauges at various locations within the pavement. Since load-induced strains are critical inputs to performance predictions, this effort was critical relative to the applicability of the 3D-Move model. Field calibration brings together many other important issues that include pavement layer and material characterization, which are essential components of the pavement response estimation.

2. Using the calibrated 3D-Move software, an analytical investigation was then undertaken to explore relationships between load-induced pavement structural-related response and the corresponding surface deflection basin related indices. A key element was the simulation of pavement deflections using the 3D-Move model with a focus on understanding the parameters that affect the TSDD measurements that included vehicle speed and loadings, and pavement layer properties.

1.4. Description of TSDD field trials

MnROAD facility in Minnesota was selected as the primary site since it provided a multitude of test sections in one location. The MnROAD facility consists of a 5.6 km (3.5-mile) mainline roadway (Figure 1-6) comprised of 45 sections with "live traffic" as part of Interstate 94 near Albertville, Minnesota. In addition, a 4 km (2.5-mile) closed-loop low volume roadway (Figure 1-7) containing 28 sections is also available. The section lengths are typically about 150 m (500 ft).

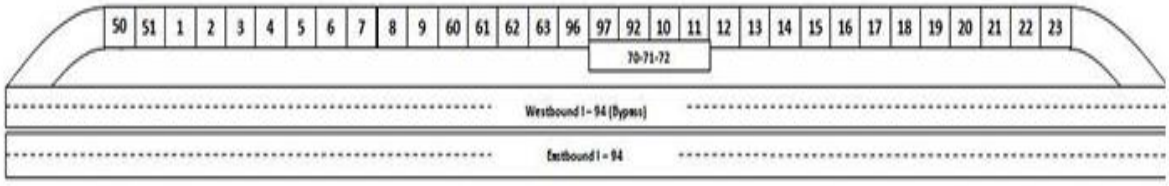

Figure 1-6. MnROAD Mainline test cell map

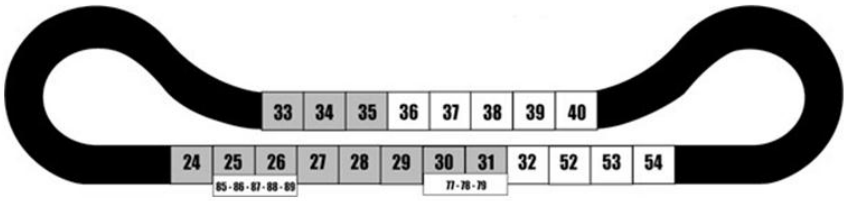

Figure 1-7. MnROAD Low Volume Road test cell map

The MnROAD sections are instrumented with different types of sensors, such as linear variable differential transformers (LVDT), strain gauges, pressure cells, moisture gauges, thermocouples and tipping buckets. Distress surveys, rutting measurements, laser profiler measurements and FWD data are collected regularly on the sections. In addition to existing sensors, four geophones and one accelerometer were installed as

embedded sensors to measure deflection velocity and displacement parameters at four MnROAD cells. Three flexible pavement section were selected. The pavement cross sections for the these cells are included in Figure 1-8. The three flexible pavement sections covered three levels of stiffness (Cell 34 soft, Cell 19 intermediate and Cell 3 stiff as judged by FWD testing and pavement structure). Geophones were primarily used since they are the least expensive, can be easily ruggedized in a steel casing, and their one-to-one correspondence to the deflection parameters measured by the TSD. In addition, one accelerometer was used at each site to verify the responses of the retrofitted geophones. The geophones had nominal resonant frequencies of 4.5-Hz and a measuring range of 160 mils (4 mm). The accelerometers were micro-electro-mechanical system (MEMS) DC accelerometer with a nominal sensitivity of 1000 mV/g.

Geophones and accelerometers were embedded in the right wheel path of each selected MnROAD cell, as shown in Figure 1-9. Two of the geophones (marked as 1 and 3) were installed along the center of the wheelpath, while the other two had 150 mm (6 inches) offset to either side of the wheel path center. The purpose for this offset was to increase the probability of having the test vehicle sensor pass directly on top of one of the sensors while data from the test vehicle and embedded sensors were being collected. The accelerometer was packaged with Geophone 3.

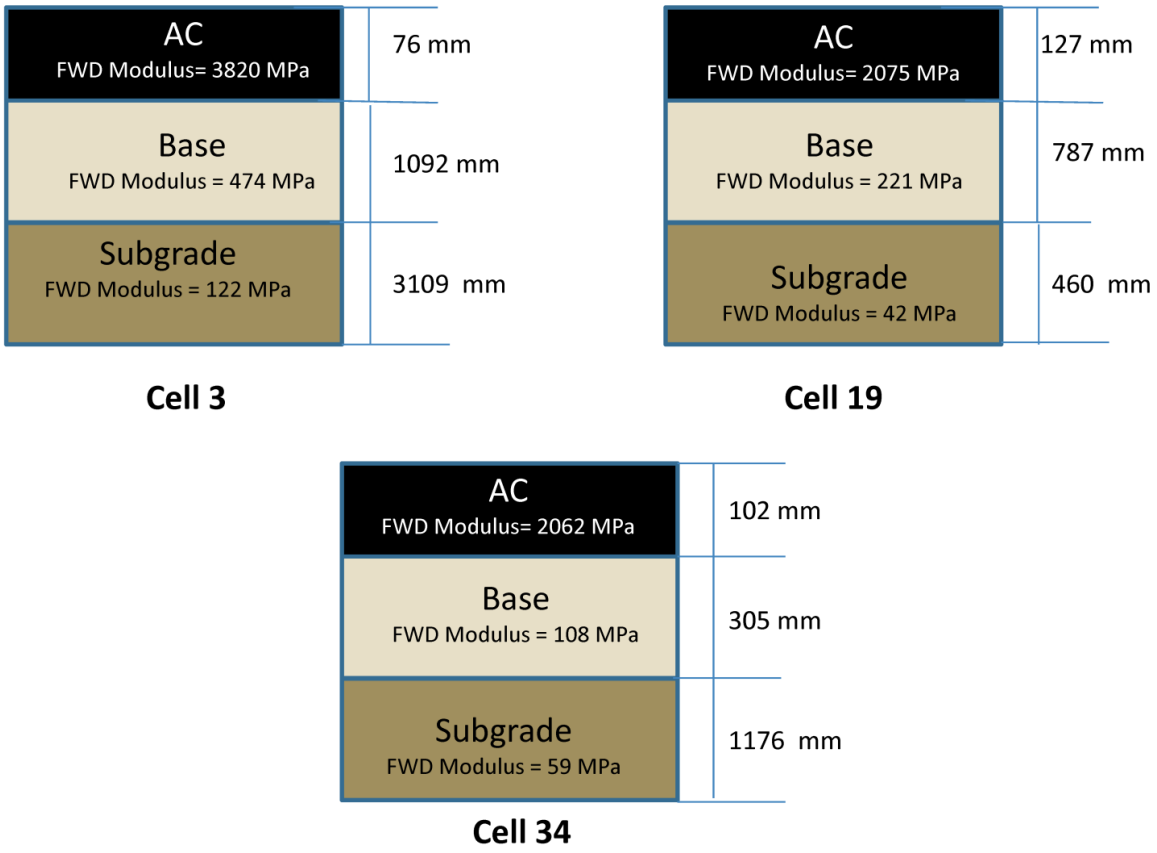

Figure 1-8. Sketch of pavement structures for Cells 3, 19, and 34

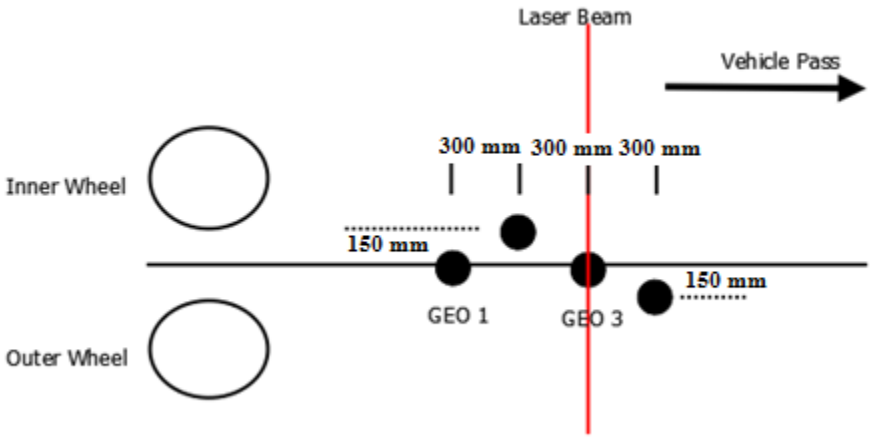

Figure 1-9. Configuration of embedded project sensors and spacing

The performance of each sensor was then verified using an FWD. For that purpose, one of the FWD sensors was placed directly on top of one of the embedded sensors. The deflections reported by the FWD were then compared with the corresponding deflections reported by the embedded geophones and accelerometers. The deflections from the two systems were quite similar. The typical accuracy of the geophones similar to those used in the FWD and installed at MnROAD is reported by the manufacturer as 2% of the measured deflection (no less than ±0.2 mils, 5 μm). Based on the reported statistics in the figure, on average the FWD and installed sensors' deflections are within about 10 μm (0.4 mils) of one another, which confirms the adequacy of the installed system given the uncertainty associated with measurements with short impulse tests (i.e., FWD).

1.5. Organization of Dissertation

This dissertation has been prepared based on four journal papers. Each paper covers a portion of study as explained in the section 1.3. The papers were converted to the same style of the other parts of the dissertation. This was possible because the author has access to the original format of each paper. For more information and to get the electronic print link, contact the corresponding author at Nasimifar@gmail.com.

The title, a short summary and publication status of each paper (at the time of dissertation submission) are described below:

Title: Dynamic analyses of traffic speed deflection devices

Short summary: This paper described the important steps used in the calibration and validation of the 3D-Move program using field data at the MnROAD facility. Several analyses were undertaken in an attempt to bracket the measured surface deflection data (peak and basin shape). In the process, due consideration was given to the selection of the inputs (material properties and loading) so that they are rationally arrived at and the adjustments are defensible. It was shown that 3D-Move computed results bracket the measured time histories from embedded geophones well. The focus of this paper was 3D-Move calibration based on TSD and RWD field trials.

Publication status: Published online in the International Journal of Pavement Engineering.

Citation: Nasimifar, M., Siddharthan, R., Rada, G., Nazarian, S., (2015). "Dynamic analyses of traffic speed deflection devices." *International Journal of Pavement Engineering*, http://dx.doi.org/10.1080/ 10298436.2015.1088152.

Title: Validation of dynamic simulation of slow moving surface deflection measurements

Short summary: In this paper, the capability of 3D-Move to evaluate slow moving surface deflection measurements was assessed using measured values from embedded sensors at the MnROAD facility during Curviametro trials. The results of this paper confirm that 3D-Move based dynamic analyses can simulate slow moving deflection measurements properly and can be used to identify surface deflection indices that correlate well with critical pavement responses.

Publication status: Accepted for presentation at the TRB Annual Meeting and is being considered for publication in the Journal of the Transportation Research Board.

Citation: Nasimifar, M., Siddharthan, Rada, G., Nazarian, S., "Validation of dynamic simulation of slow moving surface deflection measurements." *Transportation Research Record: Journal of the Transportation Research Board, Accepted for presentation at the TRB Annual Meeting and publication in the Journal of the Transportation Research Board.*

Title: Robust deflection indices from traffic speed deflectometer measurements to predict critical pavement responses for network level PMS application

Short summary: The outcomes of this paper provide an appropriate approach to enable the use of TSD in network level PMS application. The robust indices that can be readily computed from TSD measurements and best related to the pavement critical responses were identified. Then, a comprehensive sensitivity analysis on deflection basin indices and their correlations with fatigue and rutting strains were performed using a range of pavement structures.

Publication status: Accepted for publication in the Journal of Transportation Engineering, ASCE.

Citation: Nasimifar, M., Thyagarajan, S., Siddharthan, R., and Sivaneswaran, S., (2015). "Robust deflection indices from traffic speed deflectometer measurements to predict critical pavement responses for network level PMS application." *Journal of Transportation Engineering, ASCE. 10.1061/(ASCE)TE.1943-5436.0000832.*

Title: Field and numerical evaluation of traffic speed deflection measurements to estimate load-induced fatigue response

Short summary: In this paper the capability of TSDDs in prediction of fatigue strain was confirmed. Also, the location of sensors in the RWD and the TSD were evaluated and practical recommendations were made to improve the ability of TSDDs to collect more accurate measurements.

Publication status: Under review for possible publication in the Journal of testing and evaluation, ASTM.

Citation: Nasimifar, M., Siddharthan, R., Thyagarajan, S., "Field and numerical evaluation of traffic speed deflection measurements to estimate load-induced fatigue response." *Journal of testing and evaluation, ASTM* (under review).

2. 3D-Move program

As explained earlier, 3D-Move program was used as analytical model to simulate TSDD trials and develop a methodology to use the TSDD measurements in network level PMS application. This section includes a review of past literature and a brief description of the 3D-Move formulation.

2.1. Review of the literature

Many pavement engineers and researchers have argued that pavement design procedures developed on the basis of road tests are only applicable to loading conditions (i.e., tire pressures and tire types), pavement materials, and environmental conditions that were similar to those present at the locations of the road tests. On the other hand, mechanistic procedures enable pavement engineers to undertake design at a site that has different conditions (loading, materials and environment) than those of the road test sites.

Mechanistic procedures to calculate pavement responses have been evolving since 1960s to account for the changes in: characteristics of vehicle loading, pavement materials, and method of pavement construction. An important task in developing a successful mechanistic procedure is how realistically it can model the actual stress distributions at the tire-pavement interface and pavement material behavior. Most of the current mechanistic procedures used to compute pavement responses are much simpler; the stress distributions at the tire-pavement interface are modeled as static, uniform and stationary circular loads. For example, ELSYM5, WESLEA, BISAR, CIRCLY, KENLAYER, ILLIPAVE, MICHPAVE etc. are such programs. Among the above programs, some use linear layered elastic formulation, while others (e.g., ILLIPAVE and

MICHPAVE) use stress-dependent material properties and adopt the finite element approach. Researchers found that the stress distribution at the tire-pavement interface is complex and it entails: (a) noncircular loaded area, (b) non-uniform normal stresses, and (c) substantial transverse and longitudinal shear stress components *(1, 2)*. In addition, due to the moving or dynamic nature of the vehicle, the tire load that varies with time as the vehicle traverse a pavement will yield a more complex contact stress distribution. It has been shown from past research studies that characteristics of the stress distributions at the tire-pavement interface resulting from a moving load are strongly governed by three important factors: (a) road roughness; (b) vehicle speed; and (c) truck suspension system *(3, 4)*. Due to the complexities of the actual loading, influence of the dynamic nature of the tire loading is seldom considered in the mechanistic analyses.

The moving nature of the load is routinely overlooked in the conventional pavement analysis in which the loads are considered as static and stationary. It has been clearly shown from pavement responses measured in the field that the pavement strain responses are affected by the speed of the vehicle *(5)*. In general, there are two important factors that should be considered in any dynamic pavement analysis: moving nature of the load and the dependency of the material properties on the loading frequency (or vehicle speed).

Some researchers have considered the stress and frequency-dependent material properties in the pavement analysis procedure. For example, KENLAYER computer program, developed based on Burimister's layered theory, solves for an elastic multilayered system under stationary single or multiple circular loaded areas with

uniform normal contact pressure *(6)*. The asphalt layer can be treated as linear elastic or viscoelastic. The unbound layers such as base and subgrade can be divided into several sub-layers. The stress dependent moduli for the unbound layers are estimated through an iterative procedure. The moduli vary in the vertical direction but remain constant along the horizontal plane for each sub-layer. On the other hand, stationary static circular non-uniform surface stress distributions that include normal and shear (longitudinal and transverse) components can be considered in an approximate manner in CIRCLY. When axisymmetric finite element approaches are used (e.g., ILLI-PAVE and MICHPAVE) the stress-dependent material behavior can be readily incorporated.

In order to compute the dynamic response of a viscoelastic layered system subjected to stationary disk loads, Monismith and his coworkers developed a computer program called SAPSI *(7)*. The pavement structure in SAPSI consists of thin sub-layers assumed infinite in the horizontal direction. The SAPSI computes the viscoelastic pavement responses in the frequency domain. A similar approach was developed by Papagiannakis et al. where multiple loadings can be analyzed, and each loading can have a different loaded area and time history *(8)*. In these methods the load-time history on the stationary loaded areas varies as a function of the velocity of the moving vehicle. These methods fail to model the actual pavement-vehicle interaction due to the following limitations: (a) since the loaded areas are stationary, they do not account for true nature of the moving load; (b) the noncircular pressure pattern cannot be employed (e.g., wide-base tires) in the analysis as the axisymmetric formulation is used in these methods; (c) the non-uniform stress distributions at the tire-pavement interface can be considered only if

they conform to the axisymmetric condition; and (d) it is required to specify a time history of loading on the stationary circular plate that depends on vehicle velocity.

Three-dimensional finite element based models have also been proposed for pavement analysis *(9, 10)*. Limitations associated with such methods are well-known, and they include substantial computational effort and the errors resulting from the need to incorporate artificial lateral boundaries. Hardy and Cebon used the well-known convolution integral to study the pavement response to a moving load *(11)*.

The 3D-Move model considers the vehicle loading as moving with all components of contact stress distributions (normal and shear) of any shape and it is time invariant. It takes advantage of the horizontally-layered nature of the pavement structure in the formulation which makes it significantly more computer efficient than the three-dimensional finite element based models.

2.2. 3D-Move formulation

The 3D-Move model is based on finite-layer approach that uses the Fourier transform technique to evaluate the responses of layered medium subjected to a moving load traveling along x-axis at a constant speed. It is based on the work presented by Siddharthan and his co-workers *(3, 4, 12)*. The material properties for the asphalt concrete layer can be either linear elastic or viscoelastic, while material properties for the unbound layers are linear elastic. Material properties of a layer are assumed to be uniform and constant within the layer. The surface load components (normal and shear) are distributed over a loaded area of any shape that is time invariant.

3D-Move uses Fourier series expansion to decompose the loads into harmonic components in space (x and y directions) and total response at a given location is then calculated by adding the individual responses from each harmonic component. It can handle any number of layers with the complex loading at the surface and any number of response evaluation points. However, higher number of layers and response evaluation points leads to larger computational effort. The 3D-Move model is ideally suited for pavement response evaluations since only a few critical responses are needed for pavement performance evaluations. For example, maximum horizontal tensile strain at the bottom of AC layer and maximum vertical compressive strains within the layers are typically used to investigate fatigue and rutting failures of flexible pavements. Under such circumstances, 3D-Move performs much more computationally efficient than the moving load models based on the finite element method.

The following assumptions are used in the development of the model:

1. The domain is composed of horizontal layers of uniform thickness, which can be of different materials;
2. Each layer can be either linear elastic or linear viscoelastic with a set of uniform material properties (e.g., elastic modulus, Poisson's ratio, unit weight), which are time and space invariants;
3. Layers are modeled as single-phase;
4. Layers are finite, horizontally layered and rest on a rigid bottom layer;
5. The surface loads are assumed to move with constant speed (i.e., no acceleration) along the x-axis.

2.2.1. Load Idealization

The approach is based on Fourier series expansion of the applied load. Therefore, the applied load is modeled as a two-dimensional periodic function in x- and y-directions, as shown in Figure 2-1.

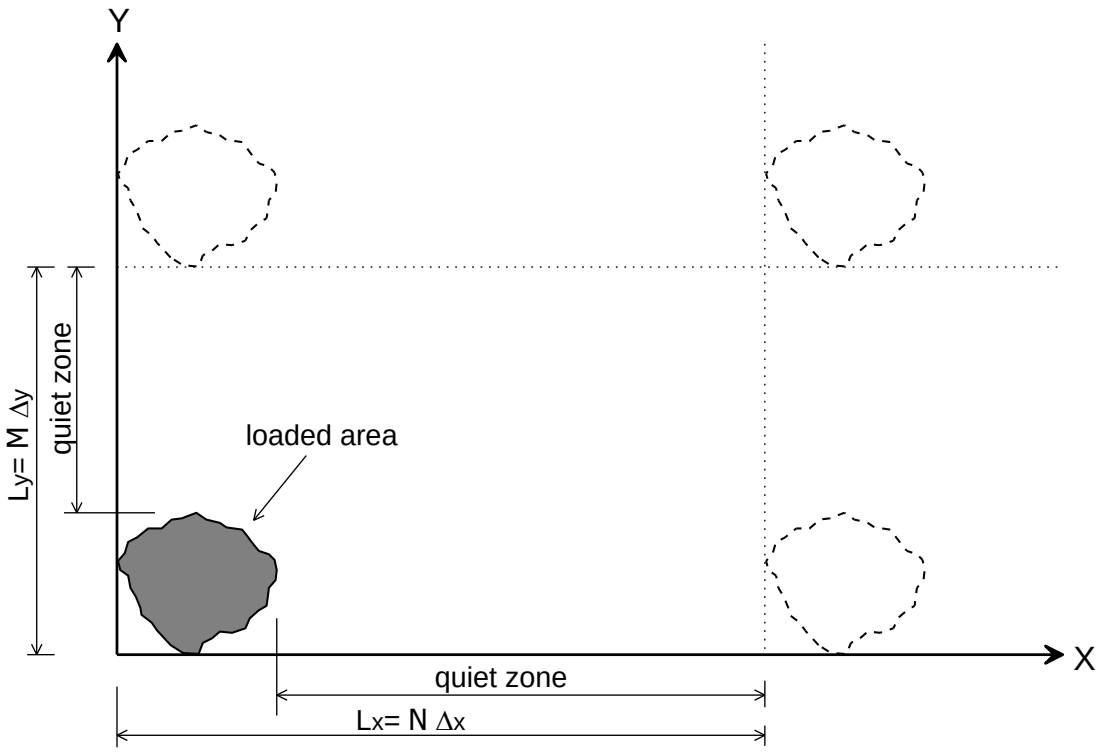

Figure 2-1. Idealization of surface loads as a two-dimensional periodic function

The wavelength is selected with sufficiently large "quiet zone" at the end of the applied load to allow time for the damping of the system to attenuate the response from one cycle before the beginning of the next cycle (i.e., no interference between the consecutive cycles). The surface (z = 0) vertical contact pressure, $q_{zz}(x, y, 0)$, can be written using partial sum of the N×M harmonics Fourier series as:

$$q_{zz}(x, y, 0) = Re\left(\sum_{n=1}^{N}\sum_{m=1}^{M} A_{mn} e^{i\alpha_n x} e^{i\beta_m y}\right) \quad (2\text{-}1)$$

where, A_{mn} are Fourier coefficients, which are calculated using Discrete Fourier Transform (DFT) of the sampled normal contact stress distribution. Parameters α_n and β_m are wave numbers given by:

$$\alpha_n = \frac{2\pi(n-1)}{N\Delta x} \quad and \quad \beta_m = \frac{2\pi(m-1)}{M\Delta y} \tag{2-2}$$

where, Δx and Δy are the sampling intervals of the normal contact stress distribution in the x and y directions, respectively.

For a moving load traveling with velocity (c) along the x-direction, Equation (2-1) can be written as:

$$q_{zz}(x, y, 0, t) = Re\left(\sum_{n=1}^{N}\sum_{m=1}^{M} A_{mn} e^{i\alpha_n(x-ct)} e^{i\beta_m y}\right) \tag{2-3}$$

Contact surface shear stress distributions of q_{xz} and q_{yz} can also be written in a similar manner.

2.2.2. Governing Equation

The equations of motion for a single-phase body are given by (Fung 1977):

$$\frac{\partial \sigma_{xx}}{\partial x} + \frac{\partial \tau_{xy}}{\partial y} + \frac{\partial \tau_{xz}}{\partial z} = -\rho \frac{\partial^2 u}{\partial t^2}$$

$$\frac{\partial \tau_{xy}}{\partial x} + \frac{\partial \sigma_{yy}}{\partial y} + \frac{\partial \tau_{yz}}{\partial z} = -\rho \frac{\partial^2 v}{\partial t^2} \tag{2-4}$$

$$\frac{\partial \tau_{xz}}{\partial x} + \frac{\partial \tau_{yz}}{\partial y} + \frac{\partial \sigma_{zz}}{\partial z} = -\rho \frac{\partial^2 w}{\partial t^2}$$

where, σ_{xx}, σ_{yy} and σ_{zz} are the normal stresses, τ_{xy}, τ_{xz} and τ_{yz} are the shear stresses, u, v and w are the displacements along the x, y and z directions, respectively, and ρ is the mass density.

The stress-displacement relationships for Hookean elastic solid are given by *(13)*:

$$\sigma_{xx} = -\left[\lambda\left(\frac{\partial u}{\partial x}+\frac{\partial v}{\partial y}+\frac{\partial w}{\partial z}\right)+2G\frac{\partial u}{\partial x}\right]$$

$$\sigma_{yy} = -\left[\lambda\left(\frac{\partial u}{\partial x}+\frac{\partial v}{\partial y}+\frac{\partial w}{\partial z}\right)+2G\frac{\partial v}{\partial y}\right]$$

$$\sigma_{zz} = -\left[\lambda\left(\frac{\partial u}{\partial x}+\frac{\partial v}{\partial y}+\frac{\partial w}{\partial z}\right)+2G\frac{\partial w}{\partial z}\right] \quad \text{(2-5)}$$

$$\tau_{xy} = -\left[G\left(\frac{\partial u}{\partial y}+\frac{\partial v}{\partial x}\right)\right]$$

$$\tau_{xz} = -\left[G\left(\frac{\partial u}{\partial z}+\frac{\partial w}{\partial x}\right)\right]$$

$$\tau_{yz} = -\left[G\left(\frac{\partial v}{\partial z}+\frac{\partial w}{\partial y}\right)\right]$$

$$\lambda = \frac{2G\nu}{1-2\upsilon}$$

where, λ is Lamé's constant, G is the shear modulus, and ν is the Poisson's ratio. Negative sign is used in these equations because compressive stresses and strains are considered positive, which is the conventional sign convention for geo-materials. It should be noted that λ and G are complex in the case of linear viscoelastic materials.

2.2.3. Solution for a Single Harmonic and Single Layer

It is known that the response (output) of a time-invariant linear system to a periodic input is also periodic *(14)*. Therefore, the displacements induced at a point within a horizontally layered system by any single harmonic (wave n,m) of the surface load (z = 0) described by Equation (2-3) can be written as shown in Equation (2-6):

$$u_{nm}(x,y,z,t) = U_{nm}(z)e^{i\alpha_n x}e^{i\beta_m y}e^{-i\alpha_n ct}$$

$$v_{nm}(x,y,z,t) = V_{nm}(z)e^{i\alpha_n x}e^{i\beta_m y}e^{-i\alpha_n ct} \quad (2\text{-}6)$$

$$w_{nm}(x,y,z,t) = W_{nm}(z)e^{i\alpha_n x}e^{i\beta_m y}e^{-i\alpha_n ct}$$

By substituting for u_{nm}, v_{nm} and w_{nm} in Equation (2-4), the partial differential equations can be converted into a set of ordinary differential equations *(4)*. Equation (2-7) lists the characteristic roots of the equation (r_1, $-r_1$, r_2 and $-r_2$):

$$r_1 = \sqrt{\alpha_n^2 + \beta_m^2 - \left(\frac{\omega_n}{c_1}\right)^2}$$

$$r_2 = \sqrt{\alpha_n^2 + \beta_m^2 - \left(\frac{\omega_n}{c_2}\right)^2} \quad (2\text{-}7)$$

where, $\omega_n = \alpha_n c$, $c_1 = \sqrt{\frac{2G+\lambda}{\rho}}$ And $c_2 = \sqrt{\frac{G}{\rho}}$

The resulting solutions of the ordinary differential equations are shown in Equation (2-8):

$$U_{nm}(z) = u_1 e^{r_1 z} + u_2 e^{-r_1 z} + u_3 e^{r_2 z} + u_4 e^{-r_2 z}$$

$$V_{nm}(z) = v_1 e^{r_1 z} + v_2 e^{-r_1 z} + v_3 e^{r_2 z} + v_4 e^{-r_2 z} \quad (2\text{-}8)$$

$$W_{nm}(z) = w_1 e^{r_1 z} + w_2 e^{-r_1 z} + w_3 e^{r_2 z} + w_4 e^{-r_2 z}$$

where, u_i, v_i and w_i are constants. By substituting the equations of (2-5), (2-6) and (2-8) into the Equation (2-4), it was found that only six constants are independent *(4)*. For each independent layer shown in Figure 2-2, the coefficients are in fact u_1, u_2, u_3, u_4, v_3 and v_4, while others are dependent on these independent coefficients.

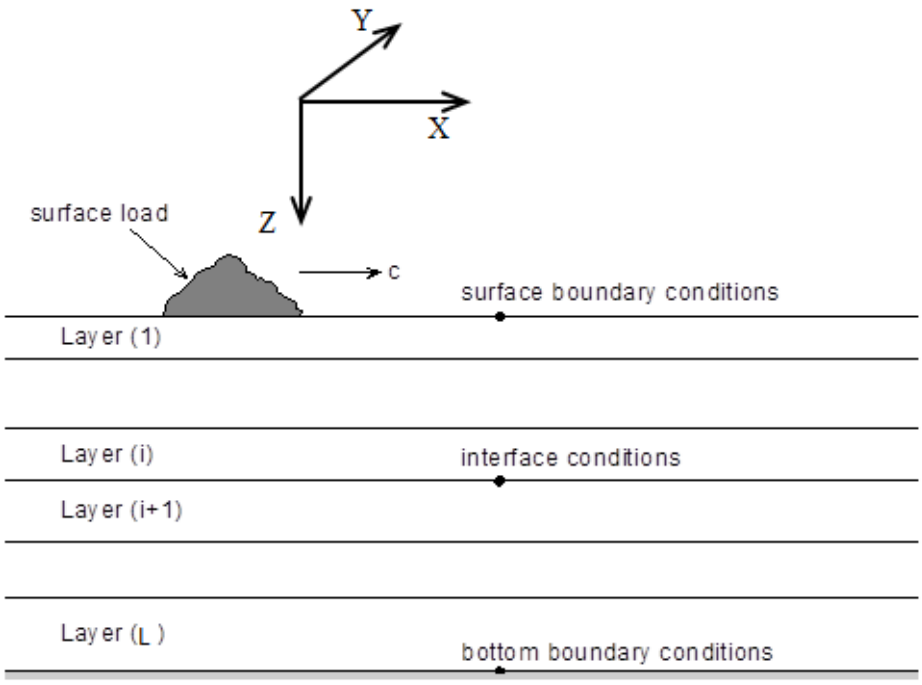

Figure 2-2. Layout and boundary conditions of layered system (L = Number of layers)

2.2.4. Solution Scheme for Layered System

It has been seen from the previous section that each layer has 6 unknowns (layer coefficients). For the layered system consisting of L layers shown in Figure 2-2, there are 6xL unknowns for each harmonic load. Therefore, 6xL equations are needed to solve the problem. These equations can be obtained from the boundary (top and bottom) and interface conditions, which are defined as follows:

(a) Equation (2-9) represents at the surface (z =0) of the layered system (3 equations):

$$\sigma_{zz} = q_{zz},\ \tau_{xz} = q_{xz} \text{ and } \tau_{yz} = q_{yz} \tag{2-9}$$

where, q_{zz}, q_{xz} and q_{yz} are the surface contact stress components.

(b) Equation (2-10) represents at the bottom of the layered system (3 equations), where a rigid bottom layer is assumed:

$$u = v = w = 0 \tag{2-10}$$

(c) Equation (2-11) represents at the interface [(L -1) x 6 equations],

$$u^+ = u^-, v^+ = v^- \text{ and } w^+ = w^-$$

$$\sigma_{zz}^+ = \sigma_{zz}^-, \tau_{xz}^+ = \tau_{xz}^- \text{ and } \tau_{yz}^+ = \tau_{yz}^- \tag{2-11}$$

in which, + and – indicate a location just above and below the interface.

These boundary and interface conditions are to be satisfied for each harmonic load, and then the complete solution is obtained by summing the responses from all harmonics.

2.2.5. Material Characterization

The dynamic modulus, |E*|, is the primary material property of AC mixes that are used in structural pavement design and analysis. Several studies have been undertaken to characterize the |E*| property of AC mixes. These studies have clearly demonstrated the importance of frequency-dependent material properties for AC relative to the estimation of stresses and strains in a pavement structure *(4, 15, 16)*.

The pavement responses given in Equation (2-6) reveal that the angular frequency, ω_n, associated with individual waves can be described by Equation (2-12).

$$\omega_n = \alpha_n c = 2\pi f_n \quad (2\text{-}12)$$

where, f_n is the frequency. From |E*| vs. frequency relationship, the |E*| at a given frequency, f_n, is evaluated for individual waves using interpolation. Unlike the dynamic and shear moduli, the Poisson's ratio decreases with frequency.

Two fundamentally different damping phenomena are associated with pavements: material (or internal) damping and radiation damping. Material damping is due to internal energy dissipation, while radiation damping is a measure of the energy loss associated with the radiation of waves away from the region of interest. For engineering applications, the internal damping of the pavement materials can be included in the analysis by writing the modulus in its complex form as shown in Equation (2-13) *(17)*:

$$E^* = E(1 + 2i\zeta_{AC}) = E_1 + iE_2 \quad (2\text{-}13)$$

where, E* = complex dynamic elastic modulus;

ζ_{AC} = a measure of material damping of the AC; and

E_1 and E_2 = real and imaginary components of E^*

Dynamic modulus, |E*| is related to E_1 and E_2 as shown in Equation (2-14).

$$|E^*| = \sqrt{{E_1}^2 + {E_2}^2} \quad (2\text{-}14)$$

For viscoelastic layers, the shear modulus G that appears in Equation (2-5) should be specified in its complex form as shown in Equation (2-15).

$$G^* = G_1 + iG_2 = \frac{E_1 + iE_2}{2(1+\nu)} \quad (2\text{-}15)$$

where, G_1 and G_2 are real and imaginary shear modulus components.

From Equations (2-13) and Equations (2-14), the relationship in Equation (2-16) may be deduced:

$$E_1 = \frac{|E^*|}{\sqrt{1+4\zeta_{AC}^2}}, E_2 = 2E_1\zeta_C \quad (2\text{-}16)$$

Material damping is included when complex modulus formulation is used. On the other hand, radiation damping is automatically accounted for since the proposed finite-layer model treats the pavement layers as infinite.

The *3D-Move* model treats the properties of unbound layers such as base and subgrade are treated as linear elastic. The internal damping for the base and subgrade layers can be included in the analysis in the same fashion as for the AC layer, by writing the elastic modulus of unbound layers, E_s^* , in its complex form shown in Equation (2-17).

$$E_s^* = E_s(1 + 2i\zeta_s) \quad (2\text{-}17)$$

where, E_s and ζ_s are real part of complex elastic modulus and damping ratio of unbound layers, respectively.

The properties of stress sensitive unbound materials may be treated as a number of linear elastic sublayers with constant modulus (without variation in lateral direction). The elastic modulus of the sublayers can be obtained based on the stresses induced by the surface loading. This a simplified approach to model the complex stress-dependent behavior of unbound materials.

The above formulation along with the material characterizations have been incorporated into the computer software "3D-Move" and it is available for free download at: http://www.arc.unr.edu/Software.html.

2.3. References

1. De Beer, M., and Fisher, C. Contact Stresses of Pneumatic Tires Measured with the Vehicle-Road Surface Pressure Transducer Array (VRSPTA) System for the University of California at Berkeley (UCB) and the Nevada Automotive Test Center(NATC). CSIR Report CR-97/053, Council for Scientific and Industrial Research, Pretoria, South Africa, 1997.
2. Sime, M., and Ashore, S.C. Tire Pavement Interface Pressure Patterns. Final Report DTFH61-96-C-00053, Federal Highway Administration, Washington, D.C., 1999.

3. Zafir, Z., Siddharthan, R. V., and Sebaaly, P. E. “Dynamic Pavement Strains from Moving Traffic Loads,” Journal of Transportation Engineering, ASCE, Vol. 120(5), 1994, pp. 821-842.

4. Siddharthan, R.V., Yao, J., and Sebaaly, P.E., “Pavement Strain from Moving Dynamic 3-D Load Distribution,” Journal of Transportation Engrg., ASCE, Vol. 124(6), Nov./Dec. 1998, pp. 557-566.

5. Sebaaly, P. E., and Tabatabaee, N. “Influence of Vehicle Speed on Dynamic Loads and Pavement Response,” Transp. Res. Rec. 1410, Transportation Research Board (TRB), Washington, D.C., 1993, pp. 107-114.

6. Huang, Y. H. “Pavement Analysis and Design,” Prentice-Hall, Inc., Englewood Cliffs, N.J. 1993.

7. Sousa, J. B., Lysmer, J., Chen, S. S., and Monismith, C. L. “Effects of Dynamic Loads on Performance of Asphalt Concrete Pavements,” Transp. Res. Record 1207, Transportation Research Board (TRB), Washington, D.C., 1988, pp. 145 – 168.

8. Papagiannakis. A. T., Amoah, N., and Taha, R. “Formulation for Viscoelastic Response of Pavement under Moving Dynamic Loads,” Journal of Transportation Engineering, ASCE, Vol. 122(2), 1996, pp. 140-145.

9. Huhtala, M. and Pihlajamaki, K. “New Concepts on Load Equivalency Measurements,” Proc. 7th Int. Conf. Asphalt Pavements, Nottingham, U.K., 1992, pp. 194-208.

10. Sousa. J. B., Weissman, S. L., Sackman, J. L., and Monismith, C. L. "Nonlinear Elastic Viscous with Damage Model to Predict Permanent Deformation of Asphalt Concrete Mixes," Transp. Res. Rec. 1384, Transportation Research Board (TRB), Washington, D.C., 1993, pp. 80-93.

11. Hardy, M. S. A., and Cebon, D. "Response of Continuous Pavements to Moving Dynamic Loads," J. Engrg. Mech., ASCE, Vol. 119(9), 1993, pp. 1762-1780.

12. Magdy, El-Desouky, "Further Developments of 3DMOVE and its Engineering Applications". PhD Dissertation, University of Nevada, Reno, 2003.

13. Fung, Y. C. "A First Course in Continuum Mechanics," Prentice-Hall, Inc., Englewood Cliffs, NJ, 2nd ed., 1997.

14. Papoulis, A. "The Fourier Integral and its Applications," McGraw-Hill Book Company, Inc., 1962.

15. Monismith, C.L., "Analytical Based Asphalt Pavement Design and Rehabilitation: Theory to Practice, 1962 – 1992" Transp. Res. Rec. 1354, Transportation Research Board (TRB), Washington, D.C., 1992, pp. 5 - 26.

16. Siddharthan, R.V., Krishnamenon, N., El-Mously, M., and Sebaaly, P.E., "Investigation of Tire Contact Stress Distributions on Pavement Response," Journal of Transportation Engineering, ASCE, Vol. 128(2), March/April, 2002, pp. 136-144.

17. Rosset, J. M. "Stiffness and Damping Coefficients of Foundations," Proc., ASCE Nat. Convention on Dynamic Response of Pile Foundations: Analytical Aspects, M. W. O'Neal and K. Dobry, eds., ASCE, New York, 1980, pp. 1-30.

3. Dynamic Analyses of Traffic Speed Deflection Devices

By
Mahdi Nasimifar (Corresponding Author)
Graduate Research Assistant
Department of Civil & Environmental Engineering
University of Nevada Reno
1664 N. Virginia St./ MS258
Reno, Nevada, 89557
Phone: (775) 682-7464
Fax: (775) 784-1390
E-mail: nasimifar@gmail.com

Raj V. Siddharthan
Professor
Department of Civil & Environmental Engineering
University of Nevada Reno
1664 N. Virginia St./ MS258
Reno, Nevada, 89557
Phone: (775) 784-1411
Fax: (775) 784-1390
E-mail: siddhart@unr.edu

Gonzalo R. Rada
Senior Principal Engineer
AMEC Foster Wheeler Environment & Infrastructure, Inc.
12000 Indian Creek Court, Suite F
Beltsville, Maryland, USA
Phone: (301) 210-5105
Fax: (301) 210-5032
E-mail: gonzalo.rada@amecfw.com

Soheil Nazarian
Professor
The University of Texas at El Paso
College of Engineering, Civil Engineering
500 W. University Av.
El Paso, Texas, USA,
Phone: (915)747-6911
Fax: (915) 747-8037
E-mail: nazarian@utep.edu

3.1. Abstract

Two Traffic Speed Deflection Devices (TSDDs) that measure surface deflections at posted traffic speeds (up to 80 – 96 kph) were evaluated through a recent Federal Highway Administration (FHWA) project that included field trials at the MnROAD facility. Four geophones were embedded near the pavement surface to measure surface deflections during field trials at each of three MnROAD cells. In addition, the MnROAD facility counted with numerous other sensors such as strain gauges to measure pavement responses and thermocouple trees to collect pavement temperature at various depths. For the implementation of TSDDs in any network-level Pavement Management System (PMS), it is important to utilize a proper analytical model that can accommodate moving load and viscoelastic properties of pavement layers in the simulation of TSDDs measurements. The 3D-Move software was chosen for this purpose. The viscoelastic properties used for the asphalt concrete (AC) layer include dynamic modulus and damping coefficient as a function of frequency relevant to the temperature at the time of the MnROAD field trials. The field trials and available data represented realistic field case scenarios to validate once more 3D-Move specifically for TSDD measurements. The proposed dynamic analytical model provided a good match with a variety of independent pavement responses that included surface deflection bowls (measured using embedded geophone sensors) as well as horizontal strains at the bottom of the AC layers (measured using MnROAD sensors).

Keywords: Traffic Speed Deflection, Dynamic simulation, Surface deflections, Pavement Response, Field Evaluation.

3.2. Introduction

The Falling Weight Deflectometer (FWD) has been an important part of the recent pavement evaluation and rehabilitation strategies. FWDs have provided valuable data relating to pavement performance to estimate suitable remedies and construction budget for network level *(1)*. FWD is a stationary device that applies a load pulse to the pavement surface at frequency of about 30 Hz *(2)* to simulate the load produced by a moving truck and measure surface deflections using multiple sensors located at varying distances from the load. The deflection basin produced by the FWD is used to backcalculate pavement material properties as well as to estimate pavement layer condition *(3)*.

The limitations of FWD, such as mobilization, traffic closure and low rate of data collections encouraged organizations in the USA and Europe to look for a faster method of pavement deflection testing for network-level data collection. The Traffic Speed Deflectometer (TSD) developed by Greenwood Engineering and Rolling Wheel Deflectometer (RWD) developed by Applied Research Associates, collectively referred to as Traffic Speed Deflection Devices (TSDDs) in this paper, have been developed to overcome many of the FWD shortcomings, as they collect surface deflections up to posted traffic speeds (up to 80 – 96 kph). Much work has been done over the past decade toward understanding the capabilities of traffic speed devices (both RWD and TSD), as a replacement for FWD data for pavement structural evaluation *(4, 5)*. However, the proper incorporation of the results from these devices to network level pavement management system (PMS) applications requires appropriate, device-specific, analysis methodology.

To assess the appropriateness of any proposed methodology, field evaluations in conjunction with analytical models to simulate the TSDDs measurements are required important steps.

The Federal Highway Administration (FHWA) commissioned the evaluation of the TSD and RWD at the MnROAD facility in September 2013 *(6)*. The surface deflections and pavement responses collected at the MnROAD facility during the field trials were used as reference values to calibrate and validate one analytical simulation tool. Since TSDDs measure surface deflection at high speeds, the moving continuous deflection measurements can be affected by the viscoelastic properties of the asphalt concrete (AC) layer. The 3D-Move program was chosen as the simulation tool since it can calculate the pavement response as a function of vehicle speed through the direct use of the frequency sweep test data (dynamic modulus and damping) of AC mixture *(7,8,9)*.

The main objective of this paper is to present the efforts toward calibrating and validating 3D-Move analytical model responses with comparable measured responses from embedded sensors at the MnROAD facility due to TSDDs field trials. The evaluation of accuracy of the devices to measure surface deflections is beyond of scope of this paper.

3.3. Field Data

During the MnROAD filed trials, the TSD used Doppler lasers to measure the deflection velocity along the midline of dual tires and in front of the axle at up to a dozen points (six in this study at 100, 200, 300, 600, 900 and 1500 mm) and the RWD measures up to two surface deflections along the midline of dual tires (in this study at 184 mm behind and

197 mm in front of the axle). To evaluate the two devices, four geophones were embedded almost flush with the pavement surface along the right wheel path of Cells 3 and 19 from the MnROAD Mainline and Cell 34 from the MnROAD Low Volume Road (see http://www.dot.state.mn.us/mnroad/ for detail).

The configuration of embedded geophones at each site is shown in Figure 3-1. Geophones 1 and 3 (GEO1 and GEO3) were placed along the midline of the wheel path. While the intent was the TSD sensors to pass directly on top of Geophones 1 and 3, the other two geophones were installed in anticipation of wheel wander, with a 150 mm offset to either side of the midline of the wheel path. In addition to the geophones, other existing instrumentations at the MnROAD facility collected data during the field trials for calibration and validation purposes. For example, longitudinal strain gauges capture the tensile strain at the bottom of the AC layer, while pavement layer temperatures were measured by thermocouple trees at a number of depths.

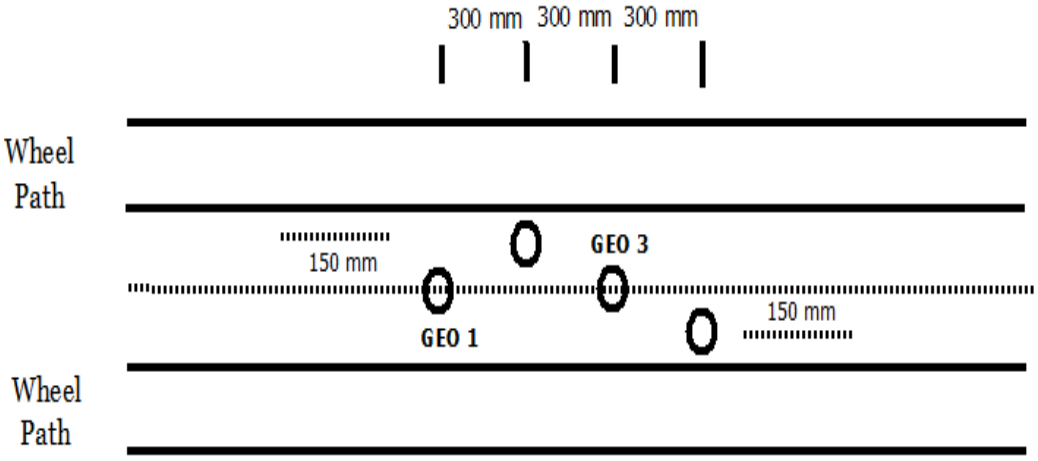

Figure 3-1. Configuration of embedded project sensors and spacing

3.4. Material Characterization

The characterization of the material properties at the three instrumented cells is an important step in the calibration process. MnROAD maintains a database containing laboratory and field-testing results on soils, aggregates, asphalt mixtures, asphalt binders, concrete mixtures, and other materials. The MnROAD database also contains cell-specific information, including layer thickness, type of layers and cross section of cells at time of construction and subsequent treatments. FWD testing performed within a few days of the field trials facilitated the characterization of the pavement layer material properties.

Table 3-1 summarizes the nominal layer thicknesses and mean and standard deviation of backcalculated moduli for each cell. The Software MODULUS *(10)* was used to estimate the values shown in the table. The properties of the unbound layers (base and subgrade) are generally unaffected by temperature above freezing temperatures; but moisture content may play a significant role. Since the FWD and TSDDs testing were performed within a short period of one other and since a careful review of climate at the site did not reveal significant changes in moisture content, the FWD backcalculated moduli for the unbound layers at the three MnROAD cells were used directly in the 3D-Move runs. However, the viscoelastic properties of the AC layers, such as dynamic modulus and damping, are highly affected with the change in temperature; therefore those input values were adjusted based on the actual temperature at the time of TSDDs testing. The procedure used for temperature adjustment is detailed in next section.

Table 3-1. Backcalculated Pavement Layer Moduli

Cell	Material	Thickness, mm. (in)	Average Modulus, MPa (ksi)	Standard Deviation, MPa, (ksi)	Coefficient of Variation (%)
3	AC	76 (3)	3820 (554)	234 (34.0)	14.0
	Base	1092 (43)	474 (68.8)	94(13.6)	19.8
	Subgrade	3109 (122.4)	122 (17.7)	15(2.2)	12.3
19	AC	127 (5)	2075 (301)	448(65)	22.0
	Base	787 (31)	221 (32)	40(5.8)	18.0
	Subgrade	460 (18.1)	42 (6.1)	4(0.6)	10.2
34	AC	102 (4)	2062 (299)	462(67.0)	22.0
	Base	305 (12)	108 (15.7)	21(3.1)	19.9
	Subgrade	1176 (46.3)	59 (8.5)	6(0.9)	10.2

3.4.1. Estimation of Average AC Layer Temperature

Thermocouple (TC) trees were used at the MnROAD cells to measure temperature within the pavement layers. The typical MnROAD TC tree is 1.8 m long. Sensor depths were selected during construction to provide a temperature profile within the AC, base and subbase layers. Table 3-2 shows the AC layer temperatures recorded by the TC devices installed at the three cells during FWD testing. As shown in Table 3-2, some of the thermocouples were out of service or out of calibration.

Table 3-2. Measured Temperatures within AC Layer during FWD Testing

Cell	Day	Hour	Temperature at location from surface, ^{o}C (^{o}F)				
			1.3cm (0.5 in.)	3.8 cm (1.5 in.)	6.4 cm (2.5 in.)	8.9 cm (3.5 in.)	11.4 cm (4.5 in.)
3	16-Sep-13	14	52 (126)	34 (93)	32 (90)	29 (84)	na
19	20-Sep-13	14	29 (84)	**	57 (135)*	23 (73)	22(72)
34	5-Sep-13	15	**	42 (108)	**	**	

*na= not applicable; * = Possible incorrect data; ** = Missing data*

Although AC temperature depth coverage seems adequate for Cell 3 with the thinnest layer (75 mm (3 in.)), coverage in the other cells are not. For example, in Cell 19 there are four data points, but one of them does not seem to follow a reasonable trend. For Cell 34, only one data point is available. Accordingly, an alternate defensible approach based on BELLS equation *(11)* was adapted to estimate temperatures within the AC layers during FWD tests and TSDDs field trials. The BELLS equation, which developed based on extensive calibration using data from the Long-Term Pavement Performance (LTPP) database, is given by:

$$T_d = 0.95 + 0.892 \times IR + \{\log(d) - 1.25\} \times \{-0.448 \times IR + 0.621 \times (1\text{-day}) + 1.83 \times \sin(hr_{18} - 15.5)\} + 0.042 \times IR \times \sin(hr_{18} - 13.5) \quad (3.1)$$

where:

- T_d = pavement temperature at depth d, °C;
- IR = pavement surface temperature, °C;
- d = depth at which pavement temperature is to be predicted, mm;
- 1-day = average air temperature the day before testing, °C;
- hr_{18} = Time of day, in a 24-hr clock system, but calculated using an 18-hr asphalt concrete (AC); and temperature rise-and-fall time cycle**.**

The BELLS equation was used to predict temperatures within the AC layer for Cells 19 and 34 at locations other than those for which measurements were available. Appropriate surface temperatures were determined based on the data available from the top-most sensor of TC device (reliable measured temperatures) and matching the prediction by the BELLS equation. The same procedure used to determine the AC layer

temperatures during the FWD testing was used to estimate the average AC layer temperatures during TSDD testing. Table 3-3 summarizes the average AC layer temperatures at the time of FWD and TSDD testing. Having the best estimate of the average AC layer temperature, the viscoelastic properties were established as described next.

Table 3-3. Average AC Layer Temperatures

Cell	Temperature at time of FWD Testing, °C (°F)	Temperature at time of TSD Testing, °C (°F)	Temperature at time of RWD Testing, °C (°F)
3	37(99)	33(91)	37(99)
19	27 (81)	20(68)	17(63)
34	42 (108)	33(91)	32 (90)

3.4.2. Viscoelastic Properties at Time of TSDD Trials

Since 3D-Move program considers rate-dependent material properties, damping coefficient and dynamic modulus as function of frequency at the representative AC temperature are key input parameters for simulation purposes. Using the average AC layer temperature, damping coefficient was estimated using dynamic modulus test data available in the MnROAD database. In those tests, the phase angles of the AC layer at several temperatures and frequencies were measured. In its complex form, the dynamic modulus is given by *(12):*

$$E^*=E'(1+2i\zeta_{AC}) \quad (3.2)$$

where E*= complex dynamic modulus; and

ζ_{AC} = measure of internal damping of the AC.

For viscoelastic layers, the complex modulus can be presented as the sum of the real and imaginary components, which is given by:

$$E^*=E_1+iE_2 \quad (3.3)$$

where E_1 and E_2 = real and imaginary modulus components. The above equations may be re-written as follows:

$$E_2 = 2E_1\zeta_{AC} \quad (3.4a)$$

$$\zeta_{AC} = E_2/(2E_1) = 0.5\tan(\varphi) \quad (3.4b)$$

where φ= phase angle associated with time lag between the load and deformation. Table 3-4 and Table 3-5 show the values of damping coefficient associated with the TSD and RWD field trials, respectively. The procedure used to obtain these values consisted of fitting a best curve through the available AC dynamic modulus test (phase angle measured at given frequencies) results and then interpolating the phase angles for the temperature corresponding with the TSDDs field trials.

Table 3-4. Phase Angle and Damping for Instrumented Cells for TSD Field Trials

TSD – Cell 3 Temperature = 33 °C			**TSD - Cell 19 Temperature = 20 °C**			**TSD - Cell 34 Temperature = 33 °C**		
Frequency (Hz)	Phase angle (°)	Damping (%)	Frequency (Hz)	Phase angle (°)	Damping (%)	Frequency (Hz)	Phase angle (°)	Damping (%)
0.1	36.3	36.8	0.1	34.2	33.9	0.01	29.0	27.8
0.5	36.7	37.3	0.5	26.4	24.8	0.1	32.0	31.2
1	36.2	36.6	1	23.7	21.9	1	31.6	30.7
5	33.2	32.7	5	19.1	17.3	25	27.6	26.1
10	34.4	34.2	10	16.9	15.1			
25	31.6	30.7	25	13.5	11.9			

The FWD backcalculated AC layer modulus is appropriate for the temperature at the time of testing and a loading frequency of about 30 Hz (2). Using this AC layer modulus and frequency as an anchoring point, the AC master curve (i.e., modulus versus frequency) was established.

Table 3-5. Phase Angle and Damping for Instrumented Cells for RWD Field Trials

RWD - Cell 3 Temperature = 37 °C			**RWD - Cell 19 Temperature = 17 °C**			**RWD - Cell 34 Temperature = 32 °C**		
Frequency (Hz)	Phase angle (°)	Damping (%)	Frequency (Hz)	Phase angle (°)	Damping (%)	Frequency (Hz)	Phase angle (°)	Damping (%)
0.1	36.8	37.4	0.1	32.7	32.1	0.01	29.7	28.5
0.5	36.6	37.2	0.5	22.6	20.8	0.1	33.0	32.4
1	36.4	36.9	1	19.4	17.6	1	32.5	31.9
5	34.7	34.6	5	15.4	13.7	25	28.0	26.5
10	36.7	37.2	10	12.4	10.9			
25	34.6	34.5	25	9.4	8.3			

The undamaged dynamic modulus for MnROAD cells at actual temperatures were predicted from the Witczak-Andrei AC dynamic modulus equation *(13)* which is given by:

$$\log E^* = -1.25 + 0.029\rho_{200} - 0.0018(\rho_{200})^2 - 0.0028\rho_4 - 0.058V_a - 0.822\frac{V_{beff}}{V_{beff}+V_a} + \frac{3.872-0.0021\rho_4+0.003958(\rho_{38})-0.000017(\rho_{38})^2+0.0055\rho_{34}}{1+e^{(-0.603313-0.313351\log(f)-0.393532\log(\eta))}} \quad (3.5)$$

where E*= dynamic modulus of mix,10^5 psi

H=viscosity of binder,10^6 poise

F= loading frequency, Hz

P_{200}=% passing #200 (0.075 mm) sieve

P_4= cumulative % retained on #4 (4.76 mm) sieve

P_{38}= cumulative % retained on 3/8 in. (9.5 mm) sieve

P_{34}= cumulative % retained on 3/4 in. (19 mm) sieve

V_a= air void, % by volume

V_{beff}= effective binder content, % by volume

The MnROAD database includes the gradation data required for this equation. The viscosity can be calculated as a function of temperature based on A and VTS viscosity temperature susceptibility *(14)* as follows:

$$\log\log\eta = A + VTS.logT_R \quad (3.6)$$

where η = the viscosity, cP

T_R= the temperature at which the viscosity is estimated, Rankine

A = Regression Intercept

VTS= Regression slope of viscosity temperature susceptibility

AASHTO T315 *(15)* gives guidelines for calculating A and VTS. The DSR test results are available in the MnROAD databases for the three cells under consideration. The PG grade for these cells, which were estimated from available data, are PG 70-16, PG 64-22 and PG 58-34 for Cells 3, 19 and 34, respectively. Accordingly, the calculated sets of A and VTS values are 10.641 and -3.548 for Cell 3, 10.98 and -3.68 for Cell 19, and 10.149 and -3.359 for Cell 34.

The undamaged dynamic modulus as function of frequency at actual temperature can be estimated from above procedure. The next step was the determination of the existing AC layer modulus at various frequencies and at the AC layer temperature corresponding to the time of TSDD testing based on the FWD backcalculated layer moduli. Figure 3-2 illustrates the procedure used to derive the AC existing modulus master curves from the undamaged AC moduli. The AC existing modulus can be estimated from the following equation *(16)*:

$$E^*_{dam} = 10^{\delta} + \frac{E^* - 10^{\delta}}{1 + e^{-0.3+5\times\log(d_{AC})}} \quad (3.7)$$

where E^*_{dam} = Existing modulus

E^* = Undamaged modulus for specific reduced time (from master curve)

δ = Regression parameter (from E^* master curve)

d_{AC} = Fatigue damage in AC layer

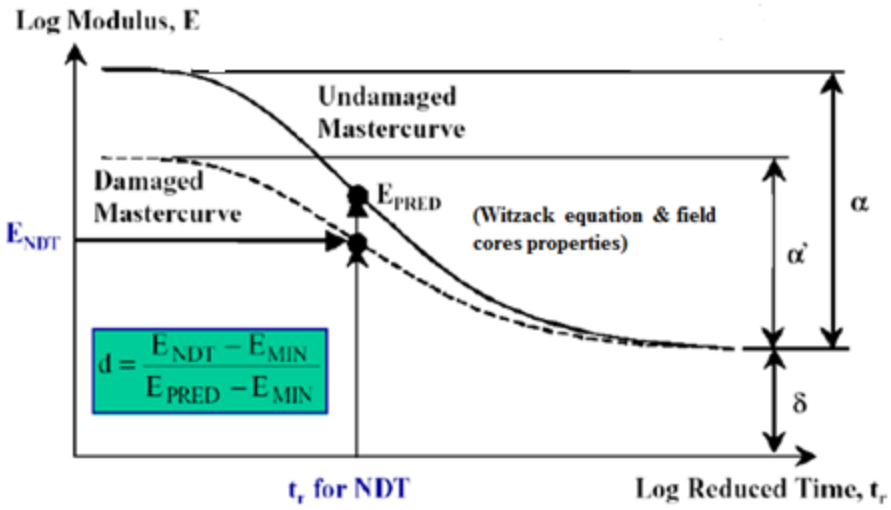

Figure 3-2. Development of AC modulus master curves from undamaged AC moduli

Accordingly, using Equation 3.5 and taking into consideration the Fatigue Damage Factor (d_{AC}), reasonable AC modulus master curves were generated. Figure 3-3 shows the resulting master curves for the temperatures associated with the TSDD field tests in Cell 34. The curve appears realistic, showing smooth variation in both the low and high frequencies and hence, they were used as input to 3D-Move. Similar curves were produced for the other two cells.

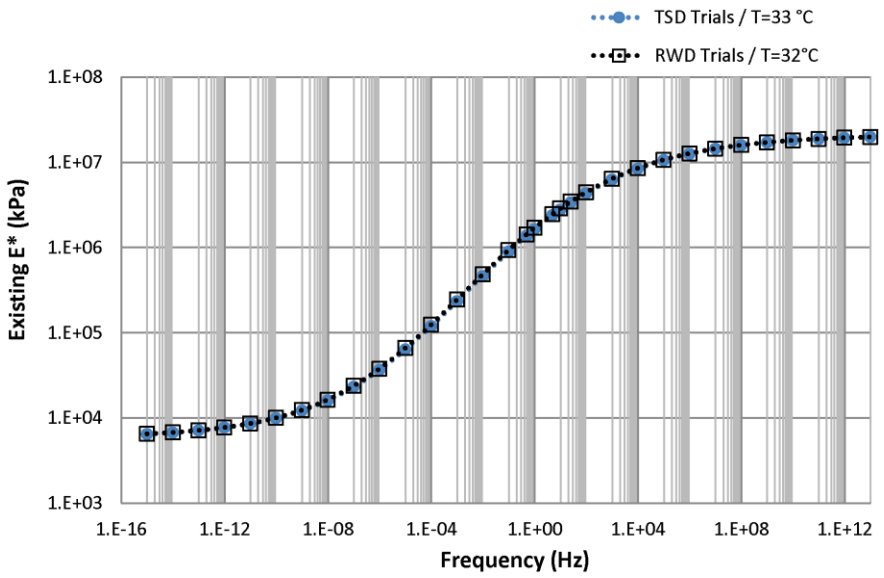

Figure 3-3. Damaged master curves for Cell 34

3.5. TSDD Loading Characteristics

Since the TSDD sensors are positioned along the midline of the rear axle dual tires, the 3D-Move comparisons in this calibration effort focused on the responses generated by those axles. Table 3-6 shows the characteristics and loads of the rear axles for the TSDD in question. The loads were determined using a MnROAD static scale.

Table 3-6. TSDD Rear Axle Configuration and Loads

	RWD Rear Tires	**TSD Rear Tires**
Tire Pressure	689.5 kPa (100 psi)	800 kPa (116 psi)
Rear Axle Load	2.37 ton/tire (4750 lbs/tire)	2.79 ton/tire (5575 lbs/tire)
Dual Tire Spacing	36.8 cm (14.5 in.)	34.3 cm (13.5 in.)

Because the weights of the devices were measured using a static scale, the 3-D Move results were used with caution when simulating moving vehicles. Figure 3-4 illustrates the variation in the rear axle load for a 5 axle truck-semitrailer traveling at 40-50 kph *(17)*. The dynamic load can vary by as much as 33% of the static load. This

suggests that the variation of axle load, which has a direct influence on the computed deflection response, should be addressed.

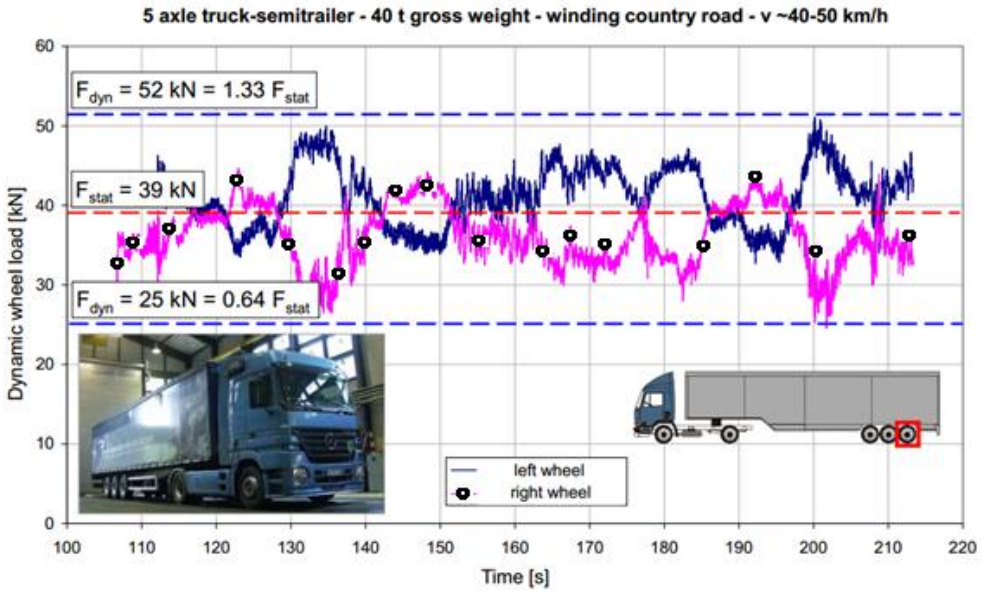

Figure 3-4. Wheel load variations of 5 axle truck-semitrailer (based on *[17]*)

3.6. Simulation Case Scenarios

So far, the material properties for the instrumented MnROAD cells and loading characteristics of the TSDDs were addressed. Observations during the field trials and a review of available data revealed that some additional factors should be considered in the 3D-Move simulations. These factors include:

(1) *Transverse wheel wander*: While it was hoped that the TSDDs would operate such that the midline of the rear axle tires coincided with the plane of the project sensor measurements (i.e., plane of GEO1 and GEO3 in Figure 3-1), this was not always achieved. Wheel wander can result in either higher or lower measured deflection data, depending on the extent of the wheel wander. The 3D-Move program is capable of providing the displacement basin as a function of wheel

wander (i.e., at various wheel locations). Since precise location of the midline relative to the plane of measurement is not available, it was decided to use only the maximum possible displacement basin given by 3D-Move.

(2) *Material properties*: The pavement layer moduli used as input into 3D-Move were based on FWD backcalculated values. The backcalculation process assumes static loading conditions and the results of the backcalculation are sensitive to small variations in the input (e.g., thickness of AC and base layers). Geology in the area suggests that the subgrade thicknesses at the instrumented cell locations are substantially greater than those that were predicted from the backcalculation effort. In addition, the viscoelastic characterization used for the AC layers was based on undamaged moduli determined using Equation 3.5 and shifting of the master curve to get the AC modulus versus frequency relationship for the existing pavements. The damping characteristics of the AC material were determined based on laboratory tests done on fresh AC samples. All of these introduce limitations, especially concerning their applicability to the aged AC layers (more than 5 years of age) at the MnROAD cells in question. To address these issues, the 3D-Move analyses considered changes to material properties and layer thicknesses when comparisons were made.

(3) Variation in axle load: The axle loads were measured under static conditions, but these loads are expected to vary during operation at high speeds. It was shown in Figure 4 that the 5 axle truck-semitrailer wheel load variations can be as high as 33% when moving across a pavement. To account for these variations in tire load

under moving conditions, adjustments to the tire loads used in the 3D-Move runs were considered.

Accordingly, after an extensive trial and error process, acceptable bracketing of the measured deflection responses was obtained with the following three 3D-Move case scenarios:

Case 1: Three layer pavement structure with same thicknesses as used in the FWD backcalculation and corresponding mean layer moduli derived from the FWD backcalculation results;

Case X: Three layer pavement with: (a) thicknesses used in the FWD backcalculation except decreasing the AC layer thickness by 1 inch (25.4 mm), (b) (mean – σ) of FWD backcalculated layer moduli for AC and base layers, (c) (mean + σ) of FWD backcalculated layer moduli for subgrade, and (d) add +25% of nominal tire load to the tire load.

Case X1: Same as Case X, but with no reduction in AC layer thickness. This case was used for Cells 3 and 34, which have the thinner AC thicknesses.

Case X was used only for Cell 19 to bracket the measured values. As will be shown later in this paper, the 3D-Move predictions based on the above three scenarios consistently bracketed well the measured responses (stresses, strains and displacements) collected by the embedded surface sensors and MnROAD sensors.

3.7. Dynamic Simulation Results: TSDD versus Embedded Sensor Measurements

The results from the analyses with 3D-Move using the case scenarios described in the previous section were initially compared with the measured values from all embedded sensors. TSDD measurements were also included in the comparisons. As indicated earlier, the TSD provides surface velocities at six points ahead of the wheels, while the RWD measures displacements at two points.

Figure 3-5 illustrates the comparison of the computed and measured deflections for Cell 34 during a TSD trial at a vehicle velocity of 48 kph (30 mph). Since the main focus is the comparison of the deflection bowls (shape and maximum value), the plots have been shifted to align so that the maximum displacement locations coincide. As shown in Figure 3-1, GEO1 and GEO3 are located along a plane parallel to the vehicle direction, so the measured values from these two sensors should be very similar. The variation between the deflection bowls given by these two sensors may be viewed as a measure of the overall variability in the measurements made by the embedded sensors and possibly any spatial variability between 30 cm of distance between geophones (Figure 3-1). The lower and upper bound of the project sensor data were arrived at by treating GEO1 and GEO3 data as independent datasets in the presentations below. In all cases, 3D-Move adequately captured the maximum and shape of measured displacements. Case X1 provides the closest deflection basin to that measured. Figure 3-6 compares the predicted and measured TSD surface velocities (maximum from

field trials). While all computed case results give similar shapes as the measured ones, the Case X1 predictions are closer to both the project sensors and TSD measurements.

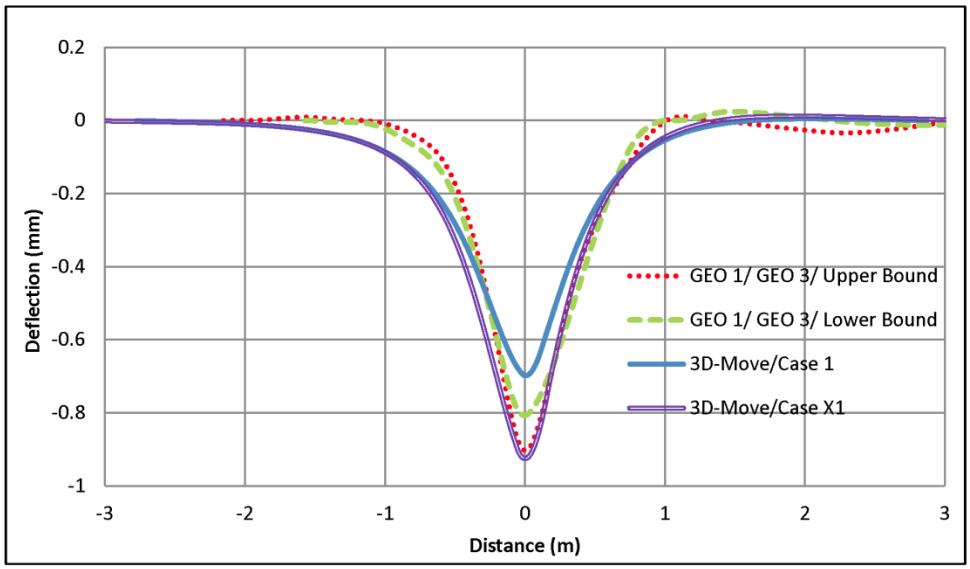

Figure 3-5. TSD trials - predicted and measured deflections (Cell 34; v = 48 kph (30 mph))

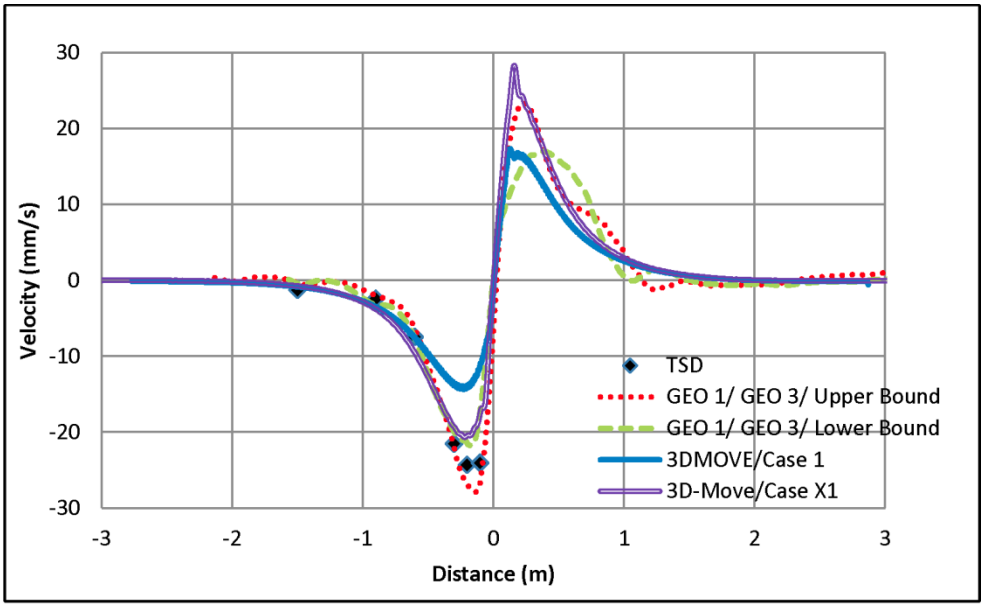

Figure 3-6. TSD trials - predicted and measured velocities (Cell 34; v = 48 kph (30 mph))

The computed results were also compared with those from the RWD device. Again, as a representative plot, Figure 3-7 shows the computed and measured deflection bowls as well as the two measured deflection values from the RWD. As shown, the computed results bracket the measured sensor values well and the RWD measurements are also close to the predicted results.

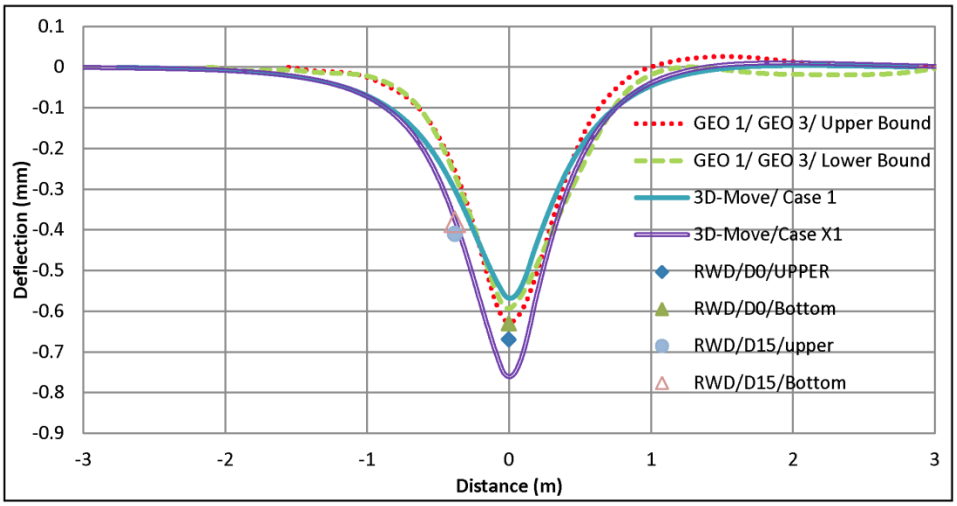

Figure 3-7. RWD trials - 3D-Move predicted and measured deflections (Cell 34; V=48 kph (30 mph))

Figure 3-8 shows the comparison of the maximum displacements computed by 3D-Move and those measured by the embedded sensors for all runs made with the TSD and RWD. When sensor measurements were plotted, the largest displacement given by either GEO1 or GEO 3 (from all field trials) was selected. The figure shows a good match between computed and measured maximum displacements.

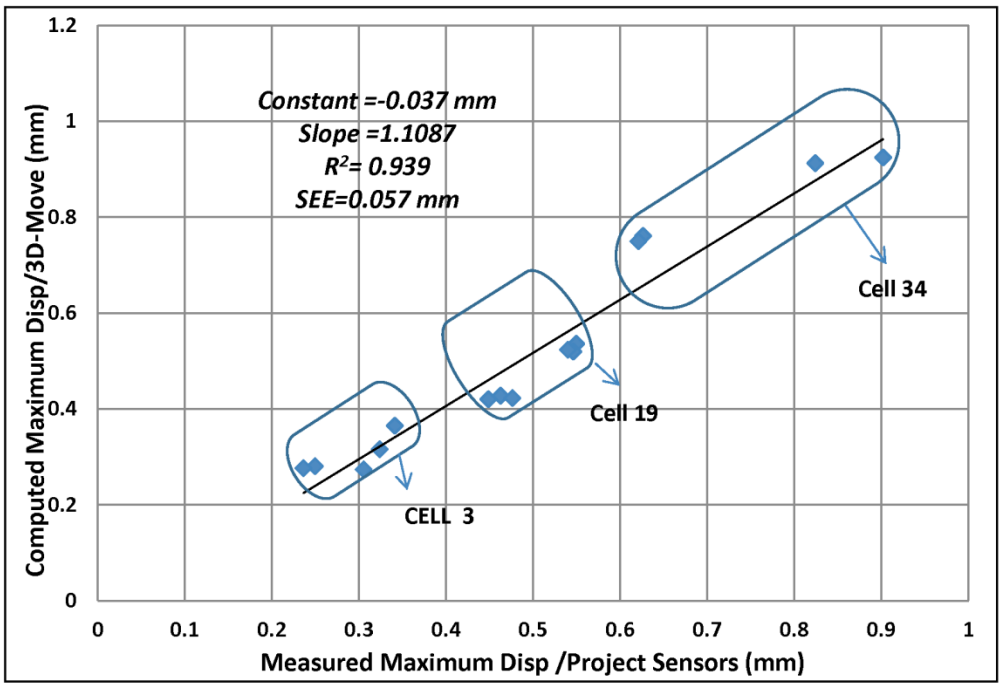

Figure 3-8. Computed maximum displacement versus measured (all cells and vehicle velocities during RWD and TSD trials)

3.8. Dynamic Simulation Results: TSDD versus MnROAD Measurements

This section presents the comparisons between the computed results and the measured MnROAD sensor data. Unlike the earlier embedded sensor comparisons, which focused on surface deflections, the comparisons presented in this section consider strains at interior pavement locations.

Figure 3-9 compares the measured and predicted longitudinal strains in Cell 34 for a TSD run. The figure shows that the calculated longitudinal strains from 3D-Move match well with the measured data from the MnROAD strain gauges. Similarly, Figure 3-10 displays the comparison of measured and computed longitudinal strain for a

RWD run in Cell 3. As shown in the figure, the measured response history is bracketed by the calculated values.

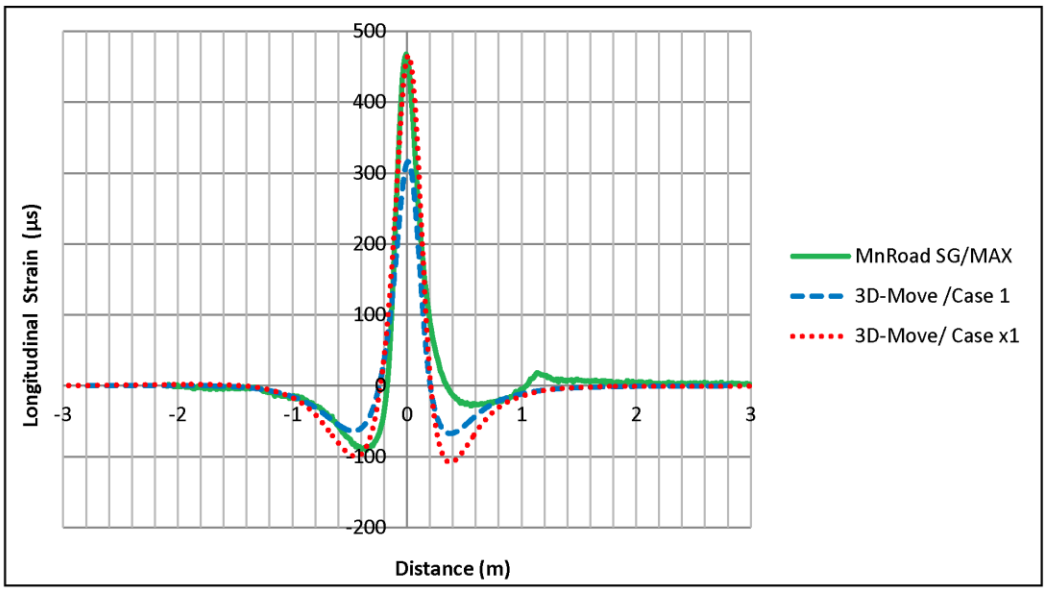

Figure 3-9. TSD trials - 3D-Move versus MnROAD strain gauge measurement (Cell 34; v=48 kph (30 mph))

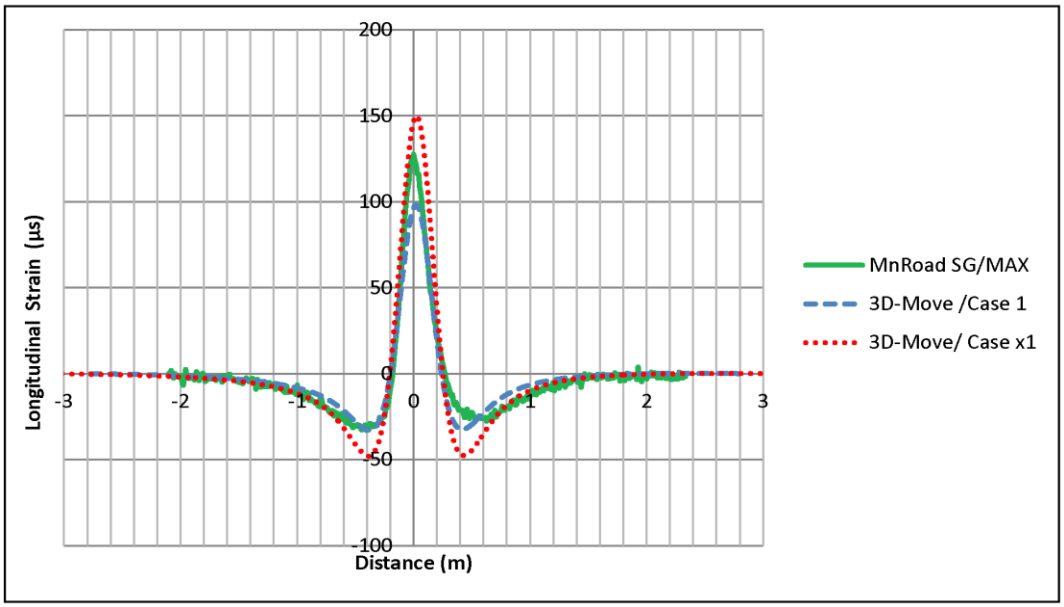

Figure 3-10. RWD trials - 3D-Move versus MnROAD strain gauge measurement (Cell 3; v=48 kph (30 mph))

Since the maximum load-induced strains are critical inputs to pavement performance predictions, this effort is seen as important in the validation of the applicability of the dynamic simulation for pavement response predictions. Figure 3-11 compares the computed and measured maximum longitudinal strains at the bottom of the AC layer for all MnROAD instrumented cells during the TSDD field trials. The dynamic simulation can capture maximum pavement responses well. The best fitted line has a slope of 1.016 with R^2 of 0.95. The standard error of estimation (SEE) for the best fitted line is 22.8 μs. The capability of the 3D-Move analytical tool to predict maximum pavement responses close to the measured values lends credibility to its use in TSDD simulations.

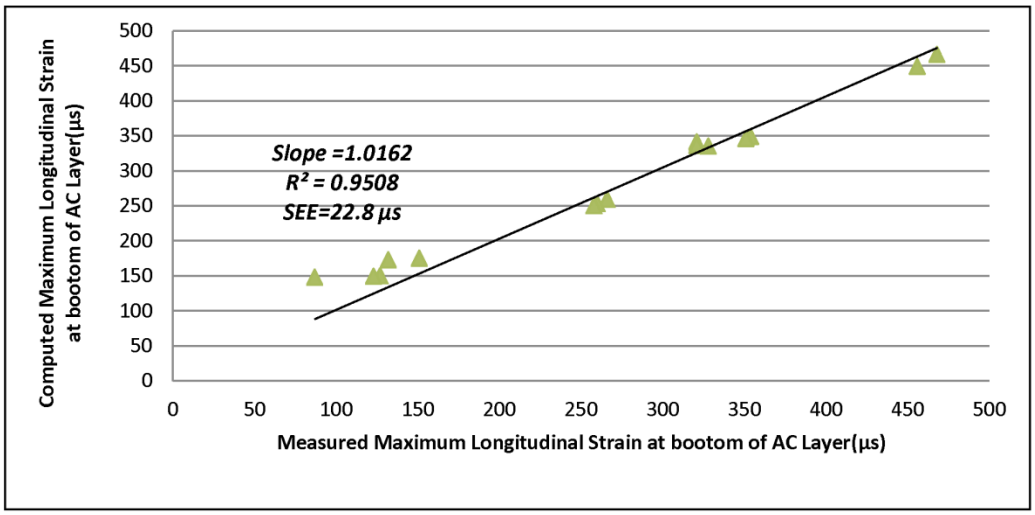

Figure 3-11. Computed versus measured maximum longitudinal strain at bottom of AC layers (all cells and vehicle velocities during RWD and TSD trials)

3.9. Summary and Conclusion

Since TSDDs measure dynamic vertical surface deflections, analytical simulation models should account for the moving nature of the load along with viscoelastic pavement layer material properties. In this study, the capability of the dynamic pavement response model 3D-Move to simulate TSSD deflection measurements and pavement responses was evaluated. TSD and RWD were investigated at the MnROAD facility with extensive instrumentations. The analyses were conducted using inputs derived based on the following considerations:

(1) Existing MnROAD database of pavement layer properties (thicknesses and physical properties) and recent FWD deflection data;

(2) Representative layer material properties based on backcalculation of FWD deflection data and subsequently, viscoelastic AC properties as a function of frequency extrapolated for the TSDD field trial temperatures using the Wictzack-Andrei model. In some cases because of lack of data, there was a need to extrapolate the AC layer temperatures at interior points using BELLS equation;

(3) Static tire loads that were measured at the MnROAD facility weighing station and dynamic load effects were addressed; and

(4) Role of wheel wander was addressed by selecting the transverse location that gave the highest deflections predictions.

Several analyses were undertaken in an attempt to bracket the measured surface deflection data (peak and basin shape). In the process, due consideration was given to the

selection of the inputs (material properties and loading) so that they are rationally arrived at and the adjustments are defensible. It was shown that 3D-Move computed results bracket the measured time histories from embedded geophones well.

Using a variety of independent pavement responses that included surface deflection bowls (measured using embedded geophone sensors) as well as horizontal strains at the bottom of the AC layers (measured using MnROAD sensors) confirmed the ability of the dynamic moving load pavement response model to simulate TSDD loading under a variety of realistic pavement conditions. A comprehensive simulation of pavement responses using dynamic simulation, but covering a larger pavement database that considers the variability in pavement condition (layer configuration and properties) is underway.

Acknowledgements

This study was funded through the FHWA study DTFH61-12-C-00031 and the support is gratefully acknowledged. The authors would like to thank Dr. Nadarajah Sivaneswaran of the FHWA and Dr. Senthil Thyagarajan of ESC, Inc. for their kind support. The authors would also like to thank Mr. Ben Worel and the rest of the MnROAD staff without whose help, the successful outcome of the project would not have been possible. The conclusions presented in this paper are solely those of these authors.

3.10. Reference

1. Noureldin, A., Zhu, K., Li, S., and Harris, D. Network Pavement Evaluation with Falling-Weight Deflectometer and Ground-Penetrating Radar. *In Transportation*

Research Record: Journal of the Transportation Research Board, No.1860. Transportation Research Board of the National Academies, Washington. D.C., 2003, pp. 90-99.

2. Irwin, L. H., Orr, D. P., and Atkins, D. *FWD Calibration Center and Operational Improvements: Redevelopment of the Calibration Protocol and Equipment*. Publication FHWA-HRT-07-040. FHWA, U.S. Department of Transportation, 2009.
3. Xu, B., Ranji Ranjithan, S., and Richard Kim, Y. New Relationships between Falling Weight Deflectometer Deflections and Asphalt Pavement Layer Condition Indicators. *In Transportation Research Record: Journal of the Transportation Research Board, No.1806 (1)*. Transportation Research Board of the National Academies, Washington. D.C., 2002, pp. 48-56.
4. Elseifi, M. A., Abdel-Khalek, A. M., Gaspard, K., Zhang, Z., and Ismail, S. Evaluation of Continuous Deflection Testing Using the Rolling Wheel Deflectometer in Louisiana. *Journal of Transportation Engineering, Vol.* 138, No. 4, 2011, pp. 414–422.
5. Flintsch, G., Katicha, S., Bryce, J., Ferne, B., Nell, S., and Diefenderfer, B. *Assessment of Continuous Pavement Deflection Measuring Technologies*. Publication SHRP 2 Report S2-R06F-RW-1, Transportation Research Board of the National Academies, 2013.
6. Rada, G., Nazarian, S., Visintine, B., Siddharthan, R.V., and Thyagarajan, S. *Pavement Structural Evaluation at the Network Level.* FHWA- DTFH61-12-C-00031, FHWA, U.S. Department of Transportation, 2015.
7. Siddharthan, R., Zafir, Z., and Norris, G. M. Moving Load Response of Layered Soil.

I: Formulation. *Journal of the Engineering Mechanic, ASCE,* Vol. 119, No. 10, 1993, pp. 2052-2071.

8. Siddharthan, R.V., Yao, J., and Sebaaly, P.E. Pavement Strain from Moving Dynamic 3-D Load Distribution," *Journal of Transportation Engineering, ASCE,* Vol. 124, No. 6, 1998, pp. 557-566.
9. Zafir, z., Siddharthan, R., and Sebbaly, P.E. Dynamic Pavement Strain from Moving Traffic Loads. *Journal of Transportation Engineering, ASCE,* Vol. 120, No. 5, 1994, pp. 821-842.
10. Liu, W. and Scullion, T. *MODULUS 6.0 for Windows: User's Manual*. FHWAS/TX-05/0-1869-2, Texas Transportation Institute, Texas A&M Uni., College Station, Texas, 2001.
11. ASTM D7228-06a. *Standard Test Method for Prediction of Asphalt-Bound Pavement Layer Temperatures*. ASTM International, West Conshohocken, PA, 2011, DOI: 10.1520/D7228-06AR11, www.astm.org.
12. Rosset, J. M. Damping and Damping Coefficients of Foundations. Special Technical Publication on Dynamic Response of Pile Foundations: Analytical Aspects, ASCE, O'Neill and Dobry, eds., ASCE, New York, 1980, pp. 1-30.
13. Kim, Y.R., Underwood, B., Sakhaei Far, M., Jackson, N., and Puccinelli, J. *LTPP Computed Parameter: Dynamic Modulus*. Publication FHWA-HRT-10-035, FHWA, U.S. Department of Transportation, 2011.
14. Velasquez, R., Hoegh, K., Yut, I., Funk, N., Cochran, G., Marasteanu , M., and Khazanovich, L. *Implementation of the MEPDG for New and Rehabilitated Pavement Structures for Design of Concrete and Asphalt Pavements in Minnesota.* Report No.

MN/RC 2009-06, Minnesota Department of Transportation, St. Paul, MN, 2009.

15. ASTM D7175-08. *Standard Method of Test for Determining the Rheological Properties of Asphalt Binder Using A Dynamic Shear Rheometer (DSR)*. ASTM International, West Conshohocken, PA, 2011.
16. Loulizi, A., Flintsch, G., and McGhee, K. Determination of In-Place Hot-Mix Asphalt Layer Modulus for Rehabilitation Projects by a Mechanistic-Empirical Procedure. *In Transportation Research Record: Journal of the Transportation Research Board, No.2037*. Transportation Research Board of the National Academies, Washington. D.C., 2007, PP. 53-62.
17. Rabe, R. Structural Pavement Monitoring with Non-Destructive Measuring Devices-Experience from a Pilot Project in Germany." *Presentation at the Ninth International Conference on Bearing Capacity of Roads, Railways and Airfields, BCRRA 2013, Trondheim, Norway.*

4. Validation of Dynamic Simulation of Slow Moving Surface Deflection Measurements

By
Mahdi Nasimifar (Corresponding Author)
Graduate Research Assistant
Department of Civil & Environmental Engineering
University of Nevada Reno
1664 N. Virginia St./ MS258
Reno, Nevada, 89557
Phone: (775) 200-8878
Fax: (775) 784-1390
E-mail: nasimifar@gmail.com

Raj V. Siddharthan
Professor
Department of Civil & Environmental Engineering
University of Nevada Reno
1664 N. Virginia St./ MS258
Reno, Nevada, 89557
Phone: (775) 784-1411
Fax: (775) 784-1390
E-mail: siddhart@unr.edu

Gonzalo R. Rada
Senior Principal Engineer
AMEC Foster Wheeler Environment & Infrastructure, Inc.
12000 Indian Creek Court, Suite F
Beltsville, Maryland, USA
Phone: (301) 210-5105
Fax: (301) 210-5032
E-mail: gonzalo.rada@amecfw.com

Soheil Nazarian
Professor
The University of Texas at El Paso
College of Engineering, Civil Engineering
500 W. University Av.
El Paso, Texas, USA,
Phone: (915)747-6911
Fax: (915) 747-8037
E-mail: nazarian@utep.edu

Word Count: 3,847 + 2×250 + 9×250 = 6,597
Number of Tables: 2
Number of Figures: 9
Submission Date: October 19, 2015

4.1. Abstract

Recent studies have concluded that measured surface deflections can be used as a low-cost pavement monitoring and condition assessment tool to determine remaining structural life and pavement performance. At present, moving load devices are being used more often to measure continuous surface deflections. They are being considered as a faster alternative to Falling Weight Deflectometer (FWD) based structural condition evaluation applications. The objective of the study presented in this paper is to compare the analytical dynamic simulation of slow moving deflection measurements with field data. The surface pavement deflections and the pavement structural responses generated by the Euroconsult Curviametro loading at the MnROAD facility near Maplewood, Minnesota were used in the evaluations. Four geophones were embedded near the pavement surface to measure surface deflections during field trials at each of three tested MnROAD cells. In addition, numerous other sensors, such as strain gauges and thermocouple trees were available at the MnROAD facility. The 3D-Move program was used in the simulations since it can accommodate moving loads and the viscoelastic properties of pavement layers, and produce continuous deflection basins. The viscoelastic properties of pavement layers were estimated based on the actual temperatures at the time of the field trials and the appropriate loading frequency of the Curviametro. The proposed dynamic analytical model provided a good match with a variety of independent pavement responses that included surface deflection basins (measured using embedded geophone sensors) as well as horizontal strains at the bottom of the AC layers (measured using MnROAD sensors).

Keywords: slow-moving surface deflection measurements, dynamic simulation, field validation, pavement response

4.2. Introduction

For decades, pavement structural condition has been assessed by measuring pavement surface deflections due to a known load. The Falling Weight Deflectometer (FWD) is known as a nondestructive stationary testing device that can simulate representative deflections of a pavement surface produced by a moving truck *(1)*. In turn, measured surface deflections have been used as a reliable indicator for assessing remaining structural life and pavement performance. The limitations of FWD such as stop-and-go operation, lane closures and low frequency of testing necessitate the need for a viable alternate device, in particular for network level pavement management applications.

At present, moving load devices are being used more often and they measure continuous surface deflections. Based on the initial investment, the daily cost of the operation of the moving load devices is currently greater than testing with the FWD. However, based on the daily productivity of the two devices, the costs per mile associated with moving load devices are substantially less than the FWDs *(2)*. The cost associated with the moving load devices may be further reduced as State Highway Agencies (SHAs) embrace their use, incentivizing more service providers to become available and the analysis algorithms to become more automated.

The Curviametro was evaluated at MnROAD facility near Maplewood, Minnesota in September 2013 *(2)*. This device operates at low speed (up to 18 kph) which is significantly slower than traffic speed devices and provides slow moving surface

deflection basins based on the measurements from geophones mounted on the truck. The MnROAD sections are instrumented with different types of sensors such as strain gauges, pressure cells and thermocouples. Four geophones were also installed to measure surface deflections at three flexible MnROAD cells, which covered three levels of stiffnesses as detailed later in this paper. The 3D-Move program was chosen to simulate slow moving surface deflection basins since it can accommodate rate-dependent (viscoelastic) material properties and can assess pavement response as a function of vehicle speed. It directly uses the frequency sweep test data (dynamic modulus and damping coefficients) of the asphalt concrete (AC) mixture.

Traditionally, SHAs have used surface condition data, such as cracking, to assess the structural condition of their pavement networks. However, surface deflections can be better correlated with load-induced pavement responses such as tensile strains at the bottom of the AC layer. Use of surface deflections measured by the slow moving devices in network level pavement management system (PMS) applications requires an appropriate methodology that relates the surface deflection indices to the pavement responses. To develop this methodology, the pavement responses under such devices need to be simulated with dynamic analyses that take in to account the realistic pavement properties as well as the moving nature of the device.

The objective of this study is to compare the analytical dynamic simulation of slow moving surface deflection basins with field data at the MnROAD facility to confirm the capability of dynamic simulations to model the pavement responses generated by the device. The pavement material properties that were relevant during the Curviametro field

trials had to be estimated for use in the simulations. The evaluation of accuracy of the Curviametro with measured surface deflections is beyond of the scope of this paper.

4.3. Overview of the Analytical Tool

The 3D-Move program was used as the analytical tool to simulate slow moving surface deflection measurements. The program is based on a finite-layer approach that uses the Fourier transform technique to evaluate the responses of a layered medium subjected to a moving load traveling at a constant speed *(3- 5)*. This model accounts for the moving nature of the vehicle load. In the program, the AC layer is considered as viscoelastic while the base course and the subgrade are considered linear elastic. The AC properties such as complex dynamic modulus vary as a function of frequency and temperature. The procedure used to get representative material properties at the MnROAD sites for use with the 3D-Move simulations during Curviametro trials is detailed in the next section.

The 3D-Move program is capable of predicting pavement responses (strain, stresses, and deflections) at selected locations. Figure 4-1 shows a sketch of vertical deflection time history from 3D-Move at a point (observation point) on the midline between the tires. Using time space superposition, the deflections at various locations along the midline between the rear tires (Curviametro measurement locations) can be calculated from the vertical deflection time history.

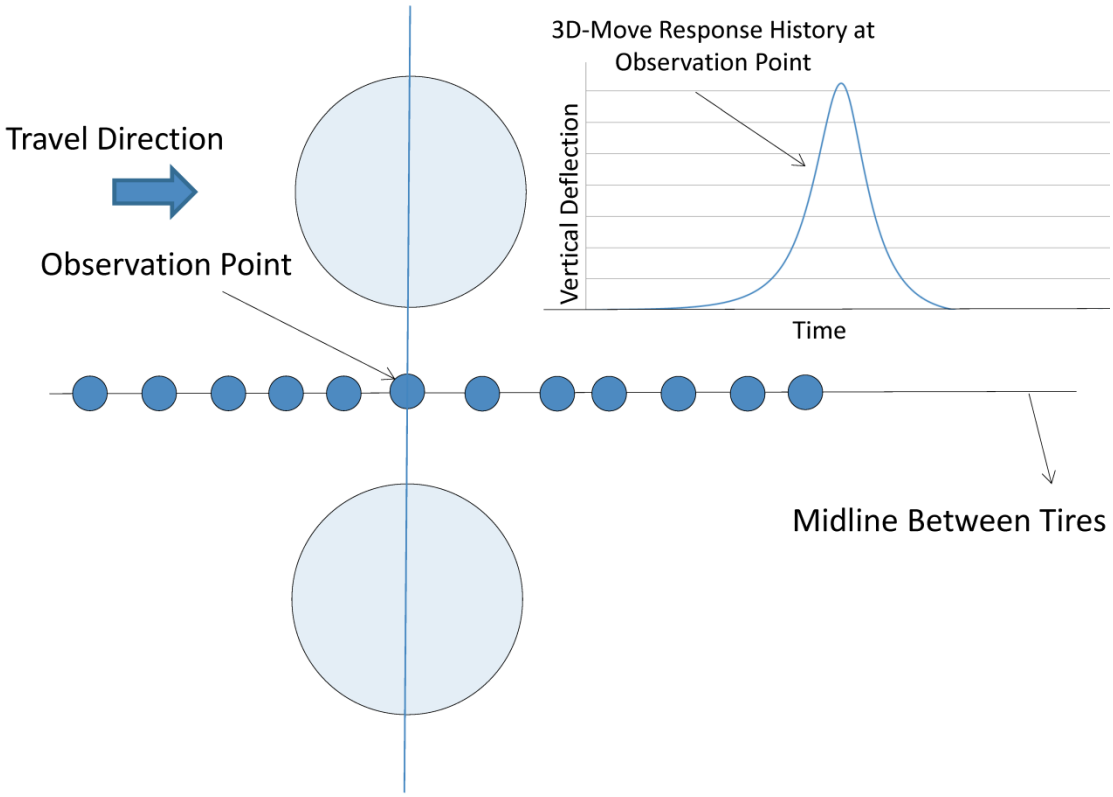

Figure 4-1. Vertical surface deflections from 3D-Move deflection time history

4.4. Field Trials

Figure 4-2 shows a Curviametro and the methodology used to measure surface deflections *(6)*. The vehicle is equipped with three geophones on a chain, but only one collects the deflection bowl at a particular point at a time. The constant speed and opposing directions of travel of the Curviametro vehicle and chain allow the geophone measurements to represent deflections at a stationary location on the pavement surface. The Curviametro geophone starts collecting data as soon as the rear axle is about 1 m (39 inches) away from the geophone's location and it stops collecting data once the rear axle has passed the geophone's location by approximately 3 m (118 inches) *(7)*. Therfore, it

can measure the entire deflection bowl. The loading characterization of the Curviametro will be explained in the next section.

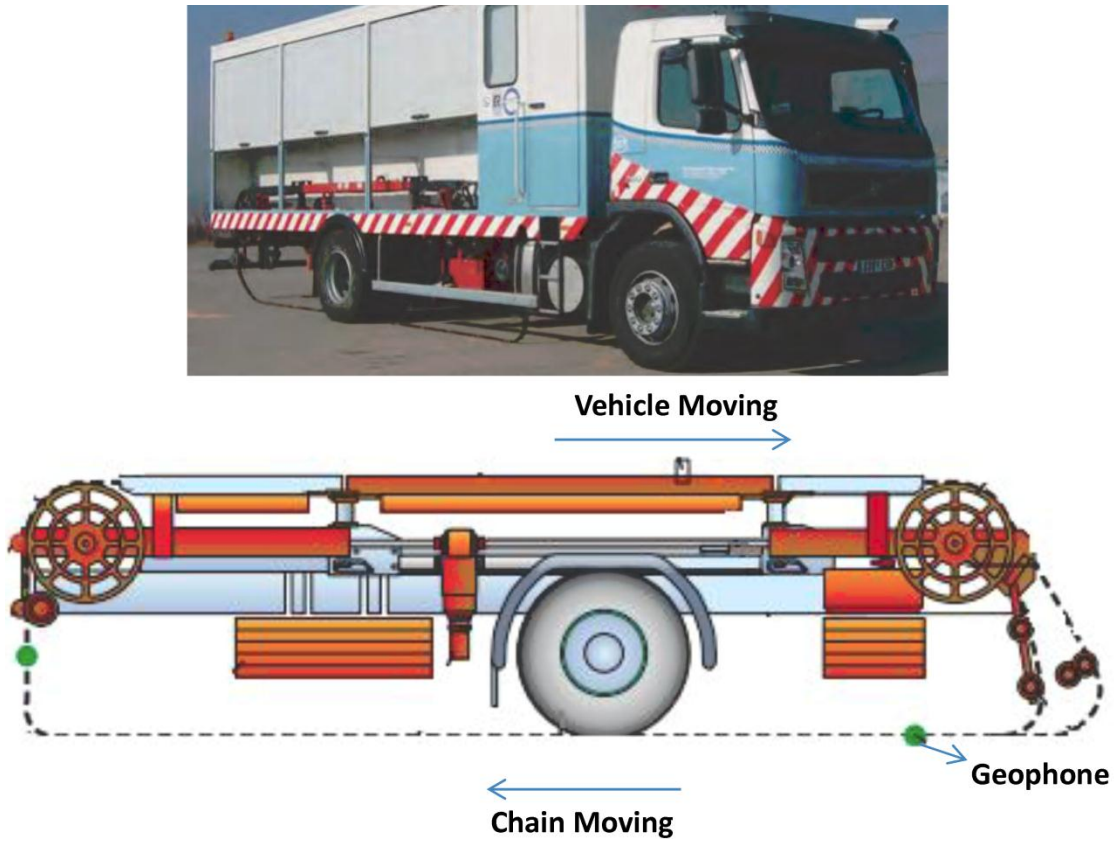

Figure 4-2. Curviametro device and schema during surface deflection measurements (6)

Four geophones were installed near the pavement surface (at the depth of 50 mm) along the right wheel path of Cells 3 and 19 of the MnROAD Mainline and Cell 34 of the MnROAD Low Volume Road. The configuration of embedded geophones at each of the sites referred to as project sensors subsequently, is shown in Figure 4-3. The intent was

for Geophones 1 and 3 to be along the midline of wheel path and during the trials, it was observed that the test vehicle geophones passed directly on top of these two sensors.

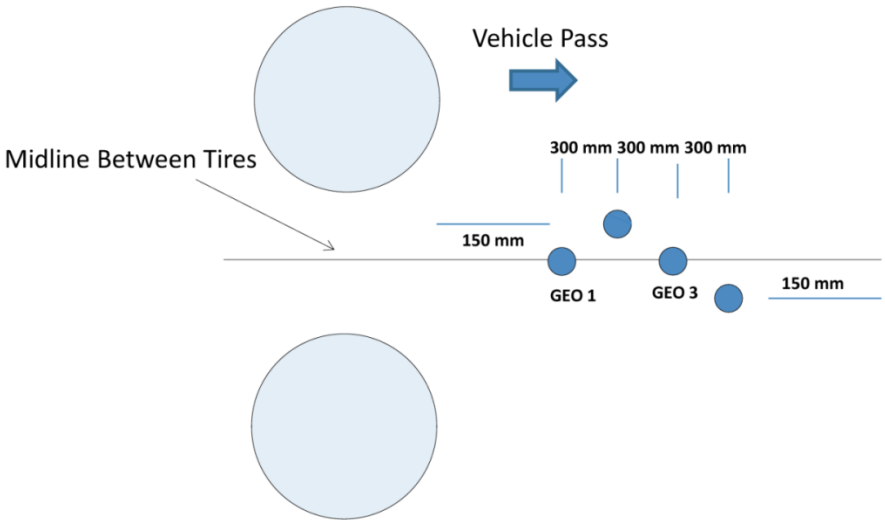

Figure 4-3. Configuration of embedded project sensors and spacing

The typical accuracy of the geophones is reported by the manufacturer as 2% of the measured deflection (no less than 5 µm, (±0.2 mils)). The performance of each project geophone was verified using an FWD. One of the FWD sensors was placed directly on top of one of the embedded sensors and then the deflection history reported by the FWD was compared with the corresponding deflections given by the embedded geophones. This effort gave quite similar deflection measurements.

Other existing instrumentations at the MnROAD facility collected data during the field trials for calibration and validation purposes. For example, longitudinal strain gauges capture the tensile strains at the bottom of the AC layer, while pavement layer temperatures were measured by thermocouple trees at a number of depths.

4.5. Material and Loading Characterization

MnROAD maintains a database containing laboratory and field-testing results on soils, aggregates, asphalt mixtures, asphalt binders, concrete mixtures, and other materials. The MnROAD database also contains cell-specific information, including layer thickness, type of layers and cross section of cells at time of construction and subsequent treatments (See http://www.dot.state.mn.us/mnroad/ for detail). FWD testing performed within a few days of the field trials facilitated the characterization of the pavement layer material properties.

Table 4-1 summarizes the backcalculated moduli and the nominal layer thicknesses for these cells, which were estimated using the widely-used MODULUS program *(8)*. The three flexible pavement sections covered three levels of stiffnesses. Cell 34, Cell 19 and Cell 3 were judged as soft, intermediate and stiff, respectively based on FWD testing.

Table 4-1. Backcalculated Pavement Layer Thicknesses and Moduli

Cell	Material	Thickness, mm. (in)	Average Modulus, MPa (ksi)	Standard Deviation, MPa, (ksi)	Coefficient of Variation (%)
3	AC	76 (3)	3820 (554)	234 (34.0)	14.0
	Base	1092 (43)	474 (68.8)	94 (13.6)	19.8
	Subgrade	3109 (122.4)	122 (17.7)	15 (2.2)	12.3
19	AC	127 (5)	2075 (301)	448 (65)	22.0
	Base	787 (31)	221 (32)	40 (5.8)	18.0
	Subgrade	460 (18.1)	42 (6.1)	4 (0.6)	10.2
34	AC	102 (4)	2062 (299)	462 (67.0)	22.0
	Base	305 (12)	108 (15.7)	21 (3.1)	19.9
	Subgrade	1176 (46.3)	59 (8.5)	6 (0.9)	10.2

These backcalculated modulus values may be considered appropriate for the site at the time of FWD testing. Since FWD testing and Curviametro trials were performed within a short period of one another and the review of climate at the site did not show significant changes in moisture content, the FWD backcalculated modulus values for the unbound layers at the three MnROAD cells were used directly as input in the 3D-Move runs. On the other hand, the AC layer moduli shown in Table 4-1 had to be temperature and frequency corrected to actual temperature and frequency corresponding to Curviametro trials for purposes of the 3D-Move simulations. This is because the existing AC moduli obtained from the backcalculation of FWD deflection data are appropriate for the temperatures at the time of FWD testing as well as for a frequency of about 30 Hz *(9)*.

A Thermocouple (TC) tree device was used at the three MnROAD cells to measure temperature within pavement layers. An alternate approach was adapted to estimate temperatures in case of missed or unreliable measured temperatures. Towards this end, the BELLS equation was selected for a number of reasons, which include its extensive calibration using data from the Long-Term Pavement Performance (LTPP study) *(10)*. Table 4-2 summarizes the average AC layer temperatures at the time of FWD and Curviametro testing.

Table 4-2. Average AC Layer Temperatures

Cell	Temperature at time of FWD, °C (°F)	Temperature at time of Curviametro, °C (°F)
3	37 (99)	38 (100)
19	27 (81)	18 (64)
34	42 (108)	30 (86)

The procedure used to develop the appropriate AC master curves took into account the following considerations:

1. Undamaged AC modulus as determined from Witczak-Andrei equation *(11)*;
2. FWD backcalculated modulus (in-situ or existing modulus); and
3. Existing modulus correction approach (Fatigue Damage Factor, d_{AC}) used in MEPDG overlay design.

One of the most comprehensive AC mixture stiffness models is Witczak-Andrei dynamic modulus predictive equation. This model predicts modulus as a function of temperature and frequency based on volumetric AC mix design information. Witczak-Andrei AC dynamic modulus equation *(11)* is given by:

$$\log E^* = -1.25 + 0.029\rho_{200} - 0.0018(\rho_{200})^2 - 0.0028\rho_4 - 0.058V_a - 0.822\frac{V_{beff}}{V_{beff}+V_a} + \frac{3.872-0.0021\rho_4+0.003958(\rho_{38})-0.000017(\rho_{38})^2+0.0055\rho_{34}}{1+e^{(-0.603313-0.313351\log(f)-0.393532\log(\eta))}} \quad (4.1)$$

where, E* = dynamic modulus of mix,10^5 psi

H = viscosity of binder,10^6 poise

f = loading frequency, Hz

ρ_{200} = % passing #200 (0.075 mm) sieve

ρ_4 = cumulative % retained on #4 (4.76 mm) sieve

ρ_{38} = cumulative % retained on 3/8 in. (9.5 mm) sieve

ρ_{34} = cumulative % retained on 3/4 in. (19 mm) sieve

V_a = air void, % by volume

V_{beff} = effective binder content, % by volume

The Equation (4.1) requires input such as gradation and viscosity; the gradation data for the three MnROAD cells were available from the MnROAD database, while viscosity values can be estimated as a function of temperature based on A and VTS viscosity temperature susceptibility *(12)* as follows:

$$\log\log\eta = A + VTS.logT_R \quad (4.2)$$

where, η = the viscosity, cP

T_R = the temperature at which the viscosity is estimated, Rankine

A = Regression Intercept

VTS = Regression slope of viscosity temperature susceptibility

The PG grades for the instrumented cells, which were estimated from available data, are PG70-16, PG64-22 and PG 58-34 for Cells 3, 19 and 34, respectively. Accordingly, the calculated A and VTS values are 10.641 and -3.548 for Cell 3, 10.98 and -3.68 for Cell 19, and 10.149 and -3.359 for Cell 34.

Having determined the A and VTS values, the Equation 4.1 was used to estimate the undamaged AC modulus as a function of temperature and frequency. The next step entailed the derivation of existing AC modulus at various frequencies and at the AC layer temperature corresponding to the time of the Curviametro testing based on the FWD backcalculated layer moduli. The existing AC moduli as a function of frequency was estimated by using the backcalculated AC layer moduli as anchor points and shifting the Witczak-derived AC modulus relationships. The AC existing modulus master curve is

obtained by applying the following equation to the E* computed from the original master curve *(13)*:

$$E^*_{dam} = 10^{\delta} + \frac{E^* - 10^{\delta}}{1 + e^{-0.3+5\times\log(d_{AC})}} \quad (4.3)$$

where, E^*_{dam} = Existing modulus

E* = Undamaged modulus for specific reduced time (from master curve)

δ = Regression parameter (from E* master curve)

d_{AC} = Fatigue damage in AC layer

Figure 4-4 shows the resulting existing moduli for the temperature associated with the Curviametro field tests at Cell 34 based on the procedure explained above. The similar curves were produced for other two cells. The master curves were used as the 3D-Move inputs. Having moduli at different frequencies provides flexibility for the program to pick the appropriate dynamic moduli corresponding to the frequency of the applied load. This is an important capability since Curviametro loading is at a lower frequency than the frequency associated with the FWD-based backcalculated AC modulus values.

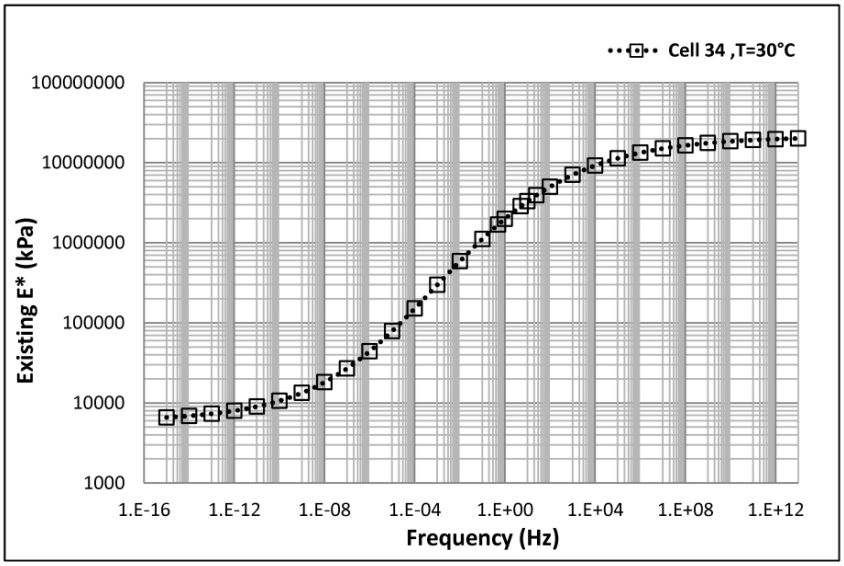

Figure 4-4. Existing moduli for Cell 34 in Curviametro field trials (average AC temperature = 30 ° C)

One of the important sets of input for analyzing pavement response is the applied load. During the Curviametro field trials, the loads carried by the axles were determined using a static scale owned and operated by MnROAD. Since the deflection measuring sensors for the Curviametro are mounted along the midline between two of the rear axle tires, the 3D-Move comparisons in this validation effort focused on the responses generated along this midline. Because data on the pavement-tire contact pressure distribution were not available, the rear axles were modelled as dual circular loads with uniform contact pressure in the 3D-Move analyses. The responses were calculated for dual tire load of 66.3 kN (14900 lb), tire pressure of 800 kPa (116 psi) and the dual tire spacing of 34.3 cm (13.5 in.).

4.6. Dynamic Simulation Results versus Field Measurements

As noted earlier, the pavement layer moduli and subgrade thickness used in the analyses were based on FWD backcalculated values. The backcalculation process assumes static loading conditions and the results of the backcalculation are sensitive to small variations in the input (e.g., thickness of AC and base layers). Geology in the area suggests that the subgrade thicknesses at the instrumented cell locations are substantially greater than those that were predicted from the backcalculation effort. A possible solution to address this issue is that analyses should consider changes to material properties and layer thicknesses when comparisons are made. As many as fifteen sets of input case scenarios were considered in the comparison effort. The following two input cases consistently provided the best comparison to the measured deflection responses.

Case 1: Three layer pavement structure with same thicknesses as used in the FWD backcalculation and corresponding mean layer moduli derived from the FWD backcalculation results;

Case X1: Three layer pavement with: (a) thicknesses used in the FWD backcalculation, (b) (mean – σ) of FWD backcalculated layer moduli for HMA and base layers, (c) (mean + σ) of FWD backcalculated layer moduli for subgrade;

As will be shown later in this section, the computed deflections and the pavement responses based on the above scenarios consistently compared well with the measured responses (strains and deflections) collected by the project and MnROAD sensors.

The computed deflection basin results from the analyses with 3D-Move using the case scenarios were initially compared with the measured values from the geophones.

Figure 4-5 illustrates the comparison of the computed and measured deflections for Cell 34 during the Curviametro runs. Since GEO1 and GEO3 are located along a plane parallel to the vehicle direction (Figure 4-3), they are expected to give very similar deflection bowls. Therefore, the responses from both of these sensors are shown in the figure. The variation between the deflection bowls given by these two sensors may be viewed as a measure of the overall variability in the measurements made by the project sensors and spatial variability that exists between the two sensor locations. The lower and upper bound of the project sensor data were arrived at by treating both GEO1 and GEO3 data as independent datasets in the presentation below. In all cases, 3D-Move adequately captured the maximum and shape of measured deflections. Maximum and minimum Curviametro measurements obtained from different trials are referred to as CRV / Max and CRV/ Min in this figure.

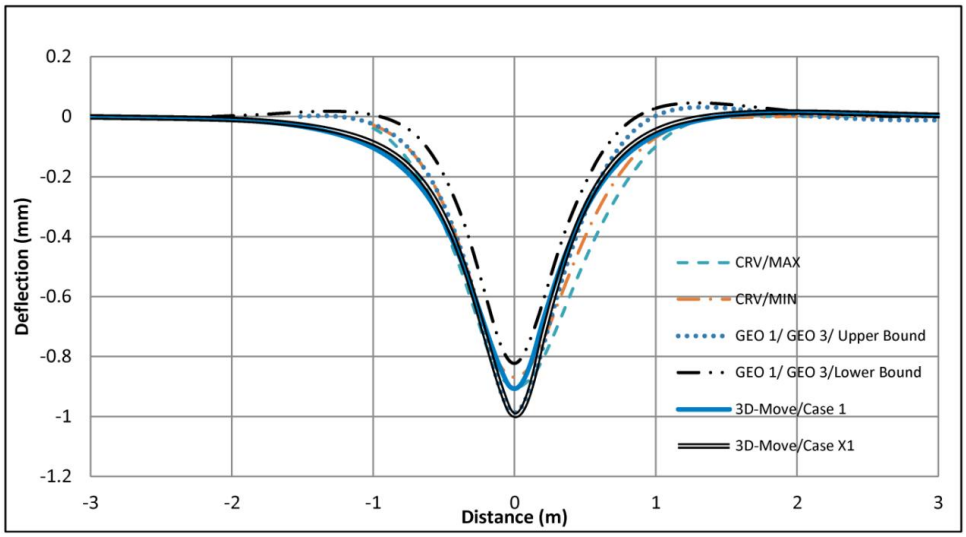

Figure 4-5. Predicted and measured surface deflections (Cell 34)

Figure 4-6 shows the comparison of maximum surface deflections computed and those measured by the project sensors for Curviametro trials. When project sensor

measurements were used, the largest deflection given by either GEO1 or GEO 3 was selected. The figure shows an excellent match between computed and measured maximum surface deflections.

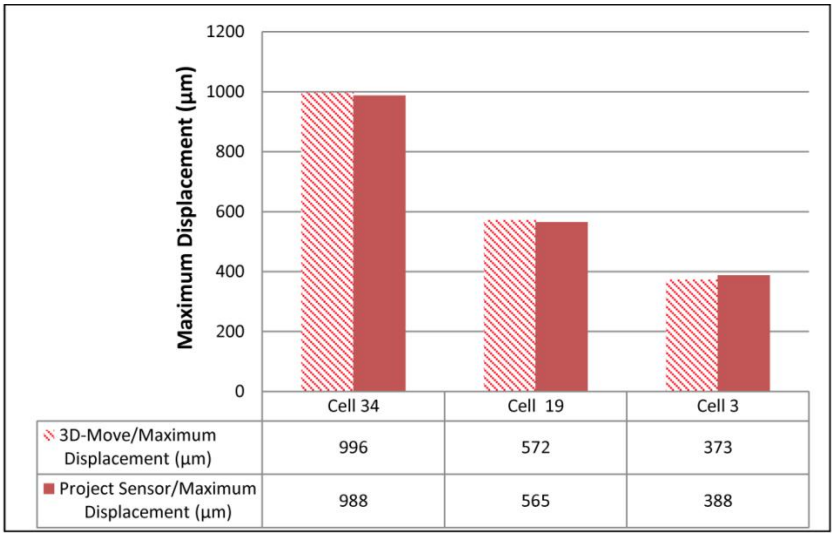

Figure 4-6. Predicted and measured maximum surface deflections

In addition to surface sensors, the measured strains at the MnROAD facility were compared with the results of analytical simulations. This comparison is important since a validated 3D-Move program can be subsequently used to obtain reliable deflection basin indices that relate well with the pavement response. The computed maximum horizontal tensile strains at the bottom of AC layers were compared with measured maximum strains from longitudinal strain gauges in the MnROAD facility. Figure 4-7 and Figure 4-8 show the comparison of results for Cells 34 and 3, which are the softest and the stiffest cells, respectively. As can be seen, the 3D-Move analyses can simulate the pavement responses well at both levels of stiffnesses. The maximum response is applicable for pavement distress predictions so the focus of the comparison was on the

maximum tensile strain. The comparison of measured and computed maximum response in all cells agreed well as shown in Figure 4-9.

The main objective of this section was the validation of the analytical tool with measured values from project and MnROAD sensors. The comparisons of computed and measured surface deflections and the pavement strain responses showed that dynamic simulations of slow moving deflection measurements could capture the measured values well. The analytical model can be used to develop the relationships between surface deflection basin indices and the pavement responses for the implementation of Curviametro in network level PMS applications.

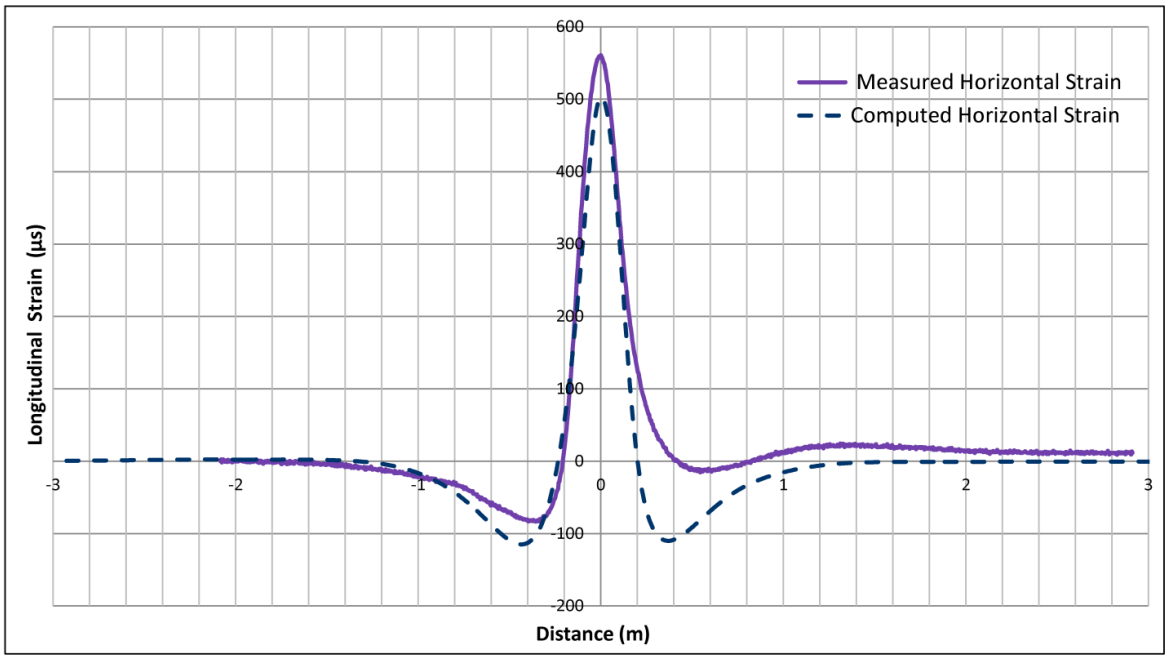

Figure 4-7. 3D-Move versus MnROAD maximum strain gauge measurements in Cell 34 (softest cell)

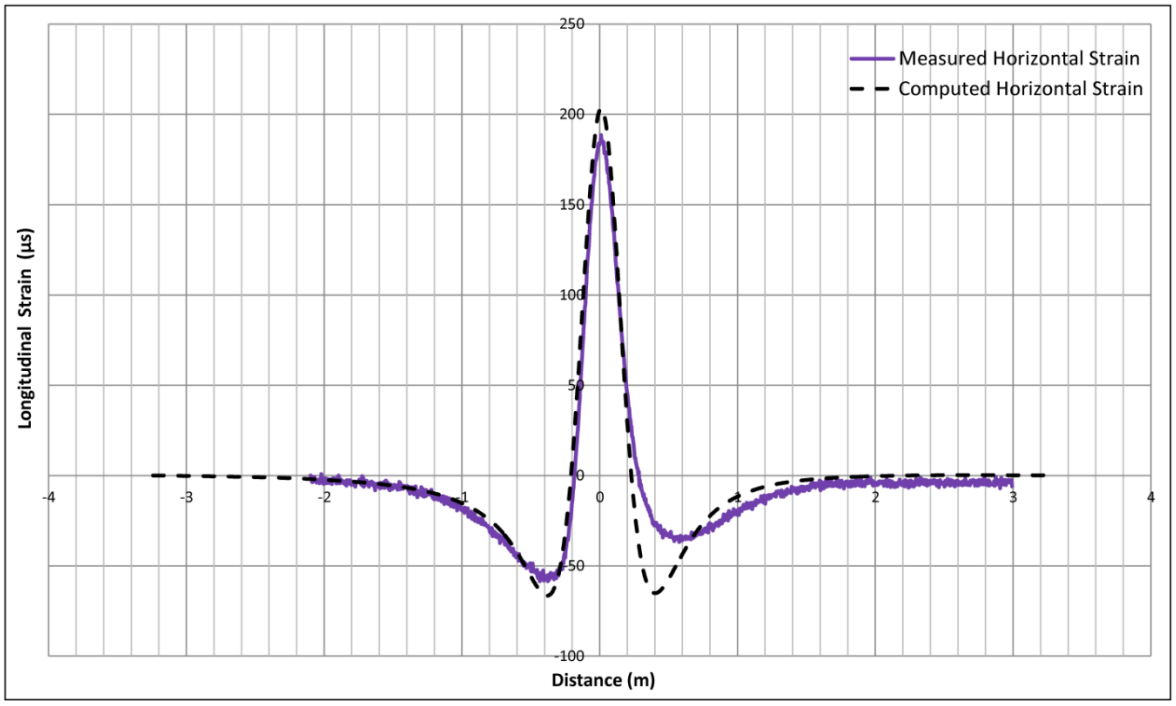

Figure 4-8. 3D-Move versus MnROAD maximum strain gauge measurements in Cell 3 (stiffest cell).

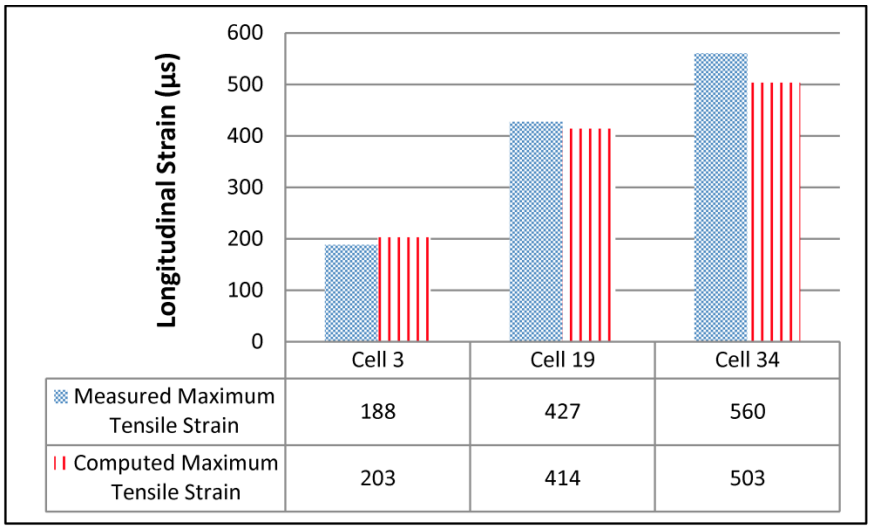

Figure 4-9. Predicted and measured maximum longitudinal strain at the bottom of AC layers

4.7. Conclusion

In this paper, the capability of dynamic simulation to evaluate slow moving surface deflection measurements was assessed using measured values from embedded sensors at the MnROAD facility during Curviametro runs conducted in September 2013. Dynamic simulations were performed based on the best estimates of the pavement layer properties that accounted for the actual pavement temperature at the time of testing and the rate of loading corresponding to Curviametro. The comparison of calculated and measured surface deflections showed that dynamic simulation can capture the entire deflection basin, including the maximum deflections well. Also, the predicted maximum tensile strains at the bottom of AC layer (considered as one of the critical pavement responses) from the analytical simulations were close to the measured responses from the MnROAD sensors. Finally, it can be concluded that 3D-Move based dynamic analyses can simulate slow moving deflection measurements properly and can be used to identify surface deflection indices that correlate well with critical pavement responses. Since such correlations can be readily incorporated into network level PMS applications, devices that measure moving deflections are seen as cost effective tools to determine remaining structural life and pavement performance.

Acknowledgements

This study was funded through the FHWA study DTFH61-12-C-00031 and their support is gratefully acknowledged. The authors would especially like to thank Dr. Nadarajah Sivaneswaran of the FHWA and Dr. Senthil Thyagarajan of ESC, Inc. for their kind support. The authors would also like to thank Mr. Ben Worel and the rest of the

MnROAD staff without whose help, the successful outcome of the project would not have been possible. The conclusions presented in this paper are solely those of the authors.

4.8. Reference

1. Schmalzer, P. N. *Long-Term Pavement Performance Program Manual for Falling Weight Deflectometer Measurements*. Publication FHWA-HRT-06-132, FHWA, U.S. Department of Transportation, 2007.
2. Rada, G., Nazarian, S., Visintine, B., Siddharthan, R.V., and Thyagarajan, S. *Pavement Structural Evaluation at the Network Level.* (under review for possible publication) FHWA- DTFH61-12-C-00031, FHWA, U.S. Department of Transportation, 2015.
3. Siddharthan, R.V., Yao, J., and Sebaaly, P.E. Pavement Strain from Moving Dynamic 3-D Load Distribution. *Journal of Transportation Engineering, ASCE,* Vol. 124, No. 6, 1998, pp. 557-566.
4. Zafir, z., Siddharthan, R., and Sebbaly, P.E. Dynamic Pavement Strain from Moving Traffic Loads. *Journal of Transportation Engineering, ASCE,* Vol. 120, No. 5, 1994, pp. 821-842.
5. Magdy, El-Desouky. *Further developments of 3DMOVE and its engineering applications*. PhD dissertation, University of Nevada, Reno, 2003.
6. COST 325. *New Road Monitoring Equipment and Method*. Final Report of the Action, European Commission Directorate General Transport, 1997.

7. Van Geem, C. Overview of Interpretation Techniques based on Measurement of Deflections and Curvature Radius Obtained with the Curviameter. *6th European FWD User's Group Meeting, Sterrebeek,* 10-11 June 2010.
8. Liu, W. and Scullion, T. *MODULUS 6.0 for Windows: User's Manual*. FHWAS/TX-05/0-1869-2, Texas Transportation Institute, Texas A&M Uni., College Station, Texas, 2001.
9. Irwin, L. H., Orr, D. P., and Atkins, D. *FWD Calibration Center and Operational Improvements: Redevelopment of the Calibration Protocol and Equipment*. Publication FHWA-HRT-07-040. FHWA, U.S. Department of Transportation, 2009.
10. ASTM D7228-06a. *Standard Test Method for Prediction of Asphalt-Bound Pavement Layer Temperatures*. ASTM International, West Conshohocken, PA, 2011, DOI: 10.1520/D7228-06AR11, www.astm.org.
11. Kim, Y.R., Underwood, B., Sakhaei Far, M., Jackson, N., and Puccinelli, J. *LTPP Computed Parameter: Dynamic Modulus*. Publication FHWA-HRT-10-035, FHWA, U.S. Department of Transportation, 2011.
12. Velasquez, R., Hoegh, K., Yut, I., Funk, N., Cochran, G., Marasteanu , M., and Khazanovich, L. *Implementation of the MEPDG for New and Rehabilitated Pavement Structures for Design of Concrete and Asphalt Pavements in Minnesota.* Report No. MN/RC 2009-06, Minnesota Department of Transportation, St. Paul, MN, 2009.
13. Loulizi, A., Flintsch, G., and McGhee, K. Determination of In-Place Hot-Mix Asphalt Layer Modulus for Rehabilitation Projects by a Mechanistic-Empirical

Procedure. *In Transportation Research Record: Journal of the Transportation Research Board, No.2037*. Transportation Research Board of the National Academies, Washington. D.C., 2007, PP. 53-62.

5. Robust Deflection Indices from Traffic Speed Deflectometer Measurements to Predict Critical Pavement Responses for Network Level PMS Application

Mahdi Nasimifar[1], Senthilmurugan Thyagarajan [2], Raj V. Siddharthan[3], Nadarajah Sivaneswaran[4]

[1] Graduate Research Assistant, University of Nevada – Reno, Department of Civil & Environmental Engineering, 1664 N. Virginia St., Reno, Nevada, USA , **nasimifar@nevada.unr.edu.**

[2] Research Engineer, ESC Inc., Turner Fairbank Highway Research Center, 6300 Georgetown Pike, McLean, Virginia, USA, **senthil.thyagarajan.ctr@dot.gov.**

[3] Professor, University of Nevada – Reno, Department of Civil & Environmental Engineering, 1664 N. Virginia St., Reno, Nevada, USA, **siddhart@unr.edu**.

[4] Senior Civil Research Engineer, Federal Highway Administration, Turner Fairbank Highway Research Center, 6300 Georgetown Pike, McLean, Virginia, USA, **nadarajah.sivaneswaran@dot.gov.**

5.1. Abstract

Traffic Speed Deflectometer (TSD) is used in several countries to evaluate the pavement structural condition at the network level. Fatigue and rutting strains are commonly used as pavement critical responses in the mechanistic-empirical design procedures to predict pavement structural performance. For successful PMS application, robust indices that can be readily computed from TSD measurements and best related to the pavement critical responses should be identified. In this study, a comprehensive sensitivity analysis on deflection basin indices and their correlations with fatigue and rutting strains was performed using a range of pavement structures. The 3D-Move program was used in the first part of the study to compute dynamic deflection basins and evaluate the effects of material properties and vehicle speed on the indices. The indices that best relate to critical responses were identified from the 3D-Move analyses and subsequently evaluated with a wider range of pavement structures analyzed using the layered linear-elastic program, JULEA. Results from the TSD accuracy field evaluation were then used to further identify the robust indices in light of measurement accuracy. The study found that classifying pavement structures based on AC thickness would be an appropriate selection for network level PMS applications. Evaluation of 67 deflection basin indices showed that Deflection Slope Indices, $DSI_{200\text{-}300}$ ($D_{200} - D_{300}$) and $DSI_{300\text{-}900}$ ($D_{300} - D_{900}$) were well related indices with fatigue and rutting strains, respectively, and were selected to establish relationships with critical pavement responses for pavement categories based on AC layer thickness.

Keywords: Load-induced pavement response, Deflection basin indices, Correlation equations, Pavement management system, Structural capacity, Traffic speed deflectometer.

5.2. Introduction and Methodology

Structural evaluation of pavement condition is an important part of a network level pavement management system (PMS) *(1)*. The maximum tensile horizontal strain at the bottom of the asphalt concrete (AC) layer and the maximum vertical compressive strain on top of the subgrade are two critical load-induced pavement responses used in the mechanistic-empirical design procedure *(2)*. These critical responses are used in performance prediction equations *(2, 3)* to predict the amount of AC fatigue cracking and subgrade rutting over time and subsequently design life (or structural capacity). For brevity, fatigue and rutting strains are used to denote the maximum horizontal strain at the bottom of the AC layer and the maximum vertical strain on top of the subgrade, respectively.

Surface deflection is the response of the pavement structural system (surface-base-subgrade) to the applied load *(4)*. Past studies *(5-7)* have shown that critical pavement responses can be estimated from correlations with vertical surface deflection basin indices. Pavement material properties influence both the magnitude and the shape of deflection basins. Thus, the effectiveness of the deflection indices to predict pavement responses need to be evaluated based on various pavement layer properties.

Traffic Speed Deflectometers (TSDs) are used in several countries to evaluate pavement structural conditions at network level. The TSD utilizes Doppler lasers to

measure the vertical surface deflection velocity (the velocity that the pavement deflects due to the moving load) at 6 points along the midline of the rear right dual tires and in front of the axle (at 100, 200, 300, 600, 900 and 1500 mm) as shown in Figure 5-1. A theoretical algorithm is used to compute the deflection basin that matches with the TSD measurements *(8)*. Currently, the measurements from TSD are mostly used to screen structurally poor from relatively stronger sections. However, the full benefit of TSD measurements can be achieved when it is periodically used to evaluate and track actual structural pavement performance to aid highway agencies in more informed decision making in PMS application.

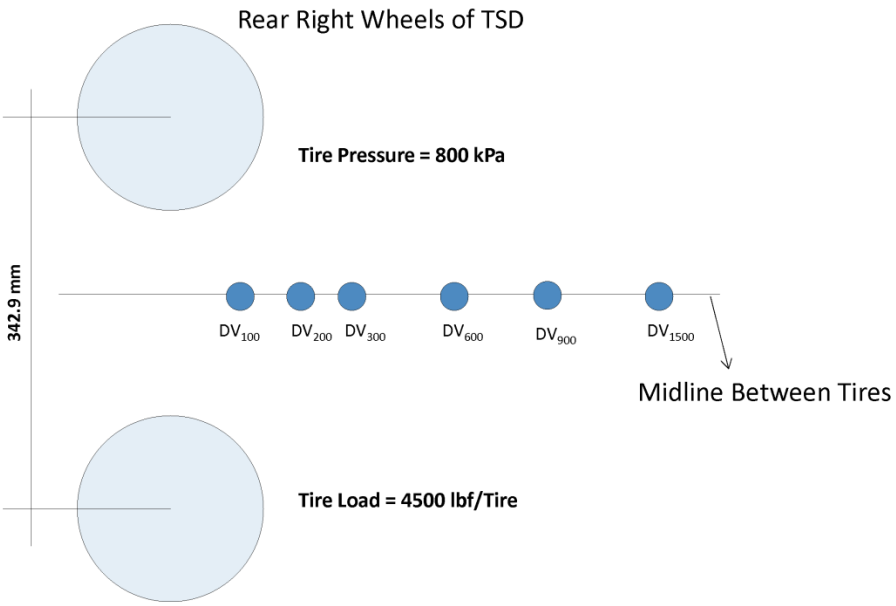

Figure 5-1. TSD rear axle configuration and location of Doppler sensors (DV= Deflection velocity)

Improved computer capabilities have enabled the consideration of a large number of influencing factors in the simulation of realistic pavement conditions. The 3D-Move program was chosen for the first part of this study as it can generate dynamic pavement responses and consider important factors such as vehicle speed and viscoelastic characterization of the AC layer. The 3D-Move model is based on finite-layer approach that uses the Fourier transform technique to evaluate the responses of layered medium subjected to moving loads traveling at a constant speed *(9-11)*. Many field calibrations that compared a variety of independently-measured pavement responses (stresses, strains, and displacements) with those computed from 3D-Move have been reported in previous studies *(12-14)*. The capability of 3D-Move program to simulate traffic speed deflectometer measurements and corresponding pavement responses was validated in a recent technical paper *(15)*.

In this study, the sensitivity analysis of the correlations between deflection basin indices and the critical pavement responses was first performed using the 3D-Move program. The analyses were done with different input values for the pavement properties (such as the AC layer thickness and modulus and the subgrade modulus) as well as the vehicle speed. The intent was to find the most important input parameters that significantly influence the correlations between the indices and the critical pavement responses. Those parameters can be used to select appropriate distinct pavement groups for developing the relationships between the indices and the pavement responses. The results were also used to identify the set of indices that have the highest correlation with fatigue and rutting strains. However, the computation time and other issues (pre-and post-processing) involved in 3D-Move analyses limited its utility in the simulation-based

sensitivity analyses. The layered linear-elastic program, JULEA, *(16)* was then used to analyze a wider range of pavement structures. A database of 15,000 pavement structures was developed using a Monte Carlo simulation covering a wide range of pavement, base and subgrade layer properties. The JULEA database was used to evaluate the most sensitive pavement properties which influence the critical pavement responses. The JULEA database was subsequently used to evaluate the set of sensitive deflection indices identified by 3D-Move sensitivity analyses in a larger database. From the set of well correlated deflection indices, those that can be accurately measured by a TSD device were identified. Relationships were then developed between selected indices and the pavement responses for possible PMS application.

5.3. Background and Objective

Much work has been done over the past decades towards finding deflection basin indices that correlated with critical pavement responses for use in Falling Weight Deflectometer (FWD) testing. Park et al. indicated that deflection basin indices and critical pavement responses are significantly affected by the structural and material properties of a flexible pavement *(17)*. Xu et al. found a correlation between rutting strain and both Base Damage Index ($BDI = D_{300} - D_{600}$) and Base Curvature Index ($BCI = D_{600} - D_{900}$) *(6)*. The subscripts refer to the distance in millimeter from the center of the FWD load. The study also used the surface curvature index ($SCI_{300} = D_o - D_{300}$) and BDI to estimate fatigue strain considering AC thickness and base thickness in the correlations. It is believed that the indices based on differences between the surface deflections can isolate

the role of individual pavement layers and best relate to the properties of certain underlying layer *(18)*.

Kilareski and Anani reported that BCI represented the strength of the lower portion of the pavement system that can relate well with the subgrade modulus *(19)*. Modified BDI ($D_{300} - D_{900}$) and modified BCI ($D_{900} - D_{1500}$) were recommended as valuable indices in identifying the location of damage in the pavement layer system *(20)*. However, they suggested that for thin asphalt layers, considering other indices is required. Horak stated that SCI_{300} indicates the strength of the upper portion of a pavement structure and thus the index is influenced by the AC and the base modulus *(5)*.

However, most of the studies considered the FWD loading and did not account for the dynamic deflection basin and loading configuration that are associated with the Traffic Speed Deflectometer (TSD) that has recently been developed for network level pavement structural evaluation. This paper presents the details of a comprehensive investigation to quantify the effects of pavement layer properties on the relationships between the critical responses and an extensive list of pavement deflection basin indices.

5.4. Evaluation of Deflection Indices using Dynamic Deflection Basin

5.4.1. Deflection Basin Indices

A list of as many as 67 indices selected for investigation is shown in Table 5-1. These indices can be calculated from the surface deflection basin parameters using the equations presented in the table. The Surface Curvature Index ($SCI = D_o - D_r$) used D_o as reference deflection, where D_o is the deflection at the midpoint between tires. The widely used index with TSD is the SCI_{300} ($D_o - D_{300}$). A new index referred to as the Deflection

Slope Index (DSI) with D_{100} and D_{200} as reference deflections was also considered in this study. In flexible pavements, viscous response lag are observed with moving load and hence maximum deflection (D_{max}) will not always be equal to D_o which is used as reference deflection in SCI. Therefore, a new index (SCI_m) is defined with D_{max} as the reference deflection. Many other indices that relate to radius of curvature, area under the deflection basin, shape factors, etc. are defined in Table 5-1. It should be noted that many of these indices have been proposed by researchers in the past. D_r in all equations in Table 5-1 is the deflection at distance r from the midpoint between dual tires.

5.4.2. Pavement Layer Configuration and Properties

A three layer pavement system was considered. 3D-Move sensitivity analyses varied the asphalt layer modulus and thickness, subgrade layer modulus and vehicle speeds, resulting in a total of 36 different analyses. Table 5-2 summarizes the different pavement layer properties and vehicle speeds used in the factorial design. The impact of pavement temperature is reflected in the AC modulus and therefore it was not considered as an independent variable. The AC modulus as a function of frequency (master curve) needs to be specified as input when the viscoelastic material characteristics are considered in 3D-Move. Typical master curves were generated for pavements at poor, moderate and good condition using the Witczak-Andrei dynamic modulus equation and the approach suggested by Seo et al. *(21)*. The AC moduli given in the table are values computed from the master curves at 30Hz.

Table 5-1. Deflection basin indices used in the evaluation**

Parameter and Number of Indices	Indices for Evaluation
Radius of Curvature (7) $R = r^2/(2D_0(D_0/D_r - 1))$	R_{200}
	R_{300}
	R_{450}
	R_{600}
	R_{900}
	R_{1200}
	R_{1500}
Surface Displacement (2)	D_0
	D_{1500}
Area (1) $A = 6[1 + 2(D_{300}/D_0) + 2(D_{600}/D_0) + D_{900}/D_0)]$	A
Shape Factors (2) $F_1 = (D_0 - D_{600}) / D_{300}$ $F_2 = (D_{300} - D_{900}) / D_{600}$	F_1
	F_2
Surface Curvature Index (7) $SCI = D_0 - D_r$	SCI_{200}
	SCI_{300}
	SCI_{450}
	SCI_{600}
	SCI_{900}
	SCI_{1200}
	SCI_{1500}
Base Curvature Index (1) $BCI = D_{600} - D_{900}$	BCI
Base Damage Index (1) $BDI = D_{300} - D_{600}$	BDI
Area Under Pavement Profile (1) $(5D_0 - 2D_{300} - 2D_{600} - D_{900})/2$	AUPP
Slope of Deflection (7) $SD = \tan^{-1}(D_0 - D_r)/r$	SD_{200}
	SD_{300}
	SD_{450}
	SD_{600}
	SD_{900}
	SD_{1200}
	SD_{1500}

Parameter and Number of Indices	Indices for Evaluation
Tangent Slope (8) TS= (dD/dr)	TS_{100}
	TS_{200}
	TS_{300}
	TS_{450}
	TS_{600}
	TS_{900}
	TS_{1200}
	TS_{1500}
Surface Curvature Index(7) $SCI_m = D_{max} - D_r$	$SCIm_{200}$
	$SCIm_{300}$
	$SCIm_{450}$
	$SCIm_{600}$
	$SCIm_{900}$
	$SCIm_{1200}$
	$SCIm_{1500}$
Deflection Slope Index(7) $DSI_{100-r} = D_{100} - D_r$	$DSI_{100-200}$
	$DSI_{100-300}$
	$DSI_{100-450}$
	$DSI_{100-600}$
	$DSI_{100-900}$
	$DSI_{100-1200}$
	$DSI_{100-1500}$
Deflection Slope Index(6) $DSI_{200-r} = D_{200} - D_r$	$DSI_{200-300}$
	$DSI_{200-450}$
	$DSI_{200-600}$
	$DSI_{200-900}$
	$DSI_{200-1200}$
	$DSI_{200-1500}$
Deflection Slope Index (4) $DSI_{300-r} = D_{300} - D_r$	$DSI_{300-450}$
	$DSI_{300-600}$=BDI
	$DSI_{300-900}$
	$DSI_{300-1200}$
	$DSI_{300-1500}$
Deflection Slope Index (4) $DSI_{450-r} = D_{450} - D_r$	$DSI_{450-600}$
	$DSI_{450-900}$
	$DSI_{450-1200}$
	$DSI_{450-1500}$
Deflection Slope Index (2) $DSI_{600-r} = D_{600} - D_r$	$DSI_{600-900}$=BCI
	$DSI_{600-1200}$
	$DSI_{600-1500}$

** Numbers within the parentheses indicate the number of indices for each deflection basin parameter

Table 5-2. Pavement structures used with the 3D-Move analyses

Vehicle Speed		**Asphalt**		**Base**		**Subgrade**
		Thickness	Modulus	Thickness	Modulus	Modulus
48 kph (30 mph)	96 kph (60 mph)	76 mm (3 in.) 152 mm (6 in.) 305 mm (12 in.)	1379 MPa (200 ksi) 3447 MPa (500 ksi) 5516 MPa (800 ksi)	305 mm (12 in.)	414 MPa (60 ksi)	69 MPa (10 ksi) 138 MPa (20 ksi)

5.4.3. 3D-Move Deflection Basins

Figure 5-2 illustrates a typical vertical surface deflection time history computed by 3D-Move for a moving load with constant speed at a point (observation point) on the midline between the dual tires where the TSD measurements are also made. The time t_o refers to the time when the midpoint of the dual tires passes over the observation point. Viscoelastic behavior of the AC layer and the moving load will cause viscous lag, i.e., the maximum deflection (D_{max}) occurs behind t_o as shown in Figure 5-2. The deflection at different individual locations along the midline can be computed from the vertical displacement time history by time-space superposition. The figure also presents the locations where the deflections are computed for the indices presented in Table 5-1.

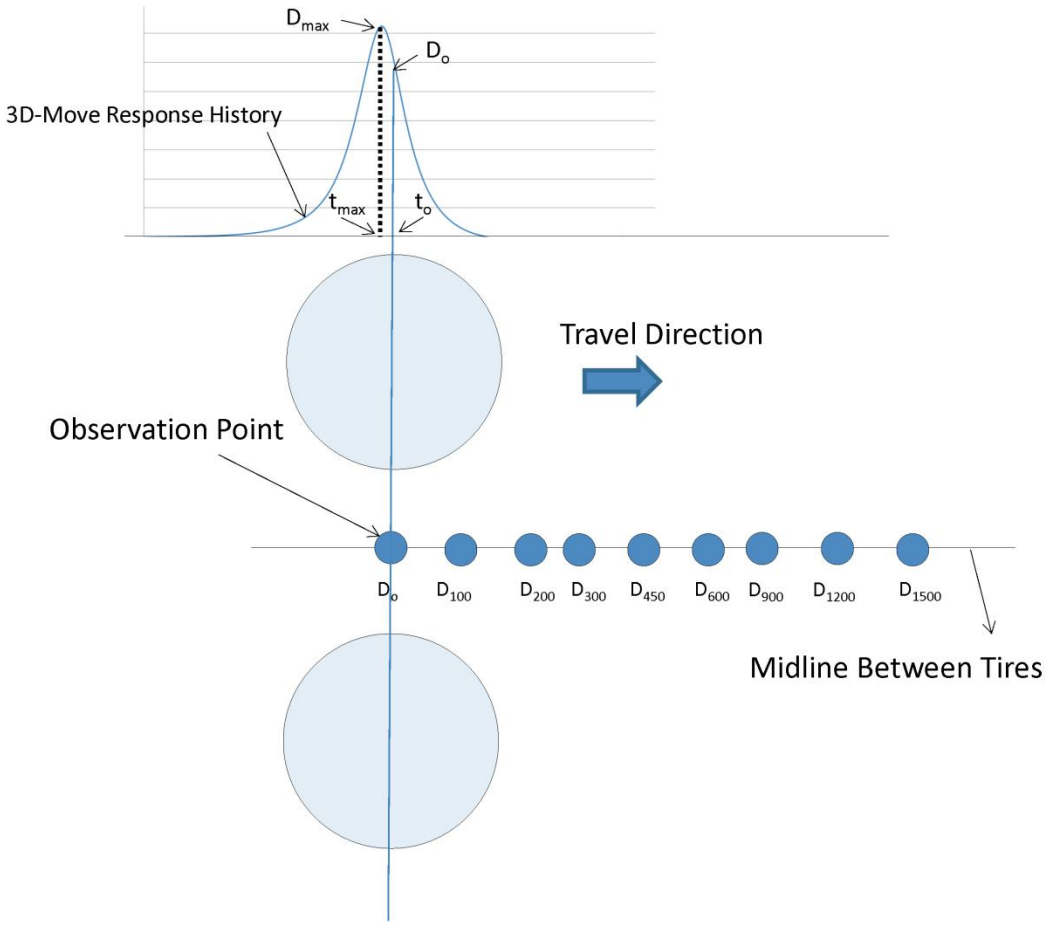

Figure 5-2. Vertical surface deflections from 3D-Move displacement time history

The maximum strain response doesn't always occur at the midline of the dual tires. Based on the pavement layer characteristics and loading configuration, the maximum strain response can occur at any of the transverse locations under the dual tires. Thus, in order to capture the maximum response computed by the 3D-Move program, the two critical responses noted above are computed at several transverse locations at 2.5 cm (1 in.) intervals as shown in Figure 5-3. The maximum computed strain is subsequently used in the analysis.

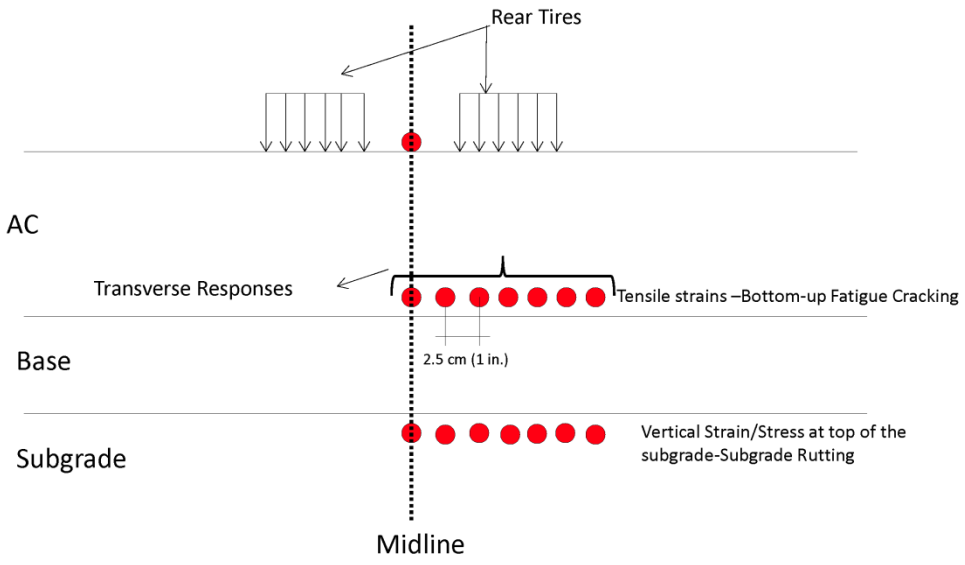

Figure 5-3. Selection of transverse response points to capture the maximum response

In general, 3D-Move sensitivity analyses show a decrease in both critical responses with an increase in the parameters under consideration (AC modulus and thickness, subgrade modulus and vehicle speed). However, for thin pavements (AC layer thickness of 76 mm (3in.)), increasing the subgrade stiffness doesn't have a clear trend on fatigue strain. Because of the limited dataset used in the 3D-Move analyses, the quantification of the sensitivity of pavement properties on responses was carried out in the next section using the much larger JULEA generated database.

The 3D-Move sensitivity analyses relative to the indices listed in Table 5-1 with respect to the AC thickness and modulus, subgrade modulus, and vehicle speed are presented in Figure 5-4 and Figure 5-5. These figures show the R^2 of the correlations of $DSI_{100\text{-}r}$ to the fatigue strain and $DSI_{300\text{-}r}$ to the subgrade rutting strain, respectively.

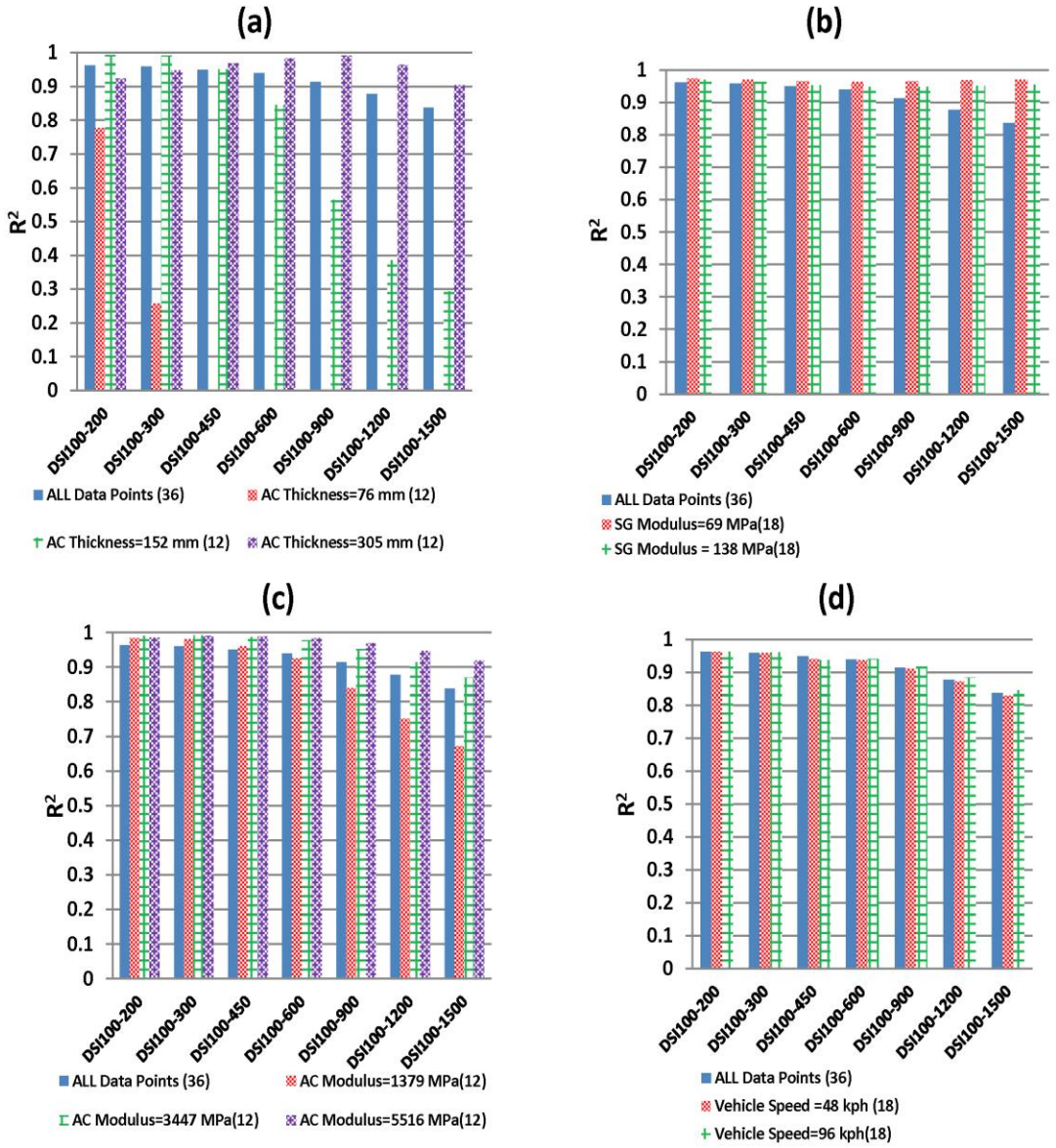

Figure 5-4. Variability of relationships of $DSI_{100\text{-}r}$ with fatigue strain for various (a)AC thickness, (b) subgrade modulus, (c) AC modulus and (d) vehicle speed (the numbers within parentheses in the legends indicate the number of data points)

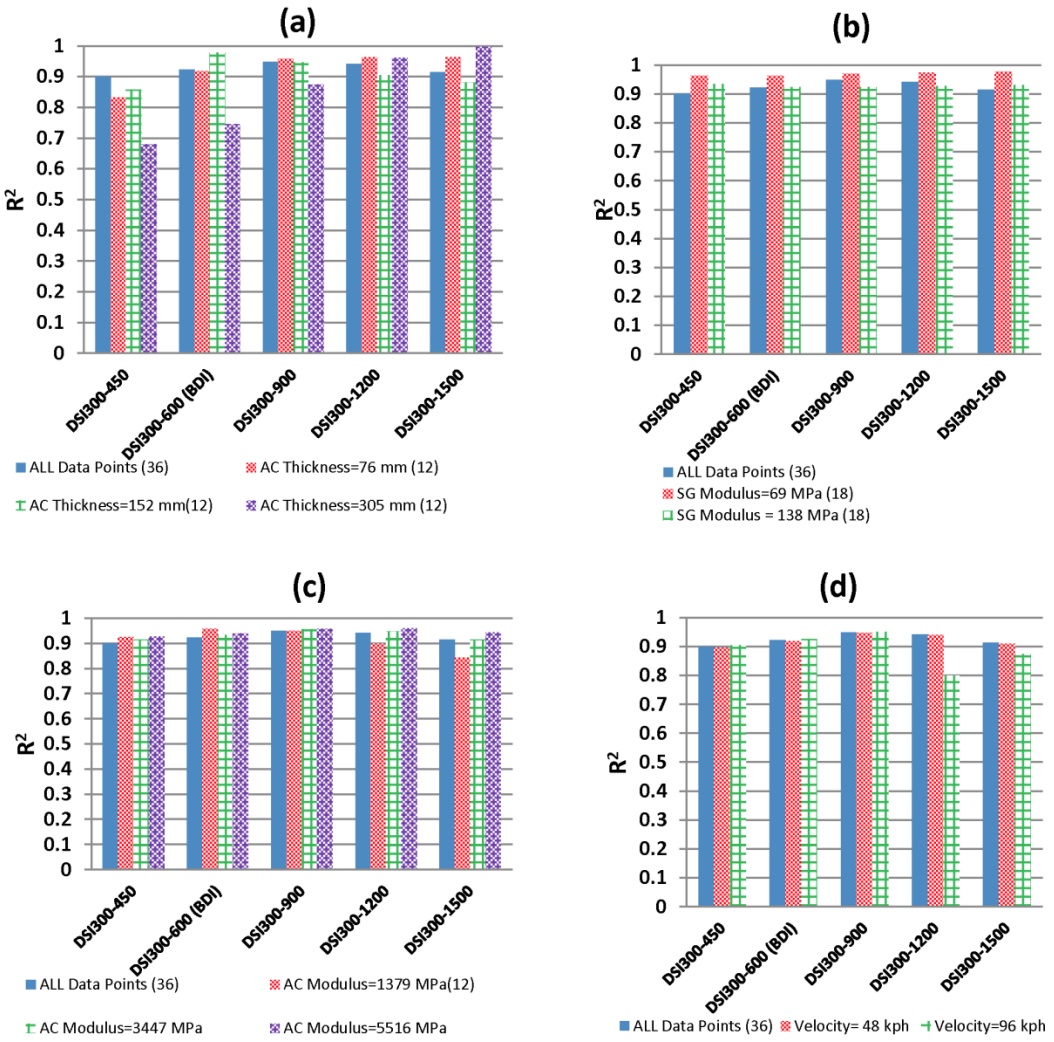

Figure 5-5. Variability of relationships of $DSI_{300\text{-}r}$ with rutting strain for various (a)AC thickness, (b) subgrade modulus, (c) AC modulus and (d) vehicle speed (the numbers within parentheses in the legends indicate the number of data points)

The coefficient of determination, R^2, is a measure of the best-fit between the variables. The sensitivity analyses for other indices showed similar trends but are not presented here because of space constraints. In summary, the following observations and conclusions were made based from the 3D-Move sensitivity analyses:

- AC thickness is the most sensitive parameter that impacts both responses (fatigue and rutting strains) as judged by changes in R^2 values with AC thickness (Figures 4.a and 5.a). However, the effect of AC thickness is less on the correlations with rutting strain as seen in Figure 5.a. Subgrade modulus, AC modulus and vehicle speed seem to affect the indices only marginally (similar values of R^2).

- It was noted that TSD users have routinely used SCI_{300} ($D_o - D_{300}$) as an index to relate pavement conditions, while it was found that the Deflection Slope Index (DSI) with D_{100} and D_{200} as reference deflections are also well correlated index families with the fatigue strain. Therefore, DSI appears to be a reliable alternative for SCI_{300} that can be used effectively to relate with fatigue strain. Index families farther away from the load ($DSI_{300\text{-}r}$, $DSI_{450\text{-}r}$ and $DSI_{600\text{-}r}$) appear to relate well with the vertical subgrade strain.

- Using D_{max} instead of D_o to calculate SCI does not significantly improve the correlation. Since TSD does not have sensors behind the wheel to capture the maximum deflection, D_{max} cannot be accurately computed from the current deflection algorithm. Therefore, SCIm indices were not given further consideration in this study.

- Based on the 3D-Move results, it was recommended that the pavements be categorized into the following three groups for selecting indices that have the highest correlation with the load-induced pavement responses:

  AC surface layer less than 76 mm (3 in.).

  AC surface layer between 76 and 152 mm (3 and 6 in.).

AC surface layer greater than 152 mm (6 in.).

Table 5-3 presents the indices that best related to fatigue and rutting strains for each class of pavement thickness based on 3D-Move results.

Table 5-3. Selective indices based on AC thickness

AC Thickness of Pavement Section	Indices Related to Fatigue Strain	Indices Related to Rutting Strain
Between 76 mm (3 in.). And 152 mm (6 in.)	$R_{300,}$ $R_{450,}$$SCI_{300}$, SCI_{200}, $DSI_{100\text{-}200}$, $DSI_{100\text{-}300}$, $DSI_{200\text{-}300}$, $DSI_{200\text{-}450}$,TS_{100},AUPP	$DSI_{300\text{-}600}$ (BDI), $DSI_{300\text{-}900}$, $DSI_{450\text{-}900}$, $DSI_{600\text{-}900}$ (BCI), $DSI_{600\text{-}1200}$,TS_{300}
Greater than 152 mm (6in.)	R_{300}, R_{450}, SCI_{300}, SCI_{450}, $DSI_{100\text{-}200}$, $DSI_{100\text{-}300}$, $DSI_{100\text{-}450}$, $DSI_{200\text{-}300}$, $DSI_{200\text{-}450,}$ TS_{100}, TS_{200}, TS_{300}, AUPP	$DSI_{450\text{-}900}$, $DSI_{600\text{-}900}$(BCI), $DSI_{300\text{-}600}$ (BDI), $DSI_{300\text{-}900}$, TS_{600}

5.5. Evaluation of Selective Indices with JULEA Simulations

An effective sensitivity analysis involves simulation technique that can (1) sample the input variables collectively based on their potential variability and (2) evaluate their effect on the specific distress of a pavement structure. The computation time involved with 3D-Move analyses limited its utility in simulation-based sensitivity analyses. Consequently, the comprehensive JULEA database was used to evaluate the results from 3D-Move sensitivity analyses and develop relationships between deflection indices and fatigue and rutting strains.

A database of 15,000 pavement structures was generated using the Monte Carlo simulation, considering a uniform distribution for the layer modulus and thickness ranges presented in Table 5-4. The loading configuration corresponding to a typical TSD was used. A static load of 40 kN (9,000 lbf) on a dual tire configuration with tire pressure of

800 kPa (116 psi) and 342.9 mm (13.5 inch) tire spacing shown in Figure 5-1, was used to compute surface deflections and critical pavement responses (fatigue and rutting strains) for each simulated pavement structure at longitudinal and transverse locations shown in Figure 5-2 and Figure 5-3, respectively. As in the 3D-Move analyses, the maximum computed critical responses were used in the subsequent analyses.

Table 5-4. Pavement property ranges used in generating database

		AC Layer	**Base Layer**	**Subgrade Layer**	**Stiff Layer**
Modulus, MPa (ksi)	Minimum	690 (100)	138 (20)	34 (5)	13790(2,000)
	Maximum	6900 (1,000)	550 (80)	138 (20)	
Thickness, mm (inch)	Minimum	51 (2)	102 (4)	610 (24)	Infinite
	Maximum	406 (16)	508 (20)	6096 (240)	

The developed JULEA database was first used to evaluate the most sensitive pavement properties that affect the critical pavement responses. It was later used to identify the most sensitive deflection indices, which correlated well with fatigue and rutting strains in the 3D-Move results presented in Table 5-3.

The degree of correlation between fatigue and rutting strains and pavement properties was calculated using a rank order correlation coefficient, which is a non-parametric technique for quantifying the relationship between two parameters. The rank order correlation coefficient, r, is independent of the relationship between the input and output. As such, it is well suited for studies that involve analytical models to predict critical responses. Rank order correlation uses the position (rank) of a data point in an ordered list to compute its correlation coefficient. The rank order correlation coefficient

known as Karl Spearman's '*r*' is calculated between the output and each dependent variable as *(22)*:

$$r = 1 - \left(\frac{6\sum (\Delta R)^2}{n(n^2 - 1)} \right) \qquad (5.1)$$

in which, ΔR is the difference in the ranks between the input and the output values in the same data pair and *n* is the number of simulations.

The magnitude of '*r*' identifies the extent of correlation between the input and output. The effect of the variable on the predicted response is high when the absolute value of r is close to one; when the r is close to zero, the effect of the variable on the predicted distress is minimal. A positive correlation value indicates that an increase in the input value will lead to an increase in the output value and a negative correlation indicates that an increase in the input value will lead to a decrease in the output value.

A Tornado plot *(22)* was used to visualize the sensitivity of pavement properties (layer stiffness and thickness) that most significantly affect the fatigue and rutting strains. Figure 5-6 shows the Tornado plot using the rank-ordered correlation coefficients, as determined from the JULEA database. The negative correlation for all pavement properties indicates that an increase in each of the simulated pavement properties reduces the pavement responses.

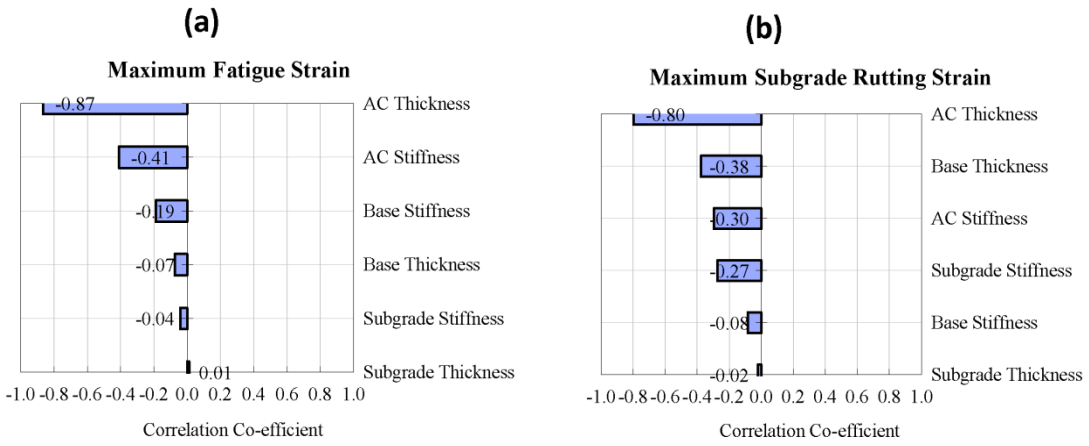

Figure 5-6. Sensitivity of pavement properties on (a) maximum fatigue strain (b) maximum subgrade rutting strain

Similar to the 3D-Move results, AC layer thickness is the most sensitive parameter and it has more influence on the fatigue strain than rutting strain. Base thickness and subgrade properties have negligible effects on the maximum fatigue strain ($|r|$ <0.07); while base thickness (r = -0.38) and subgrade stiffness (r = -0.27) have a moderate impact on rutting strain. It can be concluded that AC thickness would be an appropriate parameter to classify pavement structure and to establish deflection index-fatigue strain relationships. It may be argued that other factors may be necessary to establish deflection index- rutting strain relationships for a higher-degree of confidence. But for network-level PMS applications, a relationship should be simple and hence, such relationship was confined to categorizing the pavement based on only AC layer thickness. Three pavement categories based on AC thickness were considered for relating the pavement responses with deflection indices as explained earlier. Sensitivity of the deflection indices to maximum fatigue and rutting strains are computed using the rank order correlation coefficient 'r' as defined in Equation 5.1.

For pavement structures with an AC layer less than 76 mm (3 in.) thick, it was found that the stiffness of the base, AC and subgrade layers as well as the thickness of the base layer significantly influence the pavement responses. Accordingly, a weak correlation between the deflection indices and the strains was observed when only the AC thickness was considered for this group. However, as discussed earlier, for network-level PMS applications, a relation involving multiple material properties is not practical and therefore, such relation was not followed.

The Tornado plot shown in Figure 5-7 is created using the computed *r* value to show the sensitivity of selected deflection indices with maximum fatigue and rutting strains for pavement structures with AC layer thicknesses in the ranges of 76 mm (3 in.) to 152 mm (6 in.). Similarly, Figure 5-8 shows the Tornado plot for pavement structures with AC layer thicknesses in the ranges of 152 mm (6 in.) to 406 mm (16in.). As shown, indices identified as sensitive by 3D-Move (presented in Table 3) also have relatively good correlation with the pavement responses when evaluated with 15,000 simulated pavement structures.

5.6. Field Evaluation of Selected Indices and their Relationships with Critical Responses

In the previous sections, the indices best related to fatigue and rutting strains were identified using the sensitivity analyses based on computed surface deflections from both 3D-Move and JULEA results. It is necessary to evaluate the capability of the TSD device to accurately measure the chosen indices.

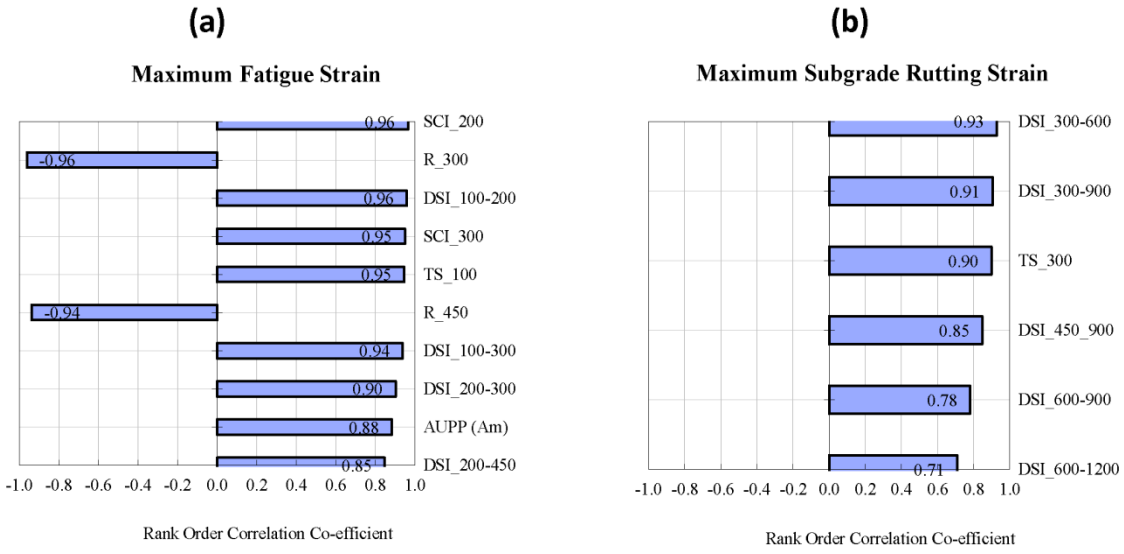

Figure 5-7. Sensitivity of the indices on (a) maximum fatigue strain (b) maximum subgrade rutting strain in 76 mm (3 in.) to 152 mm (6 in.) AC layer thickness

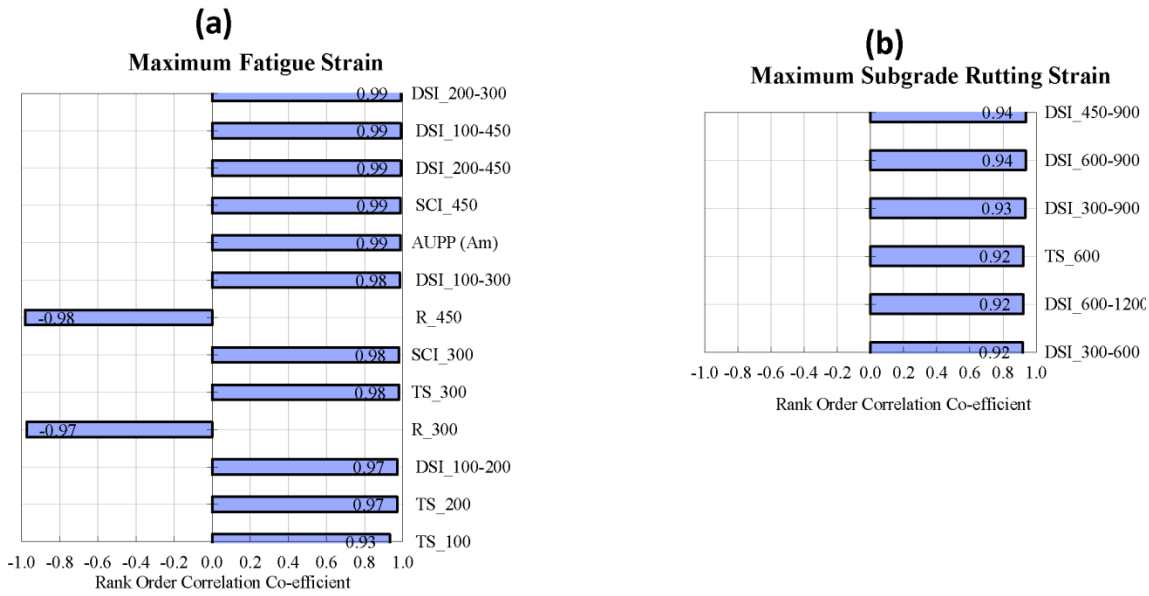

Figure 5-8. Sensitivity of the indices on (a) maximum fatigue strain (b) maximum subgrade rutting strain in 152 mm (6 in.) to 406 mm (16 in.) AC layer thickness

A recent Federal Highway Administration (FHWA) research project *(23)* evaluated the precision and accuracy of TSD measurements at the Minnesota Department of Transportation's MnROAD pavement test track facility near Maplewood, MN in September 2013. The MnROAD facility was selected as the primary site since it provided a multitude of test sections in one location (see http://www.dot.state.mn.us/mnroad/ for detail). The MnROAD test sections were instrumented with several embedded sensors (geophones) to collect surface deflection velocity and displacement parameters during TSD field trials for precision and accuracy purposes. To verify the accuracy of the embedded geophones, the performance of each sensor was validated using an FWD. For that purpose, one of the FWD sensors was placed directly on top of one of the embedded sensors. The deflections reported by the FWD were then compared with the corresponding deflections reported by the embedded geophones. The deflections from the two systems were quite similar. The deflections were within about 10 μm (0.4 mils) of one another *(23)*.

The deflection values reported by the TSD and geophones were then compared to identify the best deflection indices that can be accurately measured by the TSD. Figure 5-9 shows the accuracy of the deflection indices computed from the TSD measurements. The surface curvature indices (SCI_{200} and SCI_{300}) have differences of more than 25%. As explained earlier, the TSD uses an algorithm to compute the deflection basin that matches with the TSD measurements (deflection velocities). Since the TSD doesn't directly measure deflection velocity at 0 mm (the midline of the dual tires), D_o is estimated using assumptions regarding missing measurement at 0 mm *(24)*. This affects the estimated D_o and subsequently causes the computational error of SCI

indices. The comparison between the measured indices of embedded sensors and the TSD revealed that the indices which do not use D_o have a better accuracy. The deflection index $DSI_{200-300}$ (D_{200} - D_{300}) with a 1% difference was identified as the most accurate index that can be measured from the TSD. Similarly for predicting rutting strain, $DSI_{300-900}$ (D_{300} – D_{900}) with a 3% difference was found to be the most accurate index that can be measured from the TSD.

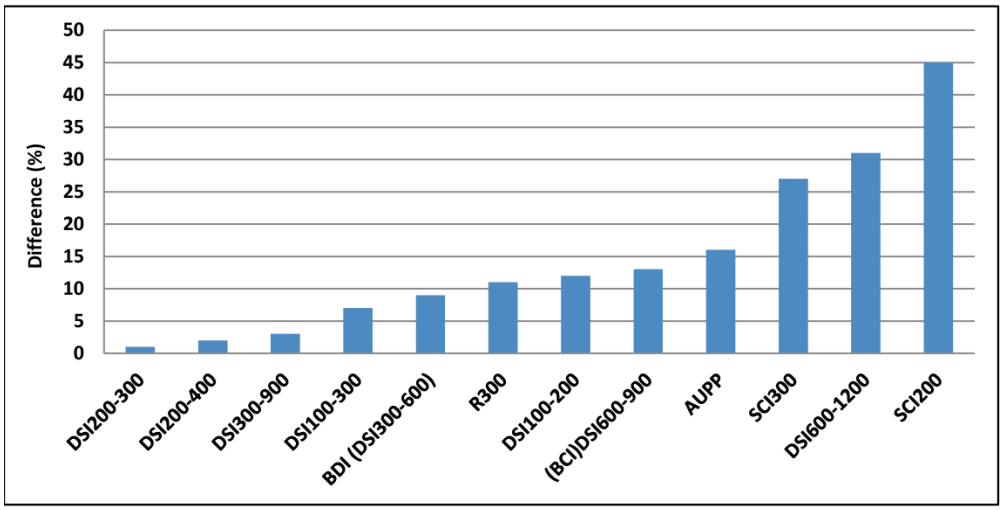

Figure 5-9. Field evaluation of accuracy of deflection indices with the highest correlation with pavement responses

Hence, these two indices were selected to establish relationships with the critical pavement responses. The relative accuracy in measuring $DSI_{200-300}$ and $DSI_{300-900}$ compared to other indices merited their use in all pavement sections irrespective of thin and thick pavement characterization arrived at through sensitivity analyses. With future improvement in the accuracy of the deflection measured by the TSD, the index $DSI_{100-200}$ that was identified by the sensitivity analyses for thin pavements could be used to relate fatigue strain.

For the selected indices, better predictions of the responses are possible when the relationship is categorized according to AC layer thickness. Therefore, relationships between the selected indices and the pavement responses were developed using the database grouped for AC layer thicknesses at 25 mm (1 in.) intervals as shown in Table 5-5. Each group contained about 1,000 pavement structures within the pavement properties presented in Table 5-4. The correlation coefficient between DSI and fatigue strain is generally higher compared to those with rutting strain because in addition to AC thickness, other layer properties can also significantly affect rutting strain (as shown in Figure 5-6).

Table 5-5. Relationships between the selective indices and critical pavement responses in various AC thicknesses

AC Layer Thickness	Relation with Maximum Fatigue Strain, μstrain*		Relation with Maximum Subgrade Rutting Strain, μstrain	
76 mm (3 in.) - 102 mm (4in.)	$135.03*DSI_{200-300}^{0.859}$	$R^2 = 0.66$	$98.622*DSI_{300-900}^{0.9661}$	$R^2 = 0.80$
102 mm (4 in.) -127 mm (5 in.)	$124.91*DSI_{200-300}^{0.987}$	$R^2 = 0.80$	$79.097*DSI_{300-900}^{1.0315}$	$R^2 = 0.85$
127 mm (5 in.) - 152 mm (6 in.)	$126.01*DSI_{200-300}^{1.0532}$	$R^2 = 0.88$	$71.138*DSI_{300-900}^{1.0629}$	$R^2 = 0.84$
152 mm (6 in.) - 178 mm (7 in.)	$136.45*DSI_{200-300}^{1.016}$	$R^2 = 0.92$	$52.141*DSI_{300-900}^{1.1805}$	$R^2 = 0.81$
178 mm (7 in.) - 203 mm (8 in.)	$139.67*DSI_{200-300}^{1.0104}$	$R^2 = 0.95$	$50.595*DSI_{300-900}^{1.2051}$	$R^2 = 0.83$
203 mm (8 in.) - 229 mm (9 in.)	$142.45*DSI_{200-300}^{0.9967}$	$R^2 = 0.97$	$53.264*DSI_{300-900}^{1.1754}$	$R^2 = 0.81$
229 mm (9 in.) - 254 mm (10 in.)	$144.45*DSI_{200-300}^{0.9749}$	$R^2 = 0.98$	$57.112*DSI_{300-900}^{1.1306}$	$R^2 = 0.81$
254 mm (10 in.) - 279 mm (11 in.)	$142.78*DSI_{200-300}^{0.9348}$	$R^2 = 0.97$	$56.95*DSI_{300-900}^{1.1444}$	$R^2 = 0.80$
279 mm (11 in.) - 305 mm (12 in.)	$141.32*DSI_{200-300}^{0.9108}$	$R^2 = 0.97$	$61.462*DSI_{300-900}^{1.0948}$	$R^2 = 0.81$
305 mm (12 in.) - 330 mm (13 in.)	$138.06*DSI_{200-300}^{0.884}$	$R^2 = 0.97$	$63.811*DSI_{300-900}^{1.0667}$	$R^2 = 0.80$
330 mm (13 in.) -356 mm (14 in.)	$131.37*DSI_{200-300}^{0.8439}$	$R^2 = 0.95$	$65.638*DSI_{300-900}^{1.0236}$	$R^2 = 0.78$
356 mm (14 in.) – 381 mm (15 in.)	$129.78*DSI_{200-300}^{0.8463}$	$R^2 = 0.96$	$67.725*DSI_{300-900}^{0.9854}$	$R^2 = 0.76$
381 mm (15 in.) – 406 mm (16 in.)	$121.04*DSI_{200-300}^{0.8079}$	$R^2 = 0.95$	$68.896*DSI_{300-900}^{0.9862}$	$R^2 = 0.79$

***** The indices are in mils. 1 mils = 25.4 μm

5.7. Conclusions

This paper describes a comprehensive sensitivity analysis on the effects of pavement layer configuration and properties on the critical responses using both 3D-Move dynamic deflection basins and as many as 15,000 pavement structure response databases generated from the layered linear elastic program, JULEA. It also evaluates many deflection basin indices to identify the best indicators of the critical pavement performance. The following conclusions are observed:

- It was found that the deflection basin indices closer to center of the loading have the highest correlation with fatigue strain and thus can best represent the structural condition of the AC layer. The sensitivity analyses showed the deflection indices SCI_{300}, $DSI_{100\text{-}200}$, and $DSI_{200\text{-}300}$ have strong correlations with fatigue strain. On the other hand, the indices based on deflections measured farther away from the center of the loading (e.g., $DSI_{300\text{-}600}$, $DSI_{300\text{-}900}$) best relate to the vertical subgrade strain.

- On the basis of the sensitivity analyses, the AC layer thickness is the most influential parameter on fatigue strain. Loading speed, subgrade and base layer properties are found to affect the fatigue strain only marginally.

- In addition to AC layer thickness that significantly affects the rutting strain, other properties such as base thickness and subgrade stiffness have a moderate impact on rutting strain. However, for network-level PMS application, it was reasonable to develop indices that relate to rutting strains by categorizing pavements based only on AC thickness.

- Measurements from the TSD and geophones are used to identify the indices that can be accurately computed from the TSD. $DSI_{200-300}$ (D_{200} - D_{300}) and $DSI_{300-900}$ (D_{300} − D_{900}) are identified as the robust indices that can be accurately measured and also have the highest correlations with fatigue and rutting strains, respectively. There is uncertainty in the estimation of the conventionally-used index (SCI) with the TSD because the TSD doesn't directly measure deflection velocity at 0 mm (the midline of the dual tires) and D_o is estimated using assumptions regarding missing measurement at 0 mm. Therefore, DSI can be a reliable alternative for SCI_{300} that can be used effectively to relate with fatigue strain.
- Relationships developed in the study can be effectively used with TSD measurements to compute two critical pavement responses that can be readily used to evaluate the structural performance of the pavement.

Acknowledgments

This study was funded through the FHWA study DTFH61-12-C-00031 and the support is gratefully acknowledged. We would like to thank Dr. Gonzalo Rada for his leadership and encouragement. The conclusions presented in this paper are solely those of these authors.

5.8. References

1. Noureldin, A., Zhu, K., Li, S., & Harris, D. (2003). "Network pavement evaluation with falling-weight deflectometer and ground-penetrating radar. "

Transportation Research Record: Journal of the Transportation Research Board, 1860, 90-99.

2. NCHRP. (2004). *Guide for mechanistic-empirical design of new and rehabilitated structures*. Final report for project 1-37A, National cooperative highway research program, Transportation Research Board, National research council, Washington, D.C.
3. Asphalt Institute. (1982). *Research and development of the asphalt institute's thickness design manual (MS-1)*, 9th Ed., Research Report 82-2.
4. Garg, N., & Thompson, M. R. (1999). "Structural response of LVR flexible pavements at Mn/road project." *J. Transportation Engineering,* 125(3), 238-244.
5. Horak E. (1987). "The Use of surface deflection basin measurements in the mechanistic analysis of flexible pavements." *Proc., Vol. 1, Sixth International Conference Structural Design of Asphalt Pavements, University of Michigan, Ann Arbor, Michigan, USA.*
6. Xu, B., Ranji Ranjithan, S., & Richard Kim, Y. (2002). "New relationships between falling weight deflectometer deflections and asphalt pavement layer condition indicators." *Transportation Research Record: J. the Transportation Research Board,* 1806(1), 48-56.
7. Thyagarajan, S., Sivaneswaran, N., Petros, K. and Muhunthan, B. (2011). "Development of a simplified method for interpreting surface deflections for in-service flexible pavement evaluation." *8th International Conference on Managing Pavement Assets, Santiago, Chile.* 15-19.

8. Pedersen, L., (2012). *Viscoelastic modeling of road deflections for use with the traffic speed deflectometer*. PhD study in collaboration with Greenwood Engineering, Technical University of Denmark and the Ministry of Science and Innovation.
9. Siddharthan, R.V., Yao, J., and Sebaaly, P.E. (1998). "Pavement strain from moving dynamic 3-d load distribution," *J. Transportation Engineering.,* ASCE, Vol. 124(6), 557-566.
10. Zafir, Z., Siddharthan, R. V., and Sebaaly, P. E. (1994). "Dynamic pavement strains from moving traffic loads," *J. Transportation Engineering,* ASCE, Vol. 120(5), 821-842.
11. Magdy, El-Desouky, (2003). *Further developments of 3DMOVE and its engineering applications*. PhD dissertation, University of Nevada, Reno.
12. Siddharthan, R.V., El-Mously, M., Krishnamenon, N., and Sebaaly, P.E. (2002). "Validation of a pavement response model using full-scale field tests," *International J. Pavement Engineering,* Vol. 3(2), 85-93.
13. Siddharthan, R., Sebaaly, P.E., El-Desouky, M., Strand, D., and Huft, D. (2005). "Heavy off-road vehicle tire-pavement interactions and response," *J. Transportation Engineering,* ASCE, Vol. 131(3), 239-247.
14. Ulloa, A., Hajj, E.Y., Siddharthan, R.V., and Sebaaly, P.E. (2012). "Equivalent loading frequencies for dynamic analysis of asphalt pavements." *J. the Materials in Civil Engineering,* 25(9), 1162-1170.

15. Nasimifar, M., Siddharthan, R., Rada, G., Nazarian, S., (2015). "Dynamic analyses of traffic speed deflection devices." International Journal of Pavement Engineering, http://dx.doi.org/10.1080/10298436.2015.1088152.

16. Uzan, J. (1976). "The Influence of the interface condition on stress distribution in a layered system." *J. Transportation Research Record* No. 616, 71-73.

17. Park, H. M., Kim, Y. R., & Wan Park, S. (2005). "Assessment of pavement layer condition with use of multi load-level falling weight deflectometer deflections." *Transportation Research Record: J. Transportation Research Board,* 1905(1), 107-116.

18. Horak E (1988). *Aspects of deflection basin parameters used in a mechanistic rehabilitation design procedure for flexible pavements in South Africa*. PhD thesis, Department of Civil Engineering at the University of Pretoria, Pretoria, South Africa.

19. Kilareski, W. P., & Anani, B. A. (1982). "Evaluation of in-situ moduli and pavement life from deflection basins." *Proc., fifth international conference on the structural design of asphalt pavements, DEFLT University of technology.*

20. Donovan, P., and Tutumluer, E. (2009). "Falling weight deflectometer testing to determine relative damage in asphalt pavement unbound aggregate layers." *Transportation Research Record: J. Transportation Research Board,* 2104(1), 12-23.

21. Seo J., Kim Y., Cho J., and Jeong S. (2013). "Estimation of in situ dynamic modulus by using MEPDG dynamic modulus and FWD data at different temperatures," *International J. Pavement Engineering,* Vol. 14(4), 343 - 353.

22. Vose, D. (1997) "Quantitative risk analysis: a guide to Monte Carlo simulation modelling." *John Wiley & Sons.New York, USA.*

23. Rada, G., Nazarian, S., Visintine, B., Siddharthan, R.V., and Thyagarajan, S. (2015). *Pavement structural evaluation at the network level,* FHWA, Final Report

24. Flintsch, G., Katicha, S., Bryce, J., Ferne, B., Nell, S., and Diefenderfer, B. (2013). *Assessment of continuous pavement deflection measuring technologies,* SHRP 2 Report S2-R06F-RW-1.

6. Field and Numerical Evaluation of Traffic Speed Surface Deflection Measurements to Estimate Load-induced Fatigue Response

Mahdi Nasimifar[1], Raj V. Siddharthan[2], Senthilmurugan Thyagarajan [3], Ramin Motamed[4]

1. Graduate Research Assistant, University of Nevada – Reno, Department of Civil & Environmental Engineering, 1664 N. Virginia St., Reno, Nevada, USA **,** *nasimifar@nevada.unr.edu***.** *(Corresponding Author).*

2. Professor, University of Nevada – Reno, Department of Civil & Environmental Engineering, 1664 N. Virginia St., Reno, Nevada, USA, siddhart@unr.edu.

3. Research Engineer, ESC Inc., Turner Fairbank Highway Research Center, 6300 Georgetown Pike, McLean, Virginia, USA, senthil.thyagarajan.ctr@dot.gov.

4. Assistant Professor, University of Nevada – Reno, Department of Civil & Environmental Engineering, 1664 N. Virginia St., Reno, Nevada, USA, Motamed@unr.edu.

6.1. Abstract

Traffic speed deflection devices (TSDDs) are actively used around the world at network level pavement management system because of their relative merits over traditional deflection devices (e.g. FWD, Benkelman beam etc.) in evaluating the pavement structural condition. Past researchers have utilized several deflection indices based on FWD surface deflections to estimate critical responses such as load induced fatigue strains at the bottom of the asphalt concrete (AC) layer. However, the differences in loading configuration and viscoelastic material behaviour under moving nature of the load of TSDDs limit the use of the FWD based indices with TSDD measurements to predict those critical responses. The two TSDDs: Traffic Speed Deflectometer (TSD) and Rolling Weight Deflectometer (RWD) were evaluated as a part of FHWA study at the MnROAD facility in September 2013. Dynamic load response data was collected during field tests along with TSDD surface deflection measurements. 3D-Move program was chosen to undertake the analytical modelling since it can model moving load and accommodate the rate-dependent material properties (viscoelastic). A number of indices that are best related to fatigue strain have been identified from 48 individual indices. The study verified the capability of TSDD surface deflection measurements to estimate fatigue strains. The TSD measurements can be used to predict the critical fatigue strains at the network level. However, the prediction accuracy can be improved if response lag between the maximum load and the deflection is accounted in the TSD deflection computation algorithm. Evaluation of the RWD device with two surface deflection measurements reveals that both RWD sensors

need to be positioned in front of the rear axle to have a better related index to fatigue strains.

Keywords: Field Evaluation, Fatigue Strain, Traffic Speed Surface Deflections, Deflection Indices, TSD, RWD

6.2. Introduction

The maximum horizontal tensile strain at the bottom of the Asphalt Concrete (AC) layer, hereafter referred simply as fatigue strain for brevity, is one of the critical load-induced pavement responses for the evaluation of existing structural capacity of a pavement [1]. The tensile strain under standard axle load is used in the performance prediction equations [2, 3] to estimate the bottom-up fatigue cracking.

The fatigue strain can be estimated from deflection-basin related indices [4, 5]. Falling Weight Deflectometer (FWD), which is a common non-destructive stationary testing device, is used at the network and project level to estimate the structural capacity of in-service pavements. Xu et al. postulated relations to estimate the load-induced pavement responses from FWD deflection indices [6]. The limitations of the FWD such as stop-and-go operation, lane closures and low frequency of testing necessitate the need for a viable alternate device, in particular for network level pavement management applications.

Several organizations in the USA and Europe have developed Traffic Speed Deflection Devices (TSDDs) over the past few decades that can continuously measure pavement deflections at traffic speed. The modern versions of the TSDDs that can work at posted traffic speeds (up to 96 kph) include Traffic Speed Deflectometer (TSD)

developed by Greenwood Engineering and Rolling Wheel Deflectometer (RWD) developed by Applied Research Associates. Recently, these two devices were evaluated at the Minnesota Department of Transportation's MnROAD pavement test track facility near Maplewood, MN through a Federal Highway Administration (FHWA) project. The surface pavement sensors were installed at the MnROAD sections to measure surface deflections and evaluate TSDD measurements [7]. The TSD used in the field evaluation utilizes Doppler lasers to measure the vertical deflection velocity (the velocity of the pavement surface due to the moving load) at 6 points (100, 200, 300, 600, 900 and 1500 mm) in front of the rear axle along the midline of the dual tires . A theoretical algorithm is used to compute the deflection basin that matches with the TSD measurements [8]. RWD uses spatial coincidence principle to measure two surface deflections along the midline of the rear dual tires at 184 mm (7.25 in.) behind and 197 mm (7.75 in.) front of the axle. More information on the devices can be found in Flintsch et al. [9].

The relationships between the deflection basin indices and the pavement responses found in the literature are based on the symmetrical FWD deflection bowls generated by an impulse load on a single circular plate. The use of TSDD measurements with the FWD based deflection indices is questionable for the dual tire loading configurations of the TSD and the RWD. In addition, unlike FWD, the TSDD moving load and viscoelastic characteristics of the AC layer produce asymmetrical deflection basins and there is response lag between the maximum load and maximum deflection [10, 11]. The 3D-Move program (explained later in this paper) was used as the analytical tool to simulate vehicle loading trials from the TSD and the RWD since it can correctly reproduce both response lag and asymmetrical deflection bowls as a function of vehicle

speed and viscoelastic properties of the AC layer. The 3D-Move program was used to theoretically identify the deflection indices that can best relate to fatigue strains and recognize the optimum sensor locations for the TSDDs. The best related indices were subsequently evaluated with field measured deflection data from the two TSDDs and corresponding fatigue strain measurements from the embedded sensors at the MnROAD facility.

6.3. Background and Objective

Researchers have proposed a number of deflection indices that best related to the critical pavement responses. Thyagarajan et al. [5] suggested that SCI_{300} (D_o - D_{300}) can be used to estimate the fatigue strains based on numerical simulation using linear elastic program (JULEA). Here, "D" refers to the vertical surface deflection and the subscript is the distance in millimetre from the center of the FWD loading plate.

There are many possible deflection indices that can be explored from the measured deflection basin. Most of the suggested indices in the literature require the center deflection, D_o, to compute the indices. Currently, center deflection is not directly measured by both TSD and RWD. In the case of TSD, an algorithm computes the center deflection by assuming the zero slope at 0 mm (midpoint of the dual tires) [9]. This assumption is valid only for pure elastic materials without response lag and this study evaluates its validity and its effect on the accuracy of the computed indices.

The objective of the paper is to identify the best related deflection indices to fatigue strains through the 3D-Move program using TSDD loading configurations and then develop deflection index-fatigue strain relationships and finally verify those using

the MnROAD field data. The outcome of the study verifies the ability of TSDD measurements to predict pavement responses in the network level pavement management applications.

6.4. Field Test Description

The field study activities were carried out at the MnROAD facility. The three flexible pavement sections, Cells 3 and 19 from MnROAD Mainline and Cell 34 from MnROAD Low Volume Road were used in the study and covered different levels of stiffness. Figure 6-1 illustrates layer thicknesses and FWD backcalculated moduli for these cells. The three flexible pavement sections, Cell 34, Cell 19 and Cell 3 were judged as soft, intermediate and stiff, respectively based on the FWD testing.

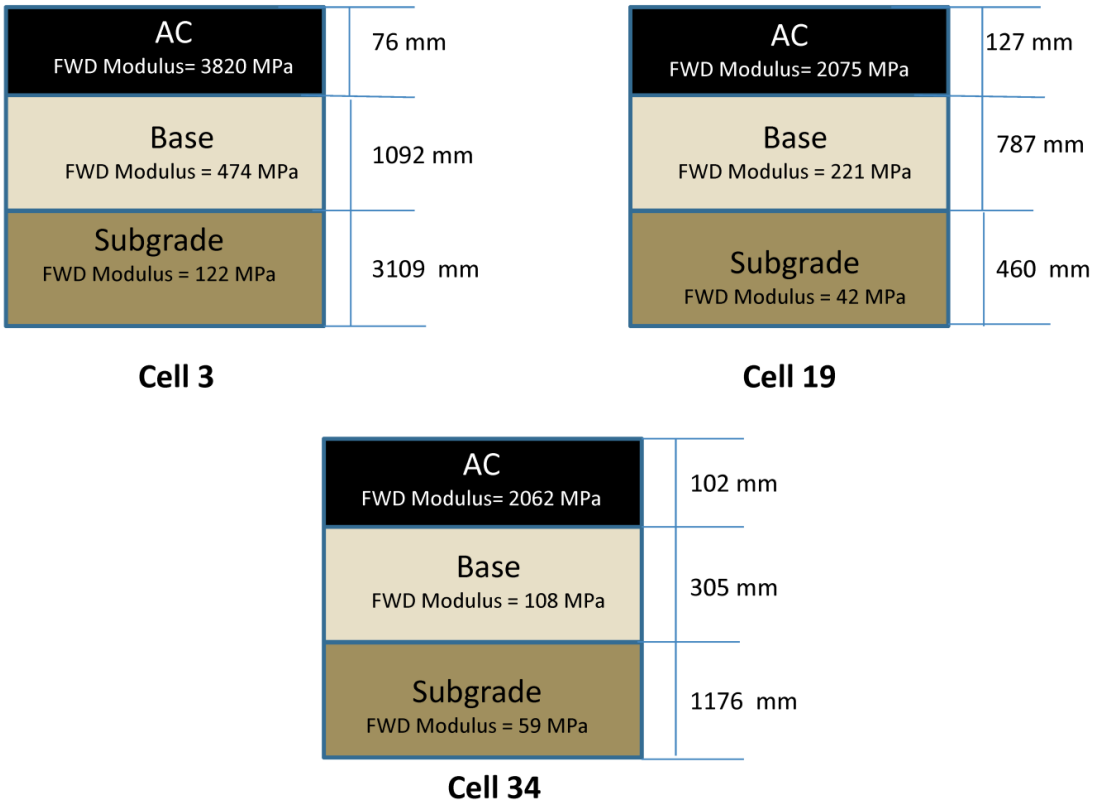

Figure 6-1. Sketch of pavement structures for Cells 3, 19, and 34

Four geophones were placed near the pavement surface in each of the three tested cells to measure surface deflections during TSDD trials. To verify the accuracy of the embedded geophones, the performance of each sensor was validated using an FWD. For that purpose, one of the FWD sensors was placed directly on top of one of the embedded sensors. The deflections reported by the FWD were then compared with the corresponding deflections reported by the embedded geophones. The deflections from the two systems were quite similar. The deflections were within about 10 μm (0.4 mils) of one another [7]. Since the measurement sensors for both devices (TSD & RWD) were located along the midline of the rear axle tires, the geophones were embedded along the midline of the right wheel path as shown in Figure 6-2**.** A laser trigger device was also installed across the travel lane (transverse plane) for time synchronizing the load and response measurements. The location of the rear wheels relative to the location of the maximum deflection (i.e., response lag) can be determined by superimposing the data from the laser device and measured deflection basins.

In addition to the newly installed geophones, the existing instrumentations (strain gages) at the MnROAD facility collected strain responses in the longitudinal direction at various depths during TSDD trials.

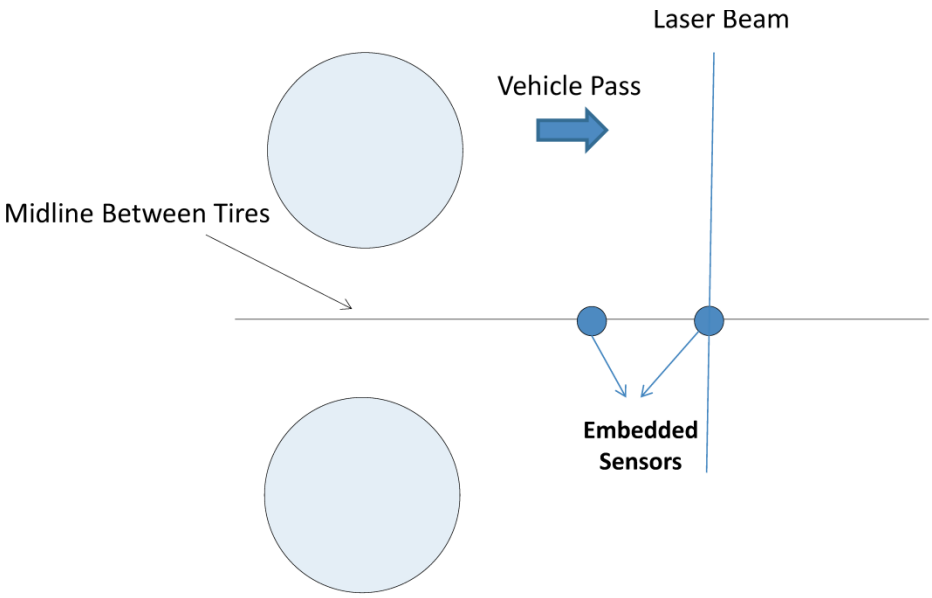

Figure 6-2. Configuration of the embedded project sensors

6.5. Analytical Approach

As explained before, it is required to use an analytical model that accounts for the moving load and viscoelastic properties of AC layers to obtain the dynamic deflection basins under TSDD loading. The 3D-Move model evaluates the pavement responses using a continuum-based finite-layer approach [12-14]. It accounts for important factors such as the moving load-induced complex 3D contact stress distributions (normal and shear) of any shape, vehicle speed, and viscoelastic material characterization for the pavement layers. Frequency-domain solutions are adopted in the 3D-Move, which enables the direct use of the frequency sweep test data of the AC mixture in the analysis. Thus, the 3D-Move has the capability of modelling moving load and the resulting dynamic pavement responses and it is ideally-suited to evaluate and compare measured pavement responses using TSDDs.

Siddharthan et al. [15, 16] reported many field calibrations that compared a variety of independently-measured pavement responses (stresses, strains, and deflections) with those computed from the 3D-Move. Chabot et al. reported on a semi-analytical dynamic multi-layer model called ViscoRoute which has viscoelastic properties in the formulation [17]. Computed maximum transverse strains (ε_{yy}) at the bottom of the AC layer under the center of the moving tire by the 3D-Move and ViscoRoute Analyses were compared for both the thin and thick pavements [18]. The computed responses are within 6% in all of the 60 cases. Nasimifar et al. confirmed the ability of the 3D-Move model to simulate TSDD loading by comparing the computed surface measurements (deflection and velocity) and the corresponding measured pavement responses from embedded sensors in the MnROAD field trials [19]. The aforementioned verification studies have validated the applicability and versatility of the 3D-Move analysis approach.

6.6. Selection of Deflection Basin Indices

Table 6-1 summarizes the 48 individual indices that were evaluated in this study. The Surface Curvature Index (SCI = D_o - D_r) used deflection at the midpoint between the dual tires, D_o, as reference deflection and D_r as the deflection at distance "r" from the midpoint between the dual tires. A new index called Deflection Slope Index (DSI) was also considered with D_{100} and D_{200} as reference deflections since estimation of D_o from the TSD measurements can introduce associated errors as explained earlier. Since D_o and D_{max} are not the same due to response lag of the moving load, a new index (SCI_m) is also considered where D_{max} instead of D_o is used as the reference deflection. The only possible index for the RWD is difference in two deflections at D_{-184} and D_{197}. Deflection velocity

indices were also considered in this study because their computation doesn't involve any assumption or integration algorithm. Other indices commonly used in literature such as radius of curvature (R), area under the deflection basin (A), shape factors (F) etc. are also considered in the study as defined in Table 6-1.

Table 6-1. Deflection basin indices used in the evaluation**

Parameter and Number of Indices	Indices for Evaluation		Parameter and Number of Indices	Indices for Evaluation
Radius of Curvature (8)** $R = r^2/(2D_o(D_o/D_r - 1))$, (m)	R_{200}		Deflection Velocity (6) DV , (mm/s)	DV_{100}
	R_{300}			DV_{200}
	R_{400}			DV_{300}
	R_{500}			DV_{600}
	R_{600}			DV_{900}
	R_{700}			DV_{1500}
	R_{800}		Surface Curvature Index(6) $SCI_m = D_{max} - D_r$, (μm)	$SCIm_{200}$
	R_{900}			$SCIm_{300}$
Area (1) $A = 6[1 + 2(D_{300}/D_o) + 2(D_{600}/D_o) + D_{900}/D_o)]$	A			$SCIm_{400}$
				$SCIm_{500}$
Shape Factors (2) $F_1 = (D_o - D_{600}) / D_{300}$ $F_2 = (D_{300} - D_{900}) / D_{600}$	F_1			$SCIm_{600}$
	F_2			$SCIm_{900}$
Surface Curvature Index (7) $SCI = D_o - D_r$, (μm)	TSD	SCI_{200}	Deflection Slope Index(5) $DSI_{100-r} = D_{100} - D_r$, (μm)	$DSI_{100-200}$
		SCI_{300}		$DSI_{100-300}$
		SCI_{400}		$DSI_{100-400}$
		SCI_{500}		$DSI_{100-500}$
		SCI_{600}		$DSI_{100-600}$
		SCI_{900}	Deflection Slope Index(4) $DSI_{200-r} = D_{200} - D_r$, (μm)	$DSI_{200-300}$
	RWD	D_{-184}-D_{197}		$DSI_{200-400}$
				$DSI_{200-500}$
				$DSI_{200-600}$
Base Curvature Index (1) $BCI = D_{600} - D_{900}$, (μm)	BCI		Slope of Deflection (6) $SD = \tan^{-1}(D_o - D_r)/r$	SD_{200}
				SD_{300}
Base Damage Index (1) $BDI = D_{300} - D_{600}$, (μm)	BDI			SD_{400}
				SD_{500}
Area Under Pavement Profile (AUPP) (1) $(5D_o - 2D_{300} - 2D_{600} - D_{900})/2$, (μm)	AUPP			SD_{600}
				SD_{900}

** Numbers within parentheses indicate the number of indices for each deflection basin parameter, r: radial distance from the center of the load, mm

6.7. Analytical Evaluation of Indices

The viscoelastic characterization (frequency-dependent) of the AC layer is required to evaluate pavement responses as a function of vehicle speed. As such, dynamic modulus of the AC layer in terms of master curve and damping coefficients are key input parameters to the 3D-Move program.

The FWD backcalculated AC layer moduli (Figure 6-1) are appropriate for the temperature at the time of FWD testing and a loading frequency of about 30 Hz [20]. The temperature corrected damaged moduli as a function of frequency for the MnROAD cells were produced using the Witczak-Andrei dynamic modulus equation [21] and appropriate procedure were utilized to generate damaged moduli from undamaged master curves [19]. Figure 6-3 shows the dynamic modulus master curve for the AC layer at the temperature measured during TSDD field tests in Cell 3. Damping coefficients were computed by fitting a best curve through the available dynamic modulus test (phase angle measured at given frequencies) results and then interpolating the phase angles for the temperature corresponding with the field trials.

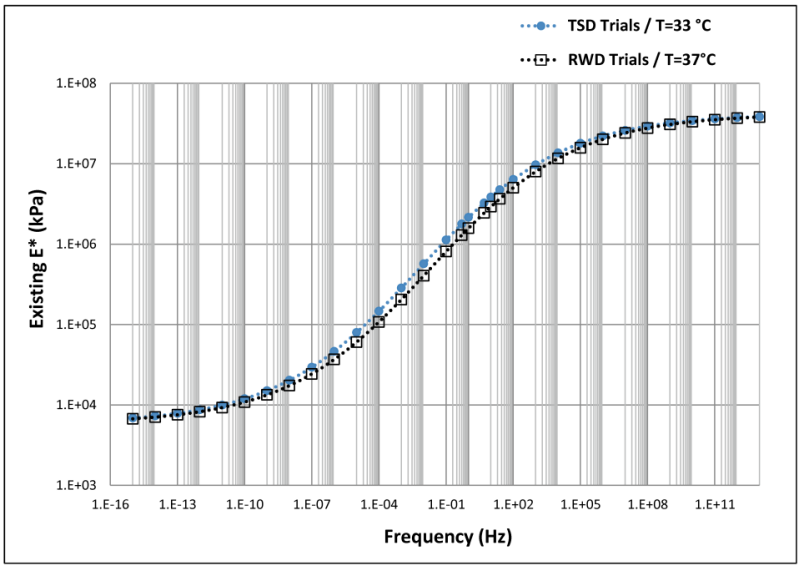

Figure 6-3. Dynamic modulus master curve for the AC layer in Cell 3 during the field trials

Figure 6-4 shows the load characterization of the rear axles in the two TSDDs. The loads were measured in a static scale operated by the MnROAD facility during the TSDD trials. The 3D-Move analyses are focussed on the rear axle where the TSDD sensors are located.

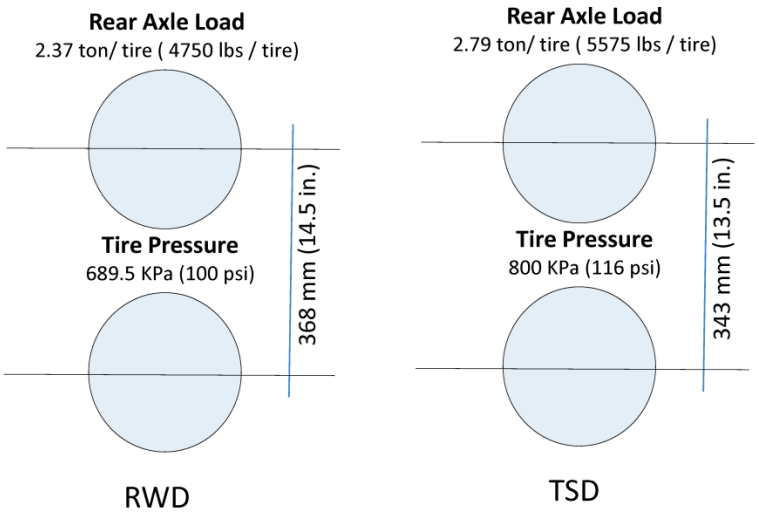

Figure 6-4. Rear axle and load configuration for the RWD and the TSD at the MnROAD test

The 3D-Move program can compute pavement response time histories under the moving load at any given location in the pavement structure. Figure 6-5 illustrates the typical vertical deflection time history computed by the 3D-Move at a point (observation point) on the midline between the tires. The figure also displays the pre-determined locations in the longitudinal direction along the midline where the deflections are computed from the vertical deflection time history by time space superposition and used to compute the indices in Table 6-1. The figure also shows the difference in the location of the maximum deflection (D_{max}) and the deflection at the midpoint between tires (D_o) termed as response lag.

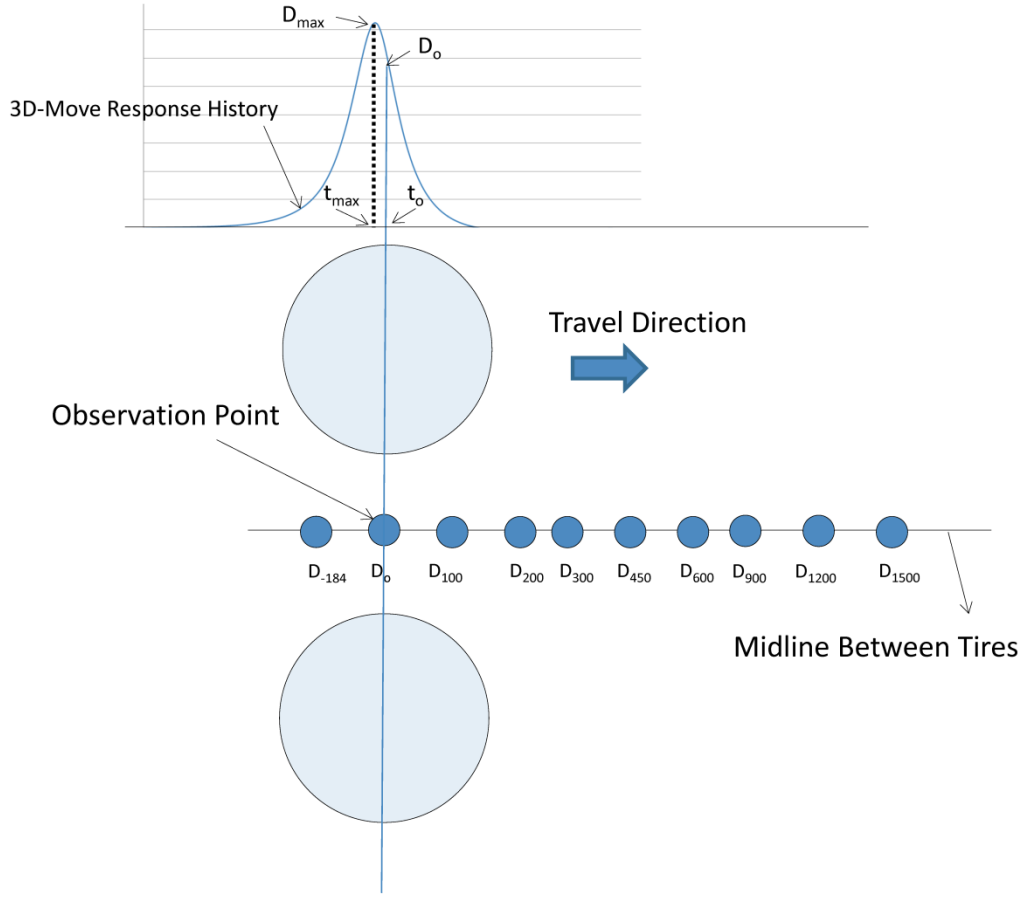

Figure 6-5. Vertical surface deflections from the 3D-Move deflection time history

Based on the pavement layer characteristics and loading configuration, the maximum fatigue strain response can occur at any of the transverse locations under the dual tire. In order to capture the maximum response predicted by the 3D-Move program, the fatigue strains are computed at several transverse locations at 25 mm (1 in.) intervals as shown in Figure 6-6. The maximum computed strain is used subsequently in the analysis.

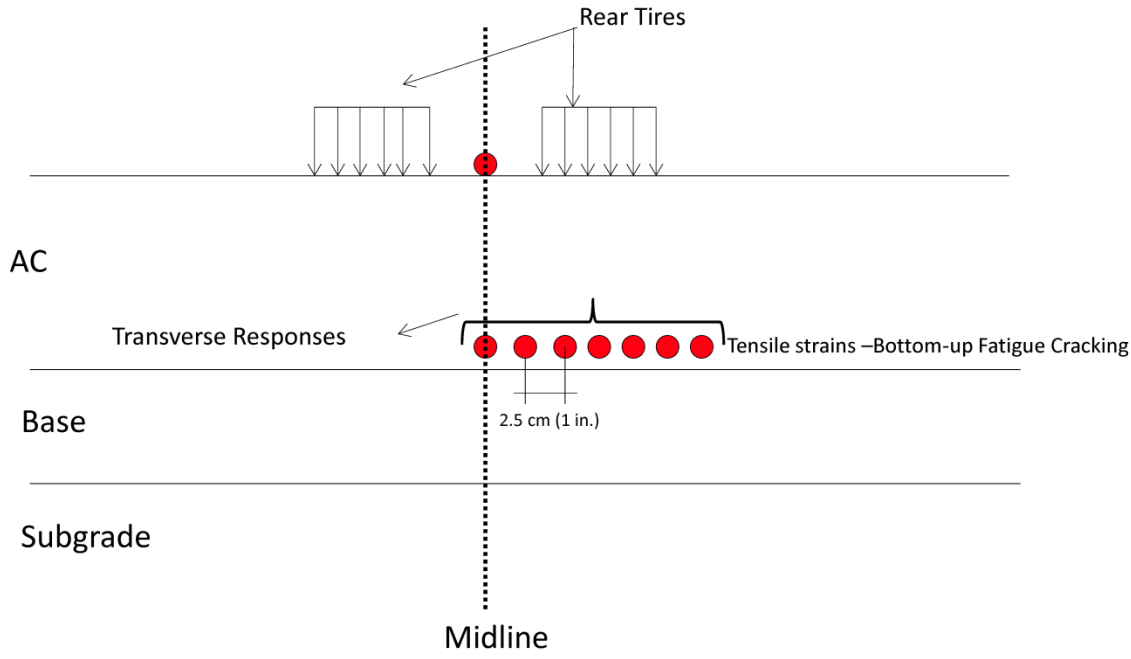

Figure 6-6. Selection of response points when using the 3D-Move

The three MnROAD test cells characterized earlier (Figure 6-1) were used with the 3D-Move program to generate 42 different analyses. The analyses covered a variety of factors that included vehicle speed, device loading configuration, and variability in the material characterization (thickness and layer properties). In each analysis, the deflections

and fatigue strains are computed at the longitudinal and transverse locations shown in Figure 6-5 and Figure 6-6 respectively.

The relationships between the 3D-Move computed deflection indices and fatigue strains were evaluated and the best promising indices were selected. Table 6-2 summarizes the most appropriate indices for the MnROAD cells. The coefficient of determination, R^2, which is a measure of the best-fit between the variables, has been shown for each index. The relationships presented in this table are based on the 3D-Move analyses and are field verified in the subsequent section using measured data from the MnROAD instrumented cells. However, a comprehensive simulation of pavement responses using dynamic model such as the 3D-Move, covering a wider range of influencing factors is seen as more appropriate for pavement management applications.

Table 6-2. Most appropriate indices and relationships related to fatigue strain at the MnROAD cells

Index	**Relation with Fatigue strain, μstrain**	
SCI_{300}, (μm)	$6.1118\ SCI_{300}^{0.7828}$	$R^2 = 0.93$
SCI_{400}, (μm)	$7.413\ SCI_{400}^{0.6954}$	$R^2 = 0.93$
$SCIm_{200}$, (μm)	$7.21\ SCIm_{200}^{0.854}$	$R^2 = 0.9$
$SCIm_{300}$, (μm)	$6.92\ SCIm_{300}^{0.751}$	$R^2 = 0.92$
SD_{300}	$118479\ SD_{300}^{0.7828}$	$R^2 = 0.93$
SD_{400}	$58278\ SD_{400}^{0.6954}$	$R^2 = 0.93$
$DSI_{100\text{-}200}$, (μm)	$11.631\ DSI_{100\text{-}200}^{0.7917}$	$R^2 = 0.90$
$DSI_{100\text{-}300}$, (μm)	$9.5962\ DSI_{100\text{-}300}^{0.7075}$	$R^2 = 0.91$
$DSI_{100\text{-}400}$, (μm)	$10.427\ DSI_{100\text{-}400}^{0.6406}$	$R^2 = 0.90$
$DSI_{200\text{-}300}$, (μm)	$20.849\ DSI_{200\text{-}300}^{0.6301}$	$R^2 = 0.90$
$DSI_{200\text{-}400}$, (μm)	$18.933\ DSI_{200\text{-}400}^{0.5692}$	$R^2 = 0.90$
AUPP, (μm)	$5.3806\ AUPP^{0.6266}$	$R^2 = 0.90$

The 3D-Move results show that indices closer to the center of the load (e.g, SCI_{300}, $DSI_{200-300}$ and SD_{300}) have good correlations with fatigue strains. The analyses revealed that using D_{max} instead of D_o to calculate SCIm does not noticeably improve the correlation. The new indices, DSI which were created to overcome the shortcomings of TSD in estimating the center deflection (D_o), were found relatively better. Thus the best indices related to fatigue strains are not necessarily depended on D_o as found in literature, consequently if D_{100} or D_{200} from the TSD is more reliably measured than D_o, they can be used as the reference deflections in the DSI calculations and subsequent relation with fatigue strains. The FHWA study [7] reported that DSI indices are measured relatively accurate than other indices based on the TSD device used in the field evaluation.

In summary, the 3D-Move analytical model that can simulate deflection basins measured from TSDD trials is used to identify the best related indices to fatigue strains. In subsequent sections, the proposed relationships are used with measured deflection indices from both TSDDs and geophones to predict fatigue strains. Following comparison of the predicted and measured fatigue strain evaluates the capability of the TSDD measurements to estimate fatigue strains.

6.8. Field Evaluation of RWD Index

As noted earlier, RWD has only two measurements at 184 mm (7.25 in.) behind and 197 mm (7.75 in.) ahead of the rear axle tire. RWD field trials were conducted at various vehicle speeds in three passes and in three cells (Cells 34, 19 and 3). Table 6-3 evaluates the capability of the RWD sensor (the sensor at 184 mm (7.25 in.) behind the rear axle tire) to capture maximum surface deflection in different vehicle speeds and levels of

pavement structure stiffness. The deflection basins measured from embedded sensors in the MnROAD instrumented cells were used for this evaluation. The actual vehicle speeds were measured during the tests and presented in the table. The trigger signal from the laser beam was used to compute the time lag between the maximum load and D_{max} from the corresponding signals. The time lag and the vehicle speed are used to compute the response lags in terms of distance between the center of wheel load and the occurrence of maximum deflection. The response lags and the percent difference between the deflections D_{-184} and D_{max} are also shown in the Table 6-3.

Table 6-3. Evaluation of RWD sensor at behind the rear axle to capture maximum deflection, D_{max}, at different vehicle speeds and pavement structures*

Cell	Target Speed kph (mph)	Pass	Actual Speed, kph(mph)	RWD Response Lag, mm (in.)	Percent Difference between Deflections at D_{max} and D_{-184}		Percent Difference between $SCIm_{200}$ and $(D_{-184} - D_{197})$	
34	48.3(30)	Pass 1	47.3 (29.4)	197.1 (7.76)	0.17%	0.13%	4.04%	1.48%
		Pass 2	49.2 (30.6)	177.8 (7.00)	0.17%		0.32%	
		Pass 3	47.1 (29.3)	183.1 (7.21)	0.05%		0.08%	
	72.4(45)	Pass 1	70.1 (43.6)	175.3 (6.90)	0.01%	0.11%	0.02%	2.22%
		Pass 2	72.8 (45.2)	171.9 (6.77)	0.28%		0.60%	
		Pass 3	71.4 (44.4)	178.6 (7.03)	0.05%		6.05%	
19	48.3(30)	Pass 1	47.4 (29.4)	125 (4.92)	2.04%	2.77%	4.07%	8.91%
		Pass 2	48.9 (30.4)	101.8 (4.01)	3.73%		12.47%	
		Pass 3	47.4 (29.4)	118.4 (4.66)	2.55%		10.19%	
	72.4(45)	Pass 1	70.8 (44)	98.3 (3.87)	4.57%	5.38%	9.65%	14.64%
		Pass 2	70.6 (43.9)	78.5 (3.09)	5.75%		12.77%	
		Pass 3	71.6 (44.5)	79.5 (3.13)	5.81%		21.51%	
	96.6(60)	Pass 1	87 (54.1)	84.6 (3.33)	5.88%	4.03%	13.43%	12.53%
		Pass 2	85.2 (52.9)	82.8 (3.26)	4.91%		20.68%	
		Pass 3	103.6 (64.4)	129.5 (5.10)	1.3%		3.47%	
3	48.3(30)	Pass 1	47.8 (29.7)	132.8 (5.23)	1.68%	3.25%	9.09%	10.79%
		Pass 2	45.2 (28.1)	94.2 (3.71)	4.18%		12.63%	
		Pass 3	44.2 (27.5)	98.3 (3.87)	3.88%		10.64%	
	72.4(45)	Pass 1	71.2 (44.2)	69 (2.72)	6.1%	6.02%	15.93%	17.32%
		Pass 2	70.8 (44)	68.6 (2.70)	5.25%		15.96%	
		Pass 3	70.9 (44.1)	49.3 (1.94)	6.71%		20.06%	
	96.6(60)	Pass 1	94.2 (58.5)	39.1 (1.54)	11.22%	11.36%	31.99%	34.09%
		Pass 2	96 (59.6)	53.3 (2.10)	10.04%		30.94%	
		Pass 3	97.3 (60.5)	26.9 (1.06)	12.83%		39.35%	

*All values were measured by geophones.

It can be seen from the table that the response lag is a function of pavement stiffness and vehicle speed as expected. The response lag is least and close to the center of the load in the stiffest cell (Cell 3) and at highest vehicle speed of 96.6 kph while it is close to 184 mm in the softest cell (Cell 34) and at lower vehicle speed of 48 kph. In summary, the hypothesis that maximum deflection occurs at 184 mm (7.25 inch) behind the tire is valid only for less stiff pavements tested at relatively lower vehicle speed and may not be valid for stiff pavement in which D_{max} occurs much closer to the center of the tire.

If the sensor at 184 mm behind the center of wheel could capture maximum deflection, RWD index defined as D_{-184}-$D_{197,}$ can be considered equivalent to $SCIm_{200}$ (D_{max} - D_{200}) which is the difference between maximum deflection and the deflection at 200mm (8 in.) in front of the midpoint between tires. It should be noted that analytical analysis has identified that this index has a good correlation with fatigue strain (Table 6-2). However, variations in the response lag can cause significant difference between the two indices as shown by percent difference between the RWD index and $SCIm_{200}$ in the Table 3. In Cell 34, which is the softest pavement, RWD index is close to $SCIm_{200}$ and can predict fatigue strain relatively well but in Cell 3, which is the stiffest pavement, the differences between RWD index and $SCIm_{200}$ can be as high as 35% at 96.6kph (60mph).

Therefore, the analyses of measured data showed that positioning only one sensor behind the wheel at a pre-determined location can’t always capture maximum deflection since response lags are highly sensitive to stiffness of pavements and vehicle speeds.

When the response lag is less than 184mm (as in the case of stiff pavements), the two RWD sensors are positioned on either side of the deflection basin reducing the device's ability to compute any robust indices to estimate fatigue strain. In order to improve the compatibility of the RWD device to wider pavement sections, it is suggested that the location of both the sensors be positioned in front of the rear axle tire.

6.9. Field Evaluation of TSD Deflection Basin Indices

In this section, the capability of deflection indices to estimate fatigue strains will be evaluated with the field data. Data used in the evaluation include:

1. Measured strains from strain gages at the MnROAD cells.

2. The measured indices from the deflection basins measured by the embedded geophones (Figure 2).

3. The measured indices from the TSD deflection basins computed by numerical integration of measured TSD deflection velocities.

4. Finally, the relationships between deflection indices and fatigue strains developed from the 3D-Move.

The above data were used to evaluate the index-fatigue strain relationships in both within and between the following scenarios:

a) Measured deflection indices from geophones with measured fatigue strains
b) Measured deflection indices from TSD with measured fatigue strains
c) Measured deflection indices from geophones with their predicted fatigue strains
d) Measured deflection indices from TSD with their predicted fatigue strains

The results of field evaluation indicated that DSI indices that use D_{100} and D_{200} as the reference deflection, are the most promising indices and can predict fatigue strains closer to the measured responses. The SCI indices that used D_o as the reference deflection are most affected by the TSD assumption of neglecting response lag in deflection computing algorithm. Among DSI indices, $DSI_{200\text{-}300}$ is the best correlated index with fatigue strain. This index should be considered for further investigations (such as sensitivity analyses) to verify the validity of the developed relationships with wide range of pavement structures [22].

Figure 6-7 shows the field evaluation of $DSI_{200\text{-}300}$ to predict fatigue strain. The general observation from this figure is that in all three cells, measured indices from the TSD are larger than those from geophones and thereby predict larger amount of fatigue strains. It should be noted that in the above analysis, the indices computed from TSD deflection basins are compared with indices computed from geophone deflection basins that are corrected for response lag. Figure 6-8 shows the direct comparison between the two measured indices. The TSD measured index, $DSI_{200\text{-}300}$ is about 13% larger than geophone index. For illustration, in Figure 8, the index computed from TSD deflection basins is also compared with index computed from geophone deflection basins that are not corrected for response lag. In which case, the comparison is better (1% difference) indicating that TSD deflection computation algorithm can be improved if it can accommodate response lag.

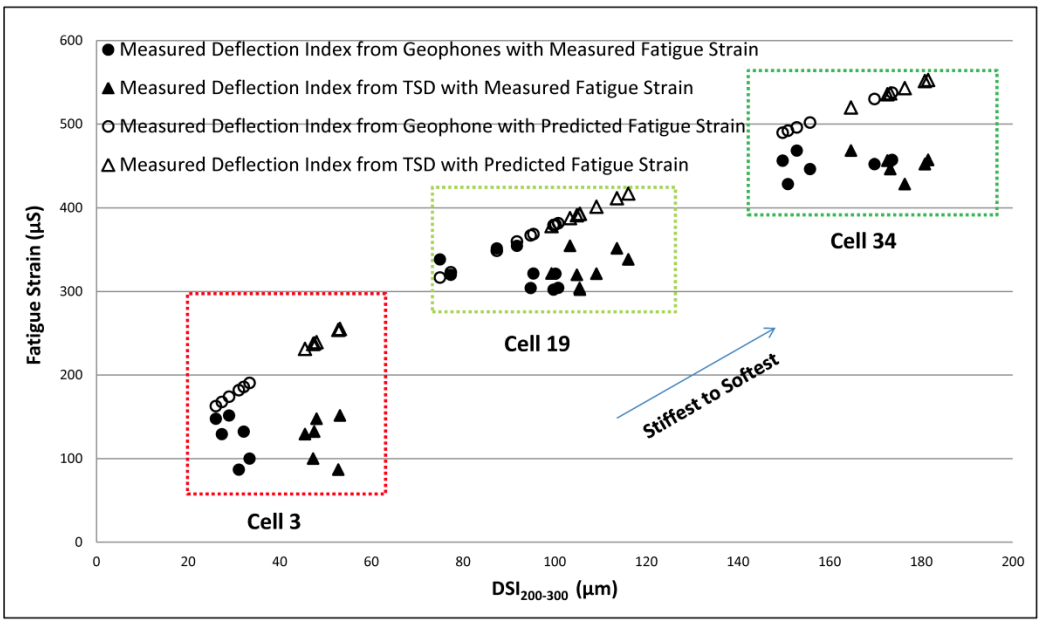

Figure 6-7. Comparison of measured and computed fatigue strains by measured $DSI_{200-300}$ from the TSD and the Geophone

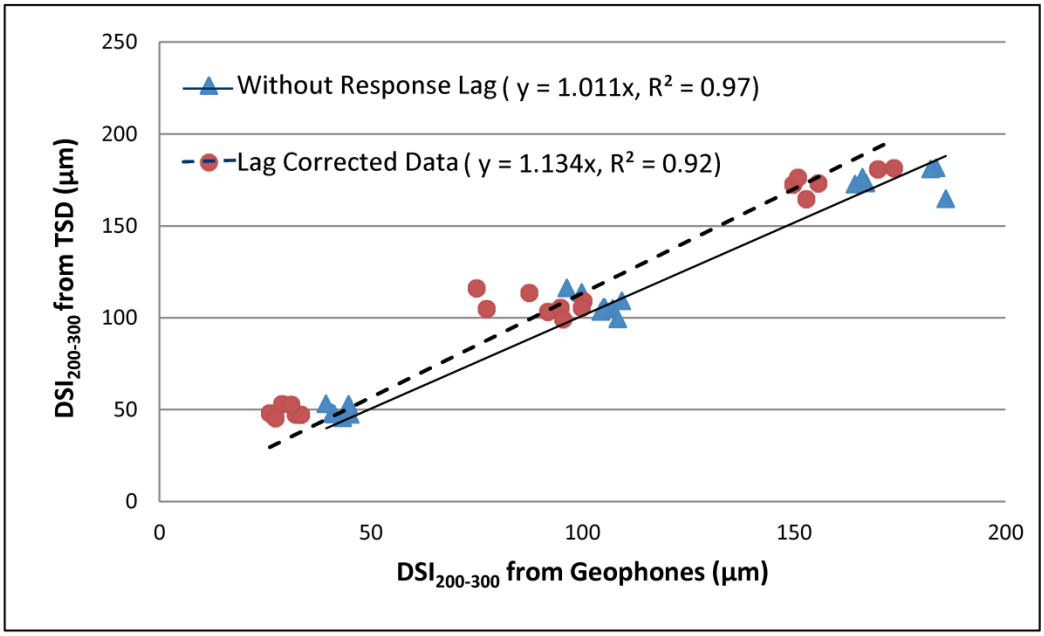

Figure 6-8. Comparison of the accuracy of $DSI_{200-300}$ measured by the TSD with Geophones data without response lag (elastic AC layer) and corrected for response lag (Viscoelastic AC layer)

Another observation from Figure 6-7 is that predicted and measured fatigue strains yielded closer values for Cells 19 and 34 which are less stiff compared to Cell 3. Figure 6-9 shows the comparison of measured fatigue strains and those predicted from $DSI_{200\text{-}300}$ measured by TSD in Cells 19 and 34 at various vehicle speeds and trail passes. This figure shows the capability of measured indices from the TSD in conjunction with analytical model to predict fatigue strain, which is one of the routinely used critical responses in pavement management. In all cases, the predicted fatigue strains are larger than measured values because as stated earlier, TSD assumption in deflection algorithm ignores viscoelastic properties.

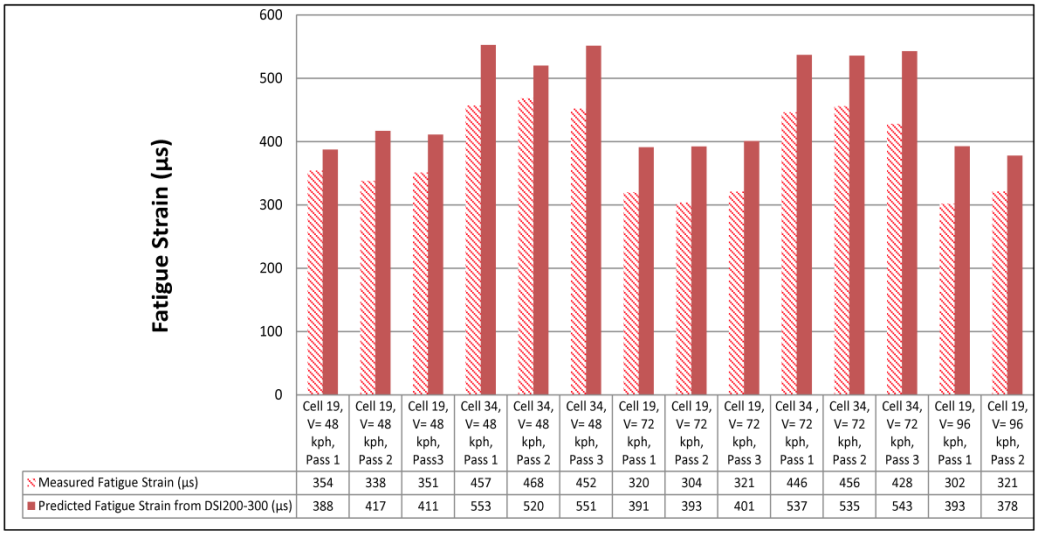

Figure 6-9. Measured versus predicted fatigue strain from $DSI_{200\text{-}300}$ measured by the TSD

6.10. Conclusions

FHWA conducted a study to evaluate traffic speed deflection devices (TSD & RWD) at the MnROAD facility. MnROAD facility was ideal location for field test since it provided many test sections in one location as well as readily accessible pavement

structure, pavement condition and dynamic load response data. An appropriate analytical program, 3D-Move, that considers moving load and viscoelastic properties of AC layer was used to develop best related indices to fatigue strains. The selected indices and relationships were evaluated with field measured data and the observations are presented below.

Results from the 3D-Move show that the indices related to the deflections close to the load center (e.g, SCI_{300}, $DSI_{200-300}$ and SD_{300}) have good relationships with fatigue strains. The new indices (DSI), which were created to overcome the shortcomings of TSD algorithm to compute deflection at D_o, were promising. Therefore the best indices related to load-induced pavement responses are not necessarily depend on D_o. Consequently if D_{100} or D_{200} from the TSD is more reliably measured than D_o, it should be used as the reference deflection in the DSI calculations.

The analyses of measured data showed that positioning only one sensor behind the rear axle tire at a pre-determined location (in RWD) can't always capture maximum deflection since response lags are highly sensitive to stiffness of pavements and vehicle speeds. With only two measurements, it is recommended that the location of the sensors be positioned in front of the rear axle to have a better related index to fatigue strains.

The TSD assumption that ignores viscoelastic properties of AC layer (zero slope at the center of the dual tires) provides conservative results i.e. high deflection index values. The comparison of TSD measured indices with indices computed from the geophone deflection basins that are corrected for response lag shows that measured indices from TSD are 13% larger than those from the geophones. Therefore, the use of

relationships with TSD measurements predicts higher fatigue strain. Accuracy can be improved if the TSD numerical algorithm can include the response lag typically observed in the moving load on viscoelastic material by possibly placing one sensor behind the rear axle.

Acknowledgments

The field measured data in this paper was originated from FHWA sponsored study "Pavement structural evaluation at the network level" DTFH61-12-C-00031. We would like to thank Dr. Nadarajah Sivaneswaran of the FHWA for his kind support. We acknowledge Dr. Gonzalo Rada and Dr.Soheil Nazarian for their leadership and encouragement. The authors would also like to thank Mr. Ben Worel and his staff's at the MnROAD facility without whose help, the successful outcome of the project would not have been possible. The conclusions presented in this paper are solely those of these authors.

6.11. References

[1] Al-Qadi, E., Scarpas, T., and Loizos, A. (2008). *Pavement cracking: mechanisms, modeling, detection*, testing, and case history, Taylor & Francis Group, London, ISBN 978-0-415-47575-4.

[2] Asphalt Institute. (1982). *Research and development of the asphalt institute's thickness design manual (MS-1)*, 9th ed., Research Report 82-2.

[3] NCHRP. (2004). *Guide for mechanistic-empirical design of new and rehabilitated structures*. Final Report for Project 1-37A, National Cooperative Highway Research Program, Transportation Research Board, National Research Council, Washington, D.C.

[4] Horak E. (1987)," The use of surface deflection basin measurements in the mechanistic analysis of flexible pavements." *Proc., Vol. 1, Sixth International Conference Structural Design of Asphalt Pavements, University of Michigan, Ann Arbor, Michigan, USA.*

[5] Thyagarajan, S., Sivaneswaran, N., Petros, K. and Muhunthan, B. (2011), "Development of a simplified method for interpreting surface deflections for in-service flexible pavement evaluation," *8th International Conference on Managing Pavement Assets, Santiago, Chile*.

[6] Xu, B., Ranji Ranjithan, S., & Richard Kim, Y. (2002). "New relationships between falling weight deflectometer deflections and asphalt pavement layer condition indicators." *Transportation Research Record: J. Transportation Research Board,* 1806(1), 48-56.

[7] Rada, G., Nazarian, S., Visintine, B., Siddharthan, R.V., and Thyagarajan, S. (2015). *Pavement structural evaluation at the network level,* FHWA, Final Report.

[8] Pedersen, L., (2012). *Viscoelastic modeling of road deflections for use with the traffic speed deflectometer*. PhD study in collaboration with Greenwood Engineering, Technical University of Denmark and the Ministry of Science and Innovation.

[9] Flintsch, G., Katicha, S., Bryce, J., Ferne, B., Nell, S., & Diefenderfer, B. (2013). *Assessment of continuous pavement deflection measuring technologies*, SHRP 2 Report S2-R06F-RW-1.

[10] Semmelink, C. J. (1999). "Evaluation of deflection bowls measured with impact, static, and in-depth deflection measuring devices on an HVS test site." *Proc., the First International Conference on Accelerated Pavement Testing, Reno, Nev.*

[11] Dasari, K. V. (2013). *Deflection based condition assessment for rolling wheel deflectometer at network level*, Doctoral dissertation, Louisiana State University.

[12] Siddharthan, R.V., Yao, J., and Sebaaly, P.E. (1998) "Pavement strain from moving dynamic 3-D load distribution." *J. Transportation Engineering. ASCE*, Vol. 124(6), pp. 557-566.

[13] Siddharthan, R.V., Krishnamenon, N., and Sebaaly, P.E. (2000). "Pavement response evaluation using finite-layer approach." *Transportation Research Record* .1709, 43-49.

[14] Siddharthan, R.V., Krishnamenon, N., El-Mously, M., and Sebaaly, P.E. (2002) "Investigation of tire contact stress distributions on pavement response." *J. Transportation Engineering, ASCE*, 128(2), 136-144.

[15] Siddharthan, R.V., El-Mously, M., Krishnamenon, N., and Sebaaly, P.E. (2002) "Validation of a pavement response model using full-scale field tests." *International Journal in Pavement Engineering*, 3(2), 85-93.

[16] Siddharthan, R., Sebaaly, P.E., El-Desouky, M., Strand, D., and Huft, D. (2005) "Heavy off-road vehicle tire-pavement interactions and response." *J. Transportation Engineering, ASCE*, 131(3), 239-247.

[17] Chabot, A., Chupin, O., Deloffre, L., and Duhamel, D. (2010) "Viscoroute 2.0: A tool for the simulation of moving load effects on asphalt pavement." *J. Road Materials and Pavement Design* , Volume 11/2, 227-250.

[18] Hajj, E.Y., Ulloa, A., Siddharthan, R.V., and Sebaaly, P.E. (2012) "Equivalent loading frequencies for dynamic analysis of asphalt pavements." *J. Materials in Civil Engineering.* 25(9), 1162-1170.

[19] Nasimifar, M., Siddharthan, R. V., Rada, G., and Nazarian, S. (2015). "Dynamic analyses of traffic speed deflection devices." *International J. Pavement Engineering*.

[20] Irwin, L. H., Orr, D. P., & Atkins, D. (2009). *FWD calibration center and operational improvements: Redevelopment of the calibration protocol and equipment*. FHWA-HRT-07-040.

[21] Kim, Y.R., Underwood, B., Sakhaei Far, M., Jackson, N., and Puccinelli, J. (2011). *LTPP computed parameter: dynamic modulus.* FHWA Publication FHWA-HRT-10-035.

[22] Nasimifar, M., Thyagarajan, S., Siddharthan, R., and Sivaneswaran, S., (2015). "Robust deflection indices from traffic speed deflectometer measurements to predict critical pavement responses for network level PMS application." *Accepted for publication in Journal of Transportation Engineering, ASCE.*

7. Summary, Conclusion and Recommendation

The Falling Weight Deflectometer (FWD) is an important part of the current pavement condition evaluation and rehabilitation strategies. FWDs have provided valuable data relating to pavement performance to estimate suitable remedies and construction budget for network level. The limitations of FWD, such as mobilization, traffic closure and low rate of data collections encouraged organizations in the USA and Europe to look for a faster method of pavement deflection testing device, especially for network-level pavement assessment. The Traffic Speed Deflectometer (TSD) developed by Greenwood Engineering and Rolling Wheel Deflectometer (RWD) developed by Applied Research Associates, collectively referred to as Traffic Speed Deflection Devices (TSDDs), have been developed to overcome many of the FWD shortcomings, as they collect surface deflections up to posted traffic speeds (up to 80 – 96 kph). Euroconsult, Curviametro (CRV) is a device that operates at low speed (up to 18 kph) which is significantly slower than traffic speed devices but provides a completed surface deflection measurements.

Much work has been done over the past decade toward understanding the capabilities of these devices, as a replacement for FWD data for pavement structural evaluation. However, the proper incorporation of the results from these devices to network level pavement management system (PMS) applications requires appropriate, device-specific, analysis methodology. To assess the appropriateness of any proposed methodology, field evaluations in conjunction with analytical models to simulate the TSDDs measurements are required important steps.

The Federal Highway Administration (FHWA) commissioned the evaluation of these devices at the MnROAD facility in September 2013. The MnROAD facility near Maplewood, Minnesota was selected as the primary site for the field trials since it provided a multitude of test sections in one location as well as a wealth of readily available information, including pavement structure, pavement condition, and environmental and TSDD load response data. In addition to the existing MnROAD sensors (strain gauges, pressure cells, etc.), four geophones and one accelerometer were installed near the pavement surface to measure deflections at three cells called accuracy cells.

3D-Move program was used as an analytical tool in this study. The analytical model (3D-Move) evaluates pavement response using a continuum-based finite-layer approach. The 3D-Move model can account for important pavement response factors such as the moving traffic-induced complex 3D contact stress distributions (normal and shear) of any shape, vehicle speed, and viscoelastic material characterization for the pavement layers. The finite-layer approach treats each pavement layer as a continuum and uses the Fourier transform technique; therefore, it can handle complex surface loadings such as multiple loads, non-uniform tire pavement contact stress distributions, and any shaped tire imprints, including those generated by wide-base tires. Since 3D-Move has the capability of modeling moving loads and the resulting dynamic pavement responses, it is ideally-suited to evaluate and compare pavement responses measured using load-response devices that move at high-speeds (e.g., TSD and RWD devices).

Having identified the TSDDs that are acceptable, the 3D-Move software was initially calibrated using data from the MnROAD facility field trials. The surface deflections and pavement responses collected at the MnROAD facility during the field trials were used as reference values to calibrate and validate 3D-Move model. The objective of this calibration was to enable the use of the 3D-Move software in the development of methodologies for incorporating TSDD measurements into network-level PMS applications. A key element in the calibration was simulating pavement surface deflections using numerical models with a focus on understanding the parameters that affect the TSDD measurements. Those parameters include changes in TSDD vehicle speed, pavement layer properties (e.g., age and moisture), and vehicle loading (e.g., tire configuration, load and inflation pressure) etc.

Numerous 3D-Move analyses were performed to bracket the computed deflection time histories (peak and basin) with the measured ones from the project geophones. The 3D-Move software was further calibrated using strain measurements taken by the MnROAD strain gauges at various interior pavement locations. Since load-induced strains are critical inputs to pavement performance predictions, this effort was considered critical in ascertaining the applicability of the 3D-Move for pavement response predictions to be used in identifying the most promising indices from TSDD measurements that best relate to pavement structure.

The 3D-Move maximum strains correlated well with the MnROAD sensor measurements. Accordingly, it was further concluded that 3D-Move captures the

pavement strain responses well, and therefore, can be used to evaluate pavement responses under TSDD loadings.

Pavement structural capacity can be estimated from performance prediction equations, which relate load-induced pavement responses to one or both of the following pavement distresses: AC fatigue cracking and rutting subgrade rutting. The critical load-induced pavement responses that relate to these two distresses are the maximum tensile strain at the bottom of the AC layer and the vertical compressive strain on top of the subgrade, respectively.

Using the calibrated 3D-Move software, an analytical investigation was then undertaken to explore relationships between load-induced pavement structural-related response and the corresponding surface deflection basin related indices. A focus was considered on understanding the parameters that affect the strength of the correlations between deflection indices and the pavement responses that included vehicle speed and loadings, and pavement layer properties.

Based on the results, the following major observations and conclusions relating to deflection indices and critical pavement responses were made:

- It was found that the deflection basin indices closer to center of the loading have the highest correlation with fatigue strain and thus can best represent the structural condition of the AC layer. The sensitivity analyses showed the deflection indices SCI_{300} (D_o - D_{300}), $DSI_{100\text{-}200}$ (D_{100} – D_{200}), and $DSI_{200\text{-}300}$ (D_{200} - D_{300}) have strong correlations with fatigue strain. On the other hand, the indices based on

deflections measured farther away from the center of the loading (e.g., $DSI_{300-600}$ ($D_{300} - D_{600}$), $DSI_{300-900}$ ($D_{300} - D_{900}$)) best relate to the vertical subgrade strain.

- On the basis of the sensitivity analyses, the AC layer thickness is the most influential parameter on fatigue strain. Loading speed, subgrade and base layer properties are found to affect the fatigue strain only marginally.

- In addition to AC layer thickness that significantly affects the rutting strain, other properties such as base thickness and subgrade stiffness have a moderate impact on rutting strain. However, for network-level PMS application, it was reasonable to develop indices that relate to rutting strains by categorizing pavements based only on AC thickness.

- Measurements from the TSD and geophones are used to identify the indices that can be accurately computed from the TSD. $DSI_{200-300}$ (D_{200} - D_{300}) and $DSI_{300-900}$ ($D_{300} - D_{900}$) are identified as the robust indices that can be accurately measured and also have the highest correlations with fatigue and rutting strains, respectively. There is uncertainty in the estimation of the conventionally-used index (SCI) with the TSD because the TSD doesn't directly measure deflection velocity at 0 mm (the midline of the dual tires) and D_o is estimated using assumptions regarding missing measurement at 0 mm. Therefore, DSI can be a reliable alternative for SCI_{300} that can be used effectively to relate with fatigue strain.

The outcome of this study facilitated use of TSDDs in network level pavement management system by categorizing pavements based only on AC thickness and then

relating $DSI_{200-300}$ (D_{200} - D_{300}) and $DSI_{300-900}$ (D_{300} − D_{900}) to fatigue and rutting strain, respectively through appropriate equations.

The study also provided some practical suggestions to improve the performance of TSDDs in PMS applications. The recommendations are as follows:

The analyses of measured data showed that positioning only one sensor behind the rear axle tire at a pre-determined location (in RWD) can't always capture maximum deflection since response lags are highly sensitive to stiffness of pavements and vehicle speeds. With only two measurements, it is recommended that the location of the sensors be positioned in front of the rear axle to have a better related index to fatigue strains. The TSD assumption that ignores viscoelastic properties of AC layer (zero slope at the center of the dual tires) provides conservative results i.e. high deflection index values. The comparison of TSD measured indices with indices computed from the geophone deflection basins that are corrected for response lag shows that measured indices from TSD are 13% larger than those from the geophones. Therefore, the use of relationships with TSD measurements predicts higher fatigue strain. Accuracy can be improved if the TSD numerical algorithm can include the response lag typically observed in the moving load on viscoelastic material by possibly placing one sensor behind the rear axle.

8. Recommended Future Study

The presented study represents the first step toward the eventual implementation of a robust system approach for the structural evaluation of pavements at the network level using TSDDs. The main objective of this research was first to calibrate and validate dynamic simulation of TSDDs (with 3D-Move program) to predict continuous deflections with measured data from the MnROAD filed trials conducted in September 2013 and then develop a methodology to use TSDDs measurements to predict pavement responses and subsequently use of these device in the evaluation of network level pavement structural condition. Beyond the study recommendations, other potential future research areas under controlled conditions may be necessary to:

- Confirm the predictive correctness of the recommended deflection indices through the use of measurements taken by strain gauges at various depths during TSDD loadings. While the data collected as part of this study served as a first step, there were issues with data limited to AC layers of around 3 to 5 in. in thickness. Accordingly, additional data for thinner and ticker pavements structures are desirable.
- Consider the impact of the non-linear response of the unbound materials in thin pavement structures on the TSDD measured responses.
- Explore methodologies for the development of robust structural performance curves based on TSDD derived structural indices measured over time with appropriate adjustments made for environmental conditions (e.g. pavement age

and time of measurement etc.) for use in pavement structural condition evaluation.

- Adjust the estimated pavement responses to a standard temperature. The pavement responses need to be corrected to a standard reference temperature for consistent evaluation and tracking of the deflection parameters over time. TSDDs measurements and their correlations with pavement responses are influenced by the viscoelastic properties of the pavement layer which are highly affected by temperature. So the adjusting the estimated pavement responses to a standard temperature can provide realistic results for PMS application.